Université de Toulouse

THÈSE

En vue de l'obtention du

DOCTORAT DE L'UNIVERSITÉ DE TOULOUSE

Délivré par **l'Institut Supérieur de l'Aéronautique et de l'Espace**
Spécialité : Systèmes automatiques

préparé en cotutelle internationale de thèse avec
l'Instituto Nacional de Pesquisas Espaciais (Brésil)

Présentée et soutenue par **Fausto De Oliveira Ramos**
le 3 mars 2011

Automatisation de la synthèse H-infinie de compensateurs
et de leurs réalisations sous forme estimation-commande

Automation of H-infinity controller design
and its observer-based realization

JURY

M. Luis Carlos Gadelha De Souza, président
M. Daniel Alazard, directeur de thèse
M. Valdemir Carrara
M. Franck Cazaurang, rapporteur
M. Waldemar De Castro Leite Filho, directeur de thèse
M. Paulo Pellanda, rapporteur

École doctorale : **Systèmes**

Unités de recherche : **Équipe d'accueil ISAE-ONERA CSDV**
Instituto Nacional de Pesquisas Espaciais (Brésil)

Directeurs de thèse : **M. Daniel Alazard – M. Waldemar De Castro Leite Filho**

Ministério da
Ciência e Tecnologia

sid.inpe.br/mtc-m19/2011/01.25.12.21-TDI

AUTOMATION OF H_∞ CONTROLLER DESIGN AND ITS OBSERVER-BASED REALIZATION

Fausto de Oliveira Ramos

Double-diploma doctoral thesis supervised by Dr. Waldemar de Castro Leite Filho (Instituto Nacional de Pesquisas Espaciais / Engenharia e Tecnologia Espaciais / Mecânica Espacial e Controle) and Prof. Daniel Alazard (Institut Supérieur de l'Aéronautique et de l'Espace / École Doctorale Systèmes / Commande des Systèmes et Dynamique du Vol), approved on Mars 3, 2011.

URL of the original document:
<http://urlib.net/8JMKD3MGP7W/393JLML>

INPE, ISAE
São José dos Campos (Brazil), Toulouse (France)
2011

PUBLISHED BY:

Instituto Nacional de Pesquisas Espaciais - INPE
Gabinete do Diretor (GB)
Serviço de Informação e Documentação (SID)
Caixa Postal 515 - CEP 12.245-970
São José dos Campos - SP - Brasil
Tel.:(012) 3945-6911/6923
Fax: (012) 3945-6919
E-mail: pubtc@sid.inpe.br

"Start by doing what's necessary; then do what's possible; and suddenly you are doing the impossible." St. Francis of Assisi

To my wife ***Célia*** *and children* ***Giuliane***, ***Fausto Jr.*** *and* ***Marcelinho***.

ACKNOWLEDGEMENTS

Institutional acknowledgements. I would like to thank the following institutions and associated academic and administrative personal:

- INPE, to allow the enrolment at the postgraduate program, and to accept the double-diploma extension with ISAE.
- ISAE, for the very good welcome and for the support in Toulouse for a one-year stay (shortened by a very agreeable reason).
- CTA, IAE, and FUNDEP, for releasing me full-time and for the financial support not only in France but also for scientific events.
- *La mairie de Belberaud*, for your directions and kindly support during the stay of my family at that village.

Academic acknowledgements. I would like to express my gratitude to the following research fellows:

- Dr. Waldemar de Castro Leite Filho, for your great confidence, incentive to pursue this doctoring program, directions and support.
- Prof. Daniel Alazard, for giving me an opportunity and providing me the best conditions at ISAE to develop the work and for your great patience.
- Dr. Luiz Carlos Gadelha de Souza, for your invaluable incentive, directions and partnership.
- Dr. Ernesto Araujo, for your essential teachings on fuzzy systems.

Personal acknowledgements.

To my family (now with a new member), who accepted to live abroad one more time, allowing me to develop the doctoring program.

To our parents, Antonio Francisco and Ephigênia, José Pinheiro and Maria Helena (*in memoriam*), aunties Lili, Lúcia and Lygia (*in memoriam*), brothers (specially Fábio - our Brazil-France connection) and relatives (thanks! Zézinho, for your high performance PC), we know that you are proud of us.

To the very warm and unexpected welcome from our neighbours of the small village called *Belberaud* (they call themselves as *Mandillais*, after the street name): Monique and Jacques, Nadia and Pierre, Geneviève and Sylvain, Annie and Christian, Tony and Dominique, Martine and Eric, Fabienne and Christoff, Jeanne-Marie and Marc, Regine and Pascal, Martine and Jacques, and Frédéric Jean (our landlord): *vous nous manquez beaucoup!*

To the office colleagues at CTA/IAE, specially the Control Team (IAE-ASE-C), many thanks for your suggestions, support and patience, mainly when producing that long series of hardware-in-the-loop simulations (Carlos and Domingos), for giving me an initial spark on computational intelligence (Alexandro) and helping me abroad (Teresa). I would like to thank also Mrs. Ana Clara and Mrs. Solange (CTA/International Affairs), Cel. Fabian Ballet and Ms. Cécilia (*Ambassade de France au Brésil / Direction du Développement International*) for the essential aid to obtain the VISAs for me and my family.

To the ISAE PhD students and personal: Leonardo, Malek, Siyuan, Baziz, Lucia, Tsan, Stephane, Pascal, Dominique, Alan, Kathia, Regine, Sophie, Odile, Maryse, thanks for your *très agreable* company and conversations at ISAE's *"labô"* and *"restô"*.

Hors concurs **acknowledgements.** There are moments in people's lives when one must face important duties - be academic, professional or personal. Besides the benefits (experience, wisdom) one can obtain in such circumstances, they frequently come accompanied of concern, doubt and discouragement; even in little proportions, they are there. However, faith in ideas keep us working hopefully for the success; thus, one must choose ideas, objectives and actions carefully, and to comprehend exactly the ultimate meaning of "success".

Thanks, God, for teaching me that in a very loving way.

LIST OF FIGURES

Pág.

2.1 Example of a Pareto-optimal set. 6
2.2 Block diagram of the computational intelligence field. 7
2.3 Basic operation cycle of a genetic algorithm. 9
2.4 Diagram of a Fuzzy System. 10
2.5 Example of a FS surface. 12
2.6 Example of a CI-based mechanism used for CSDA. 12
2.7 Satellite description. 13
2.8 Attitude control system of the satellite. 14
2.9 Satellite general standard model. 15
2.10 Fuzzy system premises of the satellite CSDA example. 18

3.1 Observer-based structure using YOULA parametrization. 25
3.2 H_∞ general standard model of the VLS launch vehicle. 30
3.3 Simulation schema comprising the attack angle estimate $\hat{\alpha}$. 35
3.4 Wind profile used as an external disturbance at the input w_v of the model. 36
3.5 Variables w, q, θ and α: comparison between real (black) and estimated (green) ones for options "A" (left) and "B" (right). 37
3.6 Variables w, q, θ and α: comparison between real (black), estimated (green) and measured (gray; only for q_m and θ_m) ones, with noise added to the sensor outputs, for options "A" (left) and "B" (right). 37
3.7 Error between real (α) and estimated (α_{hat}) angles-of-attack (options "A" and "B"). 38
3.8 Real (α) and estimated (α_{hat}) angles-of-attack, when measurement noises are taken into account (options "A" and "B"). 38
3.9 Variation of the estimated angle-of-attack when the parameters of the plant correspond to different linearisation points of the launch vehicle trajectory. (Top sub-figure, black line: nominal condition.) 39

4.1 Development of the robust control area. 42
4.2 Block diagrams used for control system analysis. 43
4.3 Singular values representing a LTV system with $A(1,2) = e^{kt}$, $k = [0.0,\ 0.1,\ \cdots 1.0]$. 48

5.1 Mission, projects and activities conducted at the Instituto de Aeronáutica e Espaço (IAE). . . . 52
5.2 VLS launch vehicle. . . . 53
5.3 Elements of the VLS hardware-in-the-loop simulation complex. . . . 55
5.4 The pseudocode of the main procedure *gen_ alg*. . . . 58
5.5 The pseudocode of the procedures *evolute* and *evaluate*. . . . 58
5.6 Mapping from constraints and indexes to cost values. . . . 59
5.7 Controller gains obtained by the CSDA-LQ design without (left, proportional gain only) and with a smoothing factor S_f in the cost function. . . . 61
5.8 Controller gains obtained by the conventional design. . . . 61
5.9 Rise time and overshoot: a comparison between the conventional and the CSDA-LQ (-) designs. . . . 61
5.10 Gain and phase margins: a comparison between the conventional and the CSDA-LQ (-) designs. . . . 62
5.11 Maximal control effort (pitch axis): a comparison between the conventional and the CSDA-LQ (-) designs (non-linear digital simulation). . . . 62
5.12 Control effort (boosters A and B of the 1^{st} stage): a comparison between conventional and CSDA-LQ (-) designs, obtained from hardware-in-the-loop phase D simulations, nominal scenario. . . . 66
5.13 GSM of the VLS launch vehicle (roll plane). . . . 67
5.14 Non-linear simplified simulation model for unit step input response. . . . 68
5.15 Part of the simulation model used for obtaining the OBR estimation. . . . 68
5.16 Estimation of the attack angle α. . . . 69
5.17 Estimation of the bias b_q. . . . 70
5.18 Estimation of the bias b_p and misalignment b_β. . . . 71
5.19 Premises of the FS no. 1. . . . 76
5.20 Indexes obtained with the CSDA-H_∞ mechanism. . . . 77
5.21 Smoothness of the closed-loop eigenvalues. . . . 78
5.22 Non-smoothed OBR vectors. . . . 78
5.23 Time variation of two elements of the closed-loop state-space matrix A_{CL}. 79
5.24 Estimate $\hat{b}_p$ produced by non-linear digital simulation. . . . 80
5.25 Elements of the state-space matrices of the discrete H_∞ controller. . . . 81

A.1 Transformation between systems of coordinate axes of the VLS vehicle. . . . 95
A.2 GSM of the VLS launch vehicle (pitch plane). . . . 110
A.3 Intervals for null coefficients of the subsets 1 and 2 (illustrative view). . . . 116
A.4 GSM of the VLS launch vehicle (roll plane). . . . 118

LIST OF TABLES

Pág.

2.1 Comparison between the four automated designs. 20

3.1 Closed-loop distribution, option "A". 34
3.2 Closed-loop distribution, option "B". 34

5.1 Case studies characterization of the VLS launch vehicle CSDA. 56
5.2 Parameter values of the cost function indexes (N. A. = not applied). . . 58
5.3 Results of the HWIL simulations, phase B, 1^{st} stage. 64
5.4 Results of the HWIL simulations, phase B, 2^{nd} stage. 65
5.5 Results of the HWIL simulations, phase B, 3^{rd} stage. 65

A.1 Parameters of the VLS model around $t_{max} \pm 1[s]$. Units in MKS, angles in radians. 99

LIST OF ABBREVIATIONS

AI	–	Artificial Intelligence
CI	–	Computational Intelligence
CACSD	–	Computer-Aided Control System Design
CSDA	–	Control System Design Automation
DISO	–	Double Input Single Output
EC	–	Evolutionary Computation
FFT	–	Fast Fourier Transform
FS	–	Fuzzy System
FUNDEP	–	*Fundação de Desenvolvimento da Pesquisa*
GA	–	Genetic Algorithm
GS	–	Gain-Scheduling
GSM	–	General Standard Model
GSP	–	General Standard Problem
GUI	–	Graphic User Interface
HWIL	–	HardWare-In-the-Loop simulation
INPE	–	*Instituto Nacional de Pesquisas Espaciais*
ISAE	–	*Institut Supérieur de l'Aéronautique et de l'Espace*
IAE	–	*Instituto de Aeronáutica e Espaço*
LQ	–	Linear-Quadratic
LTI	–	Linear Time-Invariant
LTV	–	Linear Time-Varying
MECB	–	*Missão Espacial Completa Brasileira*
MIMO	–	Multiple Input Multiple Output
NN	–	Neural Network
OBR	–	Observer-Based Realization
PID	–	Proportional-Integral-Derivative
PC	–	Personal computer
PD	–	Proportional-Derivative
SISO	–	Single Input Single Output
VLS	–	*Veículo Lançador de Satélite*

LIST OF SYMBOLS

$\mathbf{A}$, $\mathbf{B}$, $\mathbf{C}$, n	–	State-space matrices and order of the plant model or the on-board model depending on the context.
$\mathbf{A_K}$, $\mathbf{B_K}$, $\mathbf{C_K}$, $\mathbf{D_K}$, $\mathbf{n_K}$	–	Controller state-space matrices and order.
$\mathbf{A_O}$, $\mathbf{B_O}$, $\mathbf{C_O}$, $\mathbf{n_O}$	–	On-board model state-space matrices and order.
$\mathbf{A_P}$, $\mathbf{B_P}$, $\mathbf{C_P}$, $\mathbf{n_P}$	–	Plant state-space matrices and order.
f_G, f_T, f_B, f_Z	–	Respectively: Gaussian, triangular-shaped, bell-shaped and z-polynomial functions.
G_A	–	Actuator transfer function.
$G_{\phi\beta}$	–	Transfer function of the VLS roll plane decoupled model with respect to the control input.
$G_{\theta\beta}$, $G_{\theta d}$	–	Transfer function of the VLS pitch plane decoupled model with respect to the control and disturb. inputs respectively.
G_{Bi}	–	Transfer function of i^{th} VLS bending mode.
$\mathbf{H_1}$, $\mathbf{H_2}$	–	Transformation vectors from controller state vector and plant output vector respectively to physical estimates.
$\mathbf{K_c}$, $\mathbf{K_f}$, $\mathbf{Q}$	–	Respectively, state-feedback gain, state-estimation gain and Youla parameter of the observer-based realization.
m_g	–	Gain margin.
m_p	–	Phase margin.
M_p, t_r, t_s, u_{max}	–	Performance specifications, respectively: peak overshoot, rise time, settling time and maximum actuation effort.
n_i, n_m	–	Respectively, number of inputs and measurements.
p	–	Roll rate.
p_{cl}	–	Index for closed-loop smoothing and OBR estimation quality.
$\Re$	–	Set of real numbers.
$\mathbf{S}$, $\mathbf{L}$	–	Sensitivity and open loop functions.
S_f	–	Smoothing factor.
spec($\mathbf{A}$)	–	Set of eigenvalues of the matrix $\mathbf{A}$.
$\mathbf{T}$	–	Transformation matrix from controller state vector to physical estimates ($n \geq n_K$) or complementary sensitivity, depending on the context.
t_d	–	Design time.
$u_h(t)$	–	Heaviside function or unit step function.
w_v	–	Wind disturbance input.
$\breve{\mathbf{x}}$, $\hat{\mathbf{x}}$, $\bar{\mathbf{x}}$, $\dot{\mathbf{x}}$	–	Refers respectively to a balanced realization, estimate, parameter, and time derivative.
$\mathbf{x_K}$	–	Controller state vector.
α	–	Attack angle.
$\mathbf{\Phi}$	–	Transition matrix.
θ	–	Pitch attitude angle.
$\mu_\Delta(\mathbf{M})$	–	Structured singular value of the matrix $\mathbf{M}$.
Additional symbols	–	See appendix.

CONTENTS

Pág.

1 Introduction 1
1.1 Motivation and objectives 1
1.2 Bibliographic review 2
1.3 Thesis outline 3
1.4 Publications 4

2 Control system design automation 5
2.1 Introduction 5
2.1.1 Why CSDA?, overview and survey 5
2.1.2 Computational intelligence 6
2.1.3 Genetic algorithms 8
2.1.4 Fuzzy systems 10
2.1.5 Understanding a CI-based mechanism 11
2.2 Example: CSDA of a satellite controller 13
2.2.1 Satellite model and control system 13
2.2.2 The CI-based design mechanism 16
2.2.2.1 GA characteristics 16
2.2.2.2 FS characteristics 17
2.2.3 Design comparison 19
2.3 Conclusion 22

3 The observer-based realization of a controller 23
3.1 Introduction 23
3.2 OBR theory 24
3.2.1 Observer-based structure with Youla parameter 24
3.2.2 Controller order 26
3.2.3 Closed-loop combinatoric set 26
3.2.4 Complementary topics 27
3.3 CI-based combinatoric search and selection 29
3.4 Example: OBR of a launch vehicle controller 29
3.4.1 Design technique and models 29

3.4.2 On-board model . . . 31
3.4.3 Choice of the disturbance estimation dynamics . . . 32
3.4.4 Observer-based realization . . . 33
3.4.5 Simulations results . . . 35
3.4.6 Response to parameter variation . . . 36
3.5 Conclusion . . . 39

4 New robustness metric for LTV systems . . . 41
4.1 Introduction . . . 41
4.1.1 Brief history of robust control and general overview . . . 41
4.1.2 μ-analysis . . . 44
4.2 New metric for exponential uncertainty . . . 45
4.2.1 Invariant $\mathbf{x}$ time-varying systems . . . 45
4.2.2 Time-varying systems and Laplace transformation . . . 46
4.2.3 Required procedure for the new metric . . . 47
4.2.4 Example: LTV system . . . 47
4.3 Conclusion . . . 49

5 Case studies: CSDA of the VLS launch vehicle control system . 51
5.1 Introduction . . . 51
5.1.1 Overview of the Brazilian space mission . . . 51
5.1.2 Cases studied . . . 56
5.2 VLS CSDA no. 1: GS linear-quadratic controller . . . 57
5.2.1 GA characterization. . . . 57
5.2.2 Design comparison with respect to the smoothing issue . . . 59
5.2.3 Hardware-in-the-loop simulations . . . 63
5.3 VLS CSDA no. 2: GS OBR H_∞ controller . . . 65
5.3.1 Design characterization . . . 66
5.3.2 OBR characterization . . . 68
5.3.3 GA characterization . . . 72
5.3.4 FS characterization . . . 73
5.3.5 Results: smoothing closed-loop eigenvalues only . . . 76
5.3.6 Remarks on the non-linear digital simulation results . . . 79
5.4 Conclusion . . . 81

6 Conclusions . . . 83
6.1 Main facts . . . 83

6.2 Summary of contributions 84
6.3 Future research 85

REFERENCES 87

APPENDIX - REVISION OF THE VLS MODELS 93
A.1 Objective. 93
A.2 Rigid body non-linear model of the VLS launch vehicle. 93
A.3 Rigid body linear models of the VLS launch vehicle. 98
A.3.1 Numerical data. 98
A.3.2 Rigid body linear coupled model. 98
A.3.3 Rigid body linear decoupled models. 102
A.3.4 Transfer functions of the rigid body decoupled dynamics. 103
A.4 Full linear models. 105
A.4.1 Bending and torsional modes. 105
A.4.2 Full linear coupled model. 105
A.4.3 Full linear decoupled models. 108
A.5 VLS launch vehicle general standard model. 110
A.5.1 Structure of the GSM. 110
A.5.2 Development of the GSM state equations. 111
A.5.2.1 Full set of coefficients. 111
A.5.2.2 Reduced set of coefficients. 115
A.5.3 Properties of the GSM. 117
A.5.4 GSM of the roll plane. 118
A.6 Linearisation of the VLS rigid body non-linear model. 119

1 Introduction

One intends to justify in this work: (*i*) the "automation of automatics", that is, the embedding of mechanisms *for* the design (not *in* the design) of complex control systems; (*ii*) according to a perspective of fault tolerance, the convenience of controller internal reorganization as an observer; (*ii*) a suitable robustness metrics tackling time-varying uncertainty.

1.1 Motivation and objectives

As said by Einstein, "*work is 1% inspiration plus 99% transpiration*"; we could also say "999% of transpiration", because the creative (inspirational) part tends to simplify the original problem in order to make it feasible, given some time and cost constraints. In control engineering, this simplification is expressed as reduced order models for controller design, tailored formulas for industrial PID tunning, etc. . The "transpiration deflation" is a shortcut in the process of decision-making but does not necessarily mean the best sense from a pure technical perspective.

Now, let's increase even more the transpiration degree - say 9999% - considering the aerospace area, where funcionality is required not only for nominal conditions but also for time-varying, uncertain, perturbed, noisy and even faulty ones. Furthermore, multiple operating points demand for gain-scheduled design, so that each set of calculations must be repeated exhaustively, and ... did we mention the interpolation of the resulting controllers and its implication in the system stability? Well, an automated environment to carry all those tasks in a faster and deeper way is a consequent thought. In other words, inflation of the transpirational parcel[1] can be achievable by means of modern tools such as computers and computational intelligence (CI), subtly moving the (human) designer reasoning centreline from "*assuming that*" to "*what if...?*". At this level, misconceptions and prejudice raise from part of the scientific community unaccustomed to such ideas, revealing perhaps a hidden *taboo*: machines are not suitable as real-world designers. It is not our intention to join in the discussion, since the automation mechanism presented here is not effectively designing but searching and selecting designs - we leave the subject to an appropriate opportunity; the aim is to suggest a beneficial sinergy between design of complex systems and CI.

[1]The inflation of the inspirational parcel is possible as well (though it will not be considered in this work), e.g. the choice of a controller's structure in place of its parameters (FLEMING; PURSHOUSE, 2002).

Sometimes, systems (such as aircrafts or space rockets) may be found not only complex but also critical, that is, their malfunction or failure may result in serious consequences. Inevitably, some sort of fault tolerance must be conceived, where faults must be correctly detected and isolated (localised). Observers are structures frequently adopted to provide the estimations required by the FDI (Fault Detection and Isolation) logic. However, estimation is not an exclusive attribute of observers, controllers can be restructured to act as such, provided that their order is compatible with the plant one. A modern technique - the observer-based realization (OBR for short) - is adopted in this work, where again CI fulfils the needs related to the exploration of the closed-loop combinatoric set. Besides, OBR counteracts one of the main disadvantages of established multi-variable design techniques: the higher the order of the controller compared to the plant, the higher the number of variables that can be estimated - plant state variables, disturbances, faults, etc. . Finally, OBR is applied for the first time to linear time-varying (LTV) systems, and some important questions arise, *e.g.* the preservation of the estimation quality regarding the controller interpolation.

A further problem to be considered in this report is the robustness associated with LTV systems: one intends to shape an exponential variation on the plant model, thus creating a new metric which allows to study the impact due to fast variations in some of the model transfer-function coefficients on robust stability. The new metric was thought to be conceptually simple and compatible with the modern procedures for robustness evaluation (popularized by MATLAB® m-functions). Finally, one applies the ideas presented here in two case studies based on the same launch vehicle model, where a set of conflicting specifications must be achieved through CI structures by the multi-objective evolutionary optimization.

1.2 Bibliographic review

It is not easy to compile a resumed set of bibliographic references when one deals with two major areas at the same time: control engineering and computational intelligence. The work here presented was born of a previous paper (BRITO et al., 2006) where a computationally-intelligent design mechanism surpassed other three approaches for launch vehicle control system design. The problem at that time was limited to the gain-scheduling design of a launch vehicle pitch plane using a simple controller composed of three gains. A step forward (RAMOS; LEITE FILHO, 2007c) added gain smoothing - since it is also a relevant issue regarding the stability of

linear time-varying systems - to the previous objectives (stability and performance indexes), while keeping a genetic algorithm as the intelligence-based element to perform the search of linear-quadratic controllers. The cost function used for fitness evaluation was later substituted (RAMOS; LEITE FILHO, 2007a) by a fuzzy system and the entire procedure validated through hardware-in-the-loop simulations, being compared with the current LQ procedure, yielding interesting improvements, as the design optimization over the full vehicle trajectory. In (MEDEIROS et al., 2005), a H_∞ CI-designed controller with a variant tuning was adopted in order to reject the first bending mode of a launch vehicle, resulting in a similar but more robust behaviour compared with the notch filter used in a previous design.

The above mentioned works have some connection with Control System Design Automation (CSDA), because intelligent mechanisms are responsible for the creation, search and selection of controllers. CSDA is not an established field yet but it is emerging, be as complete environments covering requirements interpretation, modelling, design and analysis (MAEKAWA; PANG, 1998), be as unifying control schemes (LI et al., 2004), or simply as the majority of the recent approaches, proposing alternative and attractive ways to tackle specific problems on control system design (COELLO; VELDHUIZEN, 2007); the latter one was the motivation to combine a CI mechanism with the observer-based realization (OBR) computation of an H_∞ controller (RAMOS; ALAZARD, 2009b), resulting not only in the design of the controller itself but also supporting the search of the closed-loop combinatoric set aiming on the best estimation regarding noise and error characteristics. Finally, in this work, one considers the interpolation and sampling effects on the quality of the OBR estimations from non-linear digital simulations as well, and verifies the robust stability for a time-varying behaviour in the plant model by using a new metric.

1.3 Thesis outline

This thesis has three main subjects, discussed in the chapters 2-4. Chapter 2 introduces CSDA and other key concepts and elements as Computational Intelligence, Genetic Algorithms and so on; the purpose is to provide a minimum background to the readers not familiar to such area. A CI-based mechanism is presented and explained, and the CSDA is illustrated with a satellite model. Chapter 3 defines the observer-based realization of a controller and briefly introduces the associated theory, commenting on special features such as the choice of the closed-loop combinatoric regarding the estimation quality. Again, one presents an example of OBR

computing for a launch vehicle controller, providing results demonstrating that fault signals can be detected as if the controller behaves as an observer. Chapter 4 then proposes a new robustness metric (specially suited for the case studies presented later) according to the time-varying nature of a given plant model. Chapter 5 brings two case studies, both based on the VLS launch vehicle model, fully illustrating gain-scheduled CSDA for a linear-quadratic controller where the controller gains are to be smoothed, and an H_∞ controller where its OBR must also be computed and, at the same time, again taking into account the smoothness of both the time-varying closed-loop eigenvalues and respective OBR vectors produced from the combinatoric chosen. Finally, the last chapter presents the main findings, contributions and the perspectives for future research, including hardware-in-the-loop simulations with the system produced by the full application of the CSDA over the three control planes of manoeuvring.

1.4 Publications

The following publications directly associated with this thesis were produced:

- 11 papers presented in congresses or conferences: 6^{th} International ESA Conference on Guidance, Navigation and Control Systems (BRITO et al., 2006) (co-author), 17^{th} IFAC Symposium on Automatic Control in Aerospace (RAMOS; LEITE FILHO, 2007c), 2^{nd} European Conference for Aerospace Sciences (RAMOS; LEITE FILHO, 2007b), 19^{th} International Congress of Mechanical Engineering (RAMOS; LEITE FILHO, 2007a), IEEE World Congress on Computational Intelligence (RAMOS; ARAUJO, 2008), 9^{th} International Conference on Motion and Vibration Control (RAMOS; SOUZA, 2008), 59^{th} International Astronautical Congress (RAMOS et al., 2008), 4^{th} International Conference on Recent Advances in Space Technologies (RAMOS; ALAZARD, 2009a), AIAA Guidance, Navigation, and Control Conference (RAMOS; ALAZARD, 2009b), $10^{\text{ème}}$ Congrès des Doctorants ED-SYS (École Doctorale Systèmes) (RAMOS, 2009), and 11^{th} Pan-American Congress of Applied Mechanics (RAMOS; ALAZARD, 2010).
- Articles in periodicals: Journal of Aerospace Engineering, Sciences and Applications (RAMOS; SOUZA, 2011) and AIAA Journal of Guidance, Control and Dynamics (to be submitted).

2 Control system design automation

Concepts such as design automation and computational intelligence are probably out of the scope for control engineers. Therefore, in this chapter one briefly presents essential topics and elements required for building CI-based mechanisms. At first, design automation is justified and associated work is presented. Then, some key elements employed for building CSDA mechanisms - namely, genetic algorithms and fuzzy systems - are defined and explained. Finally, a realistic example is provided for enhanced comprehension.

2.1 Introduction

2.1.1 Why CSDA?, overview and survey

Aerospace engineering is viewed as one of the most complex and demanding areas of system design and analysis, where functionality is required not only for nominal conditions but also for time-varying, uncertain, perturbed, noisy and even faulty ones, for multiple operating points. An automated environment to carry all those D&A tasks is a consequent thought; control system design automation (CSDA, not to be confused with CACSD) area becomes to emerge as a response for this need.

Some recent efforts have been done to develop CSDA environments. (LI et al., 2004) attempted to set a unified scene for LTI schemes, by formulating various design schemes under index-based optimal design, hence transforming the present CACSD (computer-aided control system design) into CAutoCSD (computer-automated control system design). (MAEKAWA; PANG, 1998) presented a very comprehensive control system design environment for mechanics called CSDA (Control System Design Automation), composed of a requirement interpretation block, a modelling block, an analysis/design block, a data base/knowledge base block, and a verification block. However, many other works combining design and CI were produced till now, see for example (COELLO; VELDHUIZEN, 2007) regarding engineering, scientific and industrial applications.

The building blocks of CSDA come from the computational intelligence (CI) field, which will be described later, combined with a multi-objective optimization problem composed of decision variables, constraints, evaluation criteria and objective functions, where Pareto optimal sets (trade-offs between objectives) are formed from where potential solutions can be found. An example of the Pareto representation is

provided by the Fig. 2.1, related with the conflicting characteristics "rise time" and "overshoot" for a second-order underdamped system response to a unit step input. The set of solutions comprises the Pareto-optimal set and the remaining sub-optimal solutions, where a further improvement of objectives is always possible.

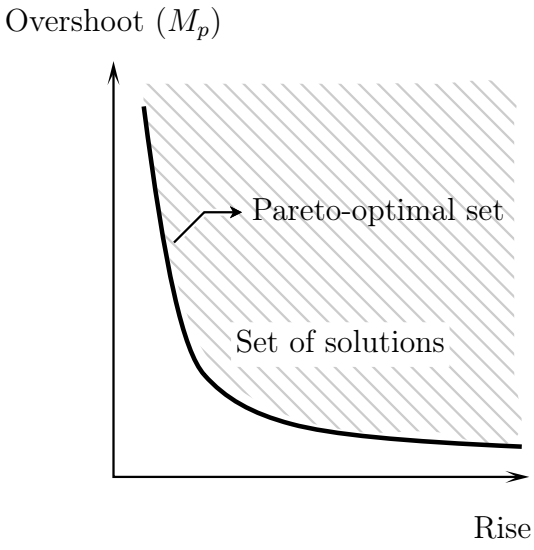

$$G(s) = \frac{\omega_n^2}{s^2 + 2\zeta\omega_n + \omega_n^2},\ 0 < \zeta < 1$$

$$t_r = \frac{1}{\omega_n\sqrt{1-\zeta^2}}\ tan^{-1}\left(\frac{\sqrt{1-\zeta^2}}{-\zeta}\right)$$

$$M_p = e^{-\pi\left(\frac{\zeta}{\sqrt{1-\zeta^2}}\right)}$$

Figure 2.1 - Example of a Pareto-optimal set.

2.1.2 Computational intelligence

Artificial Intelligence (AI) and Computational Intelligence (CI) are competing fields associated with respectively symbolic and sub-symbolic (*e.g.*, numeric) representations aimed for building intelligent systems. AI relies on a top-down strategy, that is, each system or ability is viewed as a black-box where its content is not primarily important; by the other side, CI is built from small components (as the GA chromosomes) without having a priori conception of the final system. There is low agreement on the definitions of AI and CI, but a major consensus about an overlapping nature between them; see (KONAR, 2005), (RUDAS; FODOR, 2008) and (CRAENEN; EIBEN, 2002) for terminology and discussions about it.

CI area is composed of many sub-areas (see the Fig. 2.2) such as Granular Computing (Fuzzy Systems (FS) included), Neuro-computing (Neural networks (NN) included) and Evolutionary Computation (EC, genetic algorithms (GA) included) to name the most known, along with hybrid versions of them, as well. CI presented a boost during the 90's, driven by an increasing interest of engineers, economists, and many

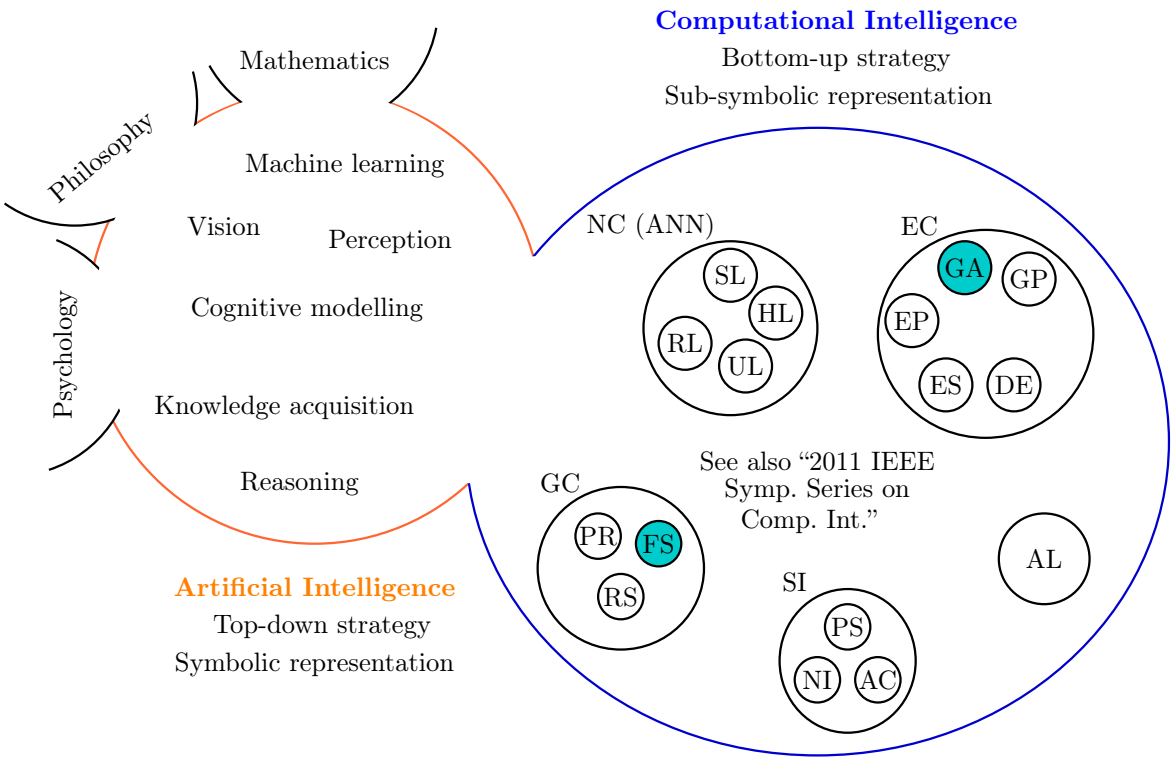

Evolutionary Computing (EC) = {Genetic Algorithms (GA), Genetic Programming (GP), Evol. Programming (EP), Evol. Strategies (ES), Differential Evolution (DE)}
Neuro-computing (NC) = Artificial Neural Networks (ANN) with {Superv. Learning (SL), Unsupervised Learning (UL), Hybrid Learning (HL) and Reinforcement Learning (RL)}
Granular Comp. (GC) = {Fuzzy Systems (FS), Probab. Reasoning (PR), Rough Sets (RS)}
Swarm Intelligence (SI) = {Particle Swarm (PS), Nature Inspired (NI), Ant Colony (AC)}
Artificial Life (AL)

Figure 2.2 - Block diagram of the computational intelligence field.
Source: adapted from (KONAR, 2005).

other professionals to apply these promising tools in their specific fields, aiming for problem solving automation and fast evaluation of possible solutions. In the Control Engineering area, CI provided the combination of classical and modern techniques (FLEMING; PURSHOUSE, 2002) for system identification and modelling, (sometimes unnecessary (TAN; LI, 2001)), design, and optimization. Off-line methods currently are the majority of the applications, reflecting their computational cost and time. However, it is only a matter of time for on-line cases to gain space, since hardware is in continuous progress (SPECTOR, 2004). Concerning the aerospace area, CI elements were applied to the control system design of launch vehicles (including the Space Shuttle), aircrafts, missiles and satellites; see references in (RAMOS; ARAUJO, 2008).

Specifically, genetic algorithms (GAs) are the preferred EC branch for control engineers ((WANG et al., 2003), (FONSECA, 1995)). The tasks required to implement EC are: (*i*) the choice (or creation) of a convenient approach which best fits the proposed problem; (*ii*) the development of an (multi-) objective or cost function; (*iii*) the tuning of the evolutionary operators in order to achieve fast convergence speed while avoiding local optima. The objective function used for fitness evaluation is generally built with specification charts (and possibly other variables of interest (RAMOS; LEITE FILHO, 2007c)), whose indexes are translated by mathematical formulae or other type of mapping into a single scalar cost, which is assigned to each individual composing the generations. The tuning of the evolutionary operators (*e.g.*, mutation rate) is a tricky and complex task, and can itself be subject to evolution, yet most applications are manually adjusted. In the former case, the operators are enclosed into each individual *genotype*, together with the parameters used to guide the search mechanism.

Two important elements are used in this work, namely GA and FS; thus, one presents them with more details.

2.1.3 Genetic algorithms

One of the most recognized pioneers in genetic algorithms is Bremermann (FOGEL; ANDERSON, 2000), who originally proposed them as general models of adaptive processes (although posteriorly applied popularly as optimization and search tools). GAs are basically the representation of the Darwinian theory of the life evolution on virtual populations or sets of individuals. Each individual is composed of chromosomes, which refer to independent entities forming the full system. By your turn,

each chromosome is characterized by a set of genes. For example, the three-axis control system of a launch vehicle could be devised as three chromosomes (each one representing the controller of the respective plane of manoeuvring), with 3 genes per chromosome (proportional, derivative and integral gains of each controller).

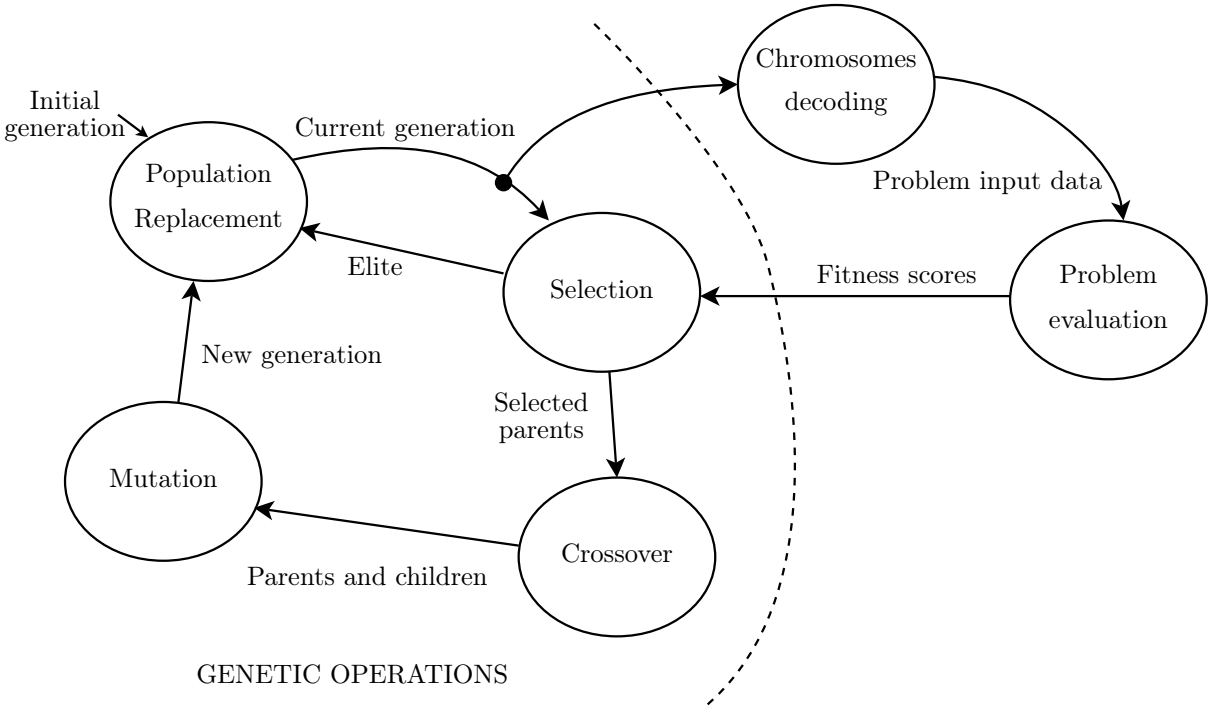

Figure 2.3 - Basic operation cycle of a genetic algorithm.

The GA operation cycle (Fig. 2.3) is composed basically of the following actions:

- **Selection.** A new set of individuals is formed with clones multiplicity proportional to the respective ratings of the individuals of the previous generation: the higher the rating of a given individual, the more the number of its clones. A popular method is known as roulette wheel, where individuals are selected based on their ratings. NOTE: the fitness evaluation is not included in the genetic operations.

- **Crossover.** Part of the new set is combined randomly in pairs by exchanging random segments of genes.

- **Mutation.** Part of the new set has some of their individuals mutated,

that is, random genes of random individuals are changed with a given probability.

- **Elite insertion.** The individual of the original set with the best rating is preserved in the new set; that is necessary due to the mutation and crossover actions.

- **Population replacement.** The original generation is replaced by the new one, or a new one is created when there is no previous one.

2.1.4 Fuzzy systems

In 1965, Lofti Zadeh defined fuzzy sets as "a class of objects with a continuum of grades of membership" (ZADEH, 1965), opposing the usual mathematical sense (*e.g.*, the sets "real numbers greater than one" and "real numbers MUCH greater than one"). A fuzzy system (Fig. 2.4) is a non-linear mapping of an input vector into a scalar output (MENDEL, 1995)[1]:

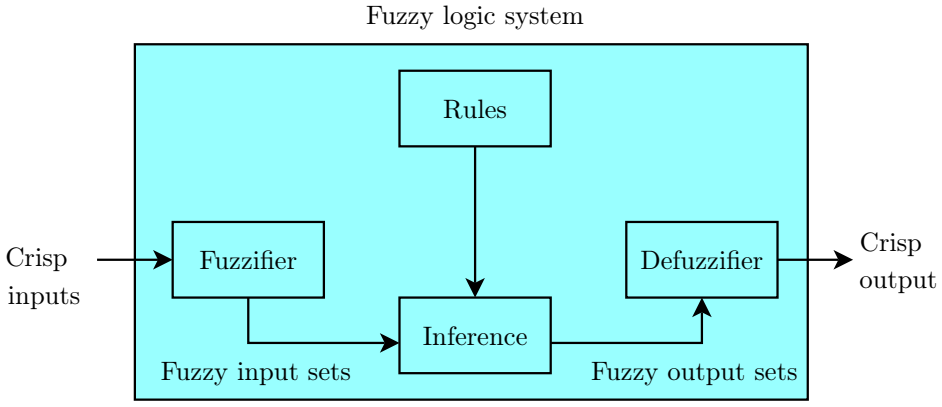

Figure 2.4 - Diagram of a Fuzzy System.
Source: (MENDEL, 1995).

- The mapping is composed of rules - expert knowledge or extracted from numerical data; it is defined as logic expressions such as IF-THEN statements (*e.g.*, "IF *settling time* IS *too slow* OR *gain margin* IS *small*, THEN *design* IS *poor*" and "IF *settling time* IS NOT *too slow* AND *gain margin*

[1]Refer to (MATHWORKS, 2010) for a lengthy and more didactic explanation of these concepts.

IS NOT *small*, THEN *design* IS *good*"; see also the graphical interpretation in the Fig. 2.5) .

- Linguistic variables deal with linguistic values which are words in a natural or artificial language rather than numbers. The combination of a linguistic variable and a linguistic value (such as "*settling time* IS *too slow*" in the previous example) is called antecedent or premise when is part of the IF section; if it is part of the THEN section, it is called consequent or conclusion.

- Fuzzifiers / defuzzifiers - interfaces (composed of membership functions) that relate the degree of the membership between input and output crisp data and the fuzzy sets.

- A crisp set is a subset of another set, whose elements uniquely belong or not to that set, while for a fuzzy set, its elements have a degree of membership with the set to which it belongs. For example, "object" may or may not belong to "fruits", while "liquid" may have infinite degrees of membership with "temperature" (cold, hot, etc.).

- Inference mechanism - maps fuzzy sets into fuzzy sets, handling the way the rules are combined; the most known are (GALICHET et al., 2008) Mamdani-type (more intuitive; large acceptance in the scientific community; well suited to human input) and Sugeno-type (computationally efficient; guaranteed continuity of the output surface; well suited to mathematical analysis; works well with linear, optimization and adaptive techniques).

2.1.5 Understanding a CI-based mechanism

An example of a CI-based mechanism used for CSDA is shown in the Fig. 2.6. The single chromosome is the controller, the genes are controller gains or weights of the linear-quadratic or H_∞ techniques. First, a GA generates, combines and mutates the individuals, reinserting the best fitted one (the elite) of the last generation in the current one. The indexes (stability, performance, etc.) are extracted from each individual and evaluated with a cost function; according to the results, the GA chooses a new elite and the process continues until a stop criterion is met.

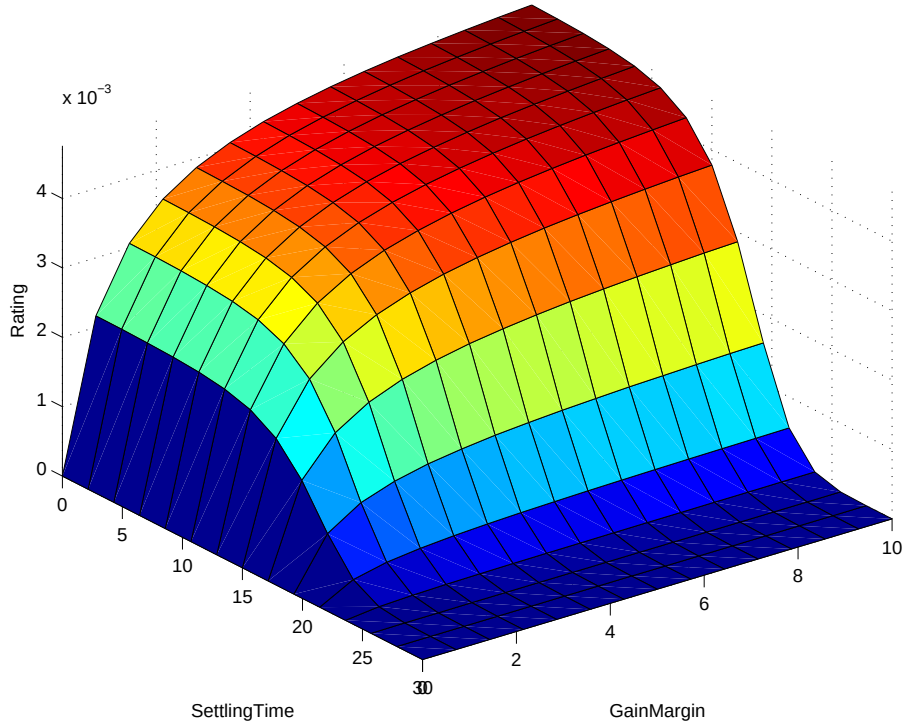

Figure 2.5 - Example of a FS surface.

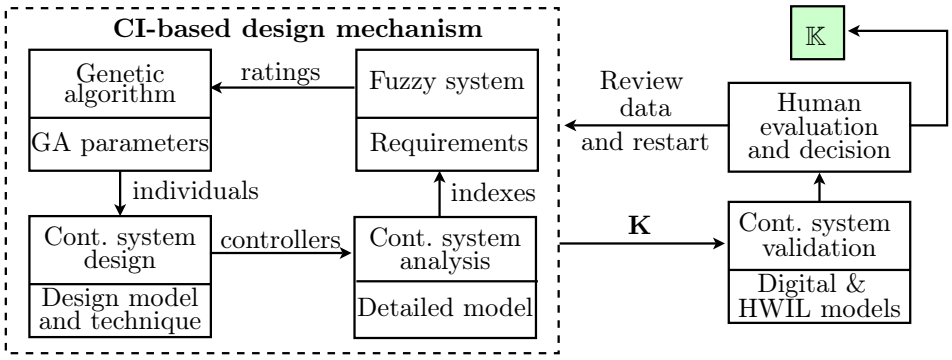

Figure 2.6 - Example of a CI-based mechanism used for CSDA.

2.2 Example: CSDA of a satellite controller

This example (RAMOS; SOUZA, 2008) employs CSDA in order to obtain controllers according to four techniques, for a satellite with appendages model.

2.2.1 Satellite model and control system

The linear model of a satellite with appendages and reaction wheel (SOUZA, 2006) is given by the Eq. 2.1, where (see the Fig. 2.7): L is the appendage length; m is the appendage mass; J_0 is the inertia moment of the rigid body related to its mass centre; J_R is the inertia moment of the reaction wheel related to its mass centre; J_P is the inertia moment of the appendage related to its mass centre; $J = J_0 + J_R + J_P$; K is the elastic constant of the appendages; K_d is the mechanic dissipation constant of the appendages; $\{X, Y, Z\}$ and $\{X_S, Y_S, Z_S\}$ are the main and satellite reference axes; $\delta(t)$ is the elastic displacement of the appendages related to the Y_S axis; $\psi(t)$ is the satellite yaw angle; $\alpha(t)$ is the angular displacement of the reaction wheel related to the Y_S axis; $\tau(t)$ is the torque applied to the reaction wheel.

NOTE: the disturbance input in the original set of equations was not considered.

$$
\begin{aligned}
\ddot{\psi}(t) &= \beta^{-1}\left[2L\,K_d\,\dot{\delta}(t) + 2L\,K\delta(t) - \tau(t)\right] \text{ where } \beta = (J - J_R - 2L^2 m) \\
\ddot{\delta}(t) &= \beta^{-1}\left[L\tau(t) - K_d\,m^{-1}\,(J - J_R)\,\dot{\delta}(t) - Km^{-1}\,(J - J_R)\,\delta(t)\right] \\
\ddot{\alpha}(t) &= \beta^{-1}\left[(J - 2L^2 m)\,J_R^{-1}\tau(t) - 2LK_d\,\dot{\delta}(t) - 2LK\delta(t)\right]
\end{aligned}
\tag{2.1}
$$

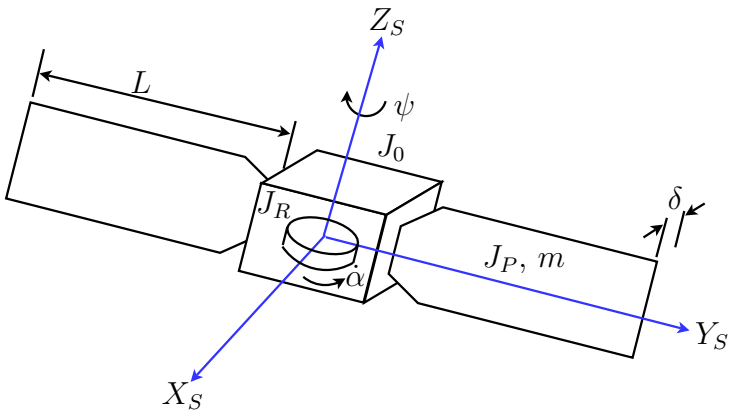

Figure 2.7 - Satellite description.

The Eq. 2.1 is a linearly dependent set; thus, only the first two sub-equations ($\ddot{\psi}$ and $\ddot{\delta}$) are considered in the design - the last one is useful to obtain the α output. The state space description of the satellite model is presented in the Eq. 2.2.

$$\dot{\mathbf{x}}(t) = \mathbf{A}\mathbf{x}(t) + \mathbf{B}\tau(t),\ \mathbf{y}(t) = \mathbf{C}\mathbf{x}(t) + \mathbf{D}\tau(t),\ \mathbf{x}(t) = \left[\psi(t)\ \delta(t)\ \dot{\psi}(t)\ \dot{\delta}(t)\right]^T$$
$$\mathbf{A} = \begin{bmatrix} 0 & 0 & 1 & 0 \\ 0 & 0 & 0 & 1 \\ 0 & 2LK\beta^{-1} & 0 & 2LK_d\beta^{-1} \\ 0 & -K\eta & 0 & -K_d\eta \end{bmatrix}, \mathbf{B} = \begin{bmatrix} 0 \\ 0 \\ -\beta^{-1} \\ L\beta^{-1} \end{bmatrix}, \quad \mathbf{C}, \mathbf{D}, \quad \eta = (J - J_R)\, m^{-1}\beta^{-1} \tag{2.2}$$

The control system of the satellite is depicted in the Fig. 2.8, where the sizes and contents of the measurement vector $\boldsymbol{\gamma}$ (reflecting the matrices $\mathbf{C}$ and $\mathbf{D}$ of the Eq. 2.2), reference input $\boldsymbol{\gamma}_{ref}$ and controller input $\mathbf{u}_c$ depend on the chosen controller.

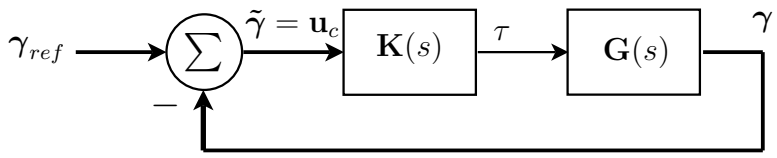

Figure 2.8 - Attitude control system of the satellite.

$\mathbf{K}(s)$ will be assigned each of the four controllers given below:

- A proportional-derivative (PD) control law (SOUZA, 2006) is defined by the Eq. 2.3, where $\mathbf{x}_c(t) = x_c(t)$, $\mathbf{A}_c = 0$, $\mathbf{B}_c = \mathbf{0}$, $\mathbf{C}_c = 1$ and $\mathbf{D}_c = \mathbf{K} = [K_P\ K_D]$.

$$\begin{aligned} &\boldsymbol{\gamma}(t) = \left[\psi(t)\ \ \dot{\psi}(t)\right]^T,\ \ \boldsymbol{\gamma}_{ref}(t) = [\psi_{ref}(t)\ \ 0]^T, \\ &\dot{\mathbf{x}}_c(t) = \mathbf{A}_c\,\mathbf{x}_c(t) + \mathbf{B}_c\,\mathbf{u}_c(t),\ \ \tau(t) = \mathbf{C}_c\,\mathbf{x}_c(t) + \mathbf{D}_c\mathbf{u}_c(t) \end{aligned} \tag{2.3}$$

- A double-input-single-output (DISO) controller with first order transfer functions $a/(s+b)$ and $c/(s+b)$ between inputs and output is defined by the Eq. 2.4.

$$\begin{aligned} \boldsymbol{\gamma}(t) &= \left[\psi(t)\ \ \dot{\psi}(t)\right]^T,\ \ \boldsymbol{\gamma}_{ref}(t) = [\psi_{ref}(t)\ \ 0]^T, \\ \dot{x}_c(t) &= -b\, x_c(t) + [a\ \ c]\, \mathbf{u}_c(t),\ \ \tau(t) = x_c(t) + \mathbf{0}\ \mathbf{u}_c(t) \end{aligned} \tag{2.4}$$

- A full-state LQ controller is given by the Eq. 2.5, where $\mathbf{K} = \mathbf{K}_{1\text{x}4}$.

  NOTES:

  a) The controller $\mathbf{K}$ is calculated upon the state-space matrices $\mathbf{A}$ and $\mathbf{B}$ of the Eq. 2.2 and the weighting values $\mathbf{Q}$ and R.

  b) For the sake of simplicity, the existence of an observer to reconstruct the full state is not considered here.

$$\begin{aligned} \boldsymbol{\gamma}(t) &= \left[\psi(t)\ \ \delta(t)\ \ \dot{\psi}(t)\ \ \dot{\delta}(t)\right]^T,\ \ \boldsymbol{\gamma}_{ref}(t) = [\psi_{ref}(t)\ \ \mathbf{0}]^T, \\ \dot{x}_c(t) &= 0\ x_c(t) + \mathbf{0}\ \mathbf{u}_c(t),\ \tau(t) = x_c(t) + \mathbf{K}\mathbf{u}_c(t) \end{aligned} \tag{2.5}$$

- An H_2 controller is given by the Eq. 2.3 and matrices $\mathbf{A}_c$, $\mathbf{B}_c$, $\mathbf{C}_c$ and $\mathbf{D}_c$. The controller is built from the general standard model of the satellite control system (Fig. 2.9); the augmented plant $\mathbf{P}$ contains the external disturbances w_τ and $\mathbf{w}_y$ at the plant input and outputs respectively, and the weighting values $\mathbf{k_y} = \text{diag}(k_\psi,\ k_r)$ (amplitude of the output vector $\mathbf{y}$), k_τ (amplitude of the actuation signal τ) and k_w (amount of the disturbance at the plant input). $\mathbf{G}$ is the transfer function matrix of the satellite model, which can be obtained from the Eq. 2.2, where matrices $\mathbf{C}$ and $\mathbf{D}$ are chosen so that $\mathbf{y} = \left[\psi\ \dot{\psi}\right]^T$; also note that $r \triangleq \dot{\psi}$.

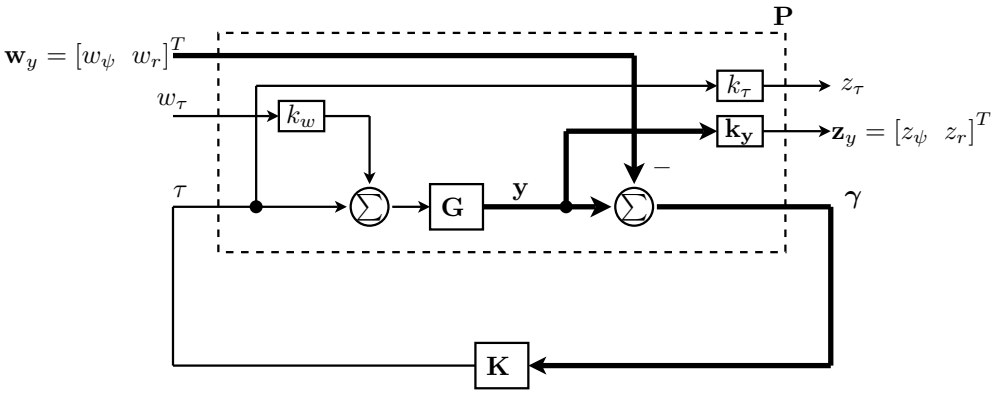

Figure 2.9 - Satellite general standard model.

The mathematical description of the general standard model is given by the Eq. 2.6.

$$\begin{bmatrix} \dot{x}_1(t) \\ \dot{x}_2(t) \\ \dot{x}_3(t) \\ \dot{x}_4(t) \\ z_\psi(t) \\ z_r(t) \\ z_\tau(t) \\ \gamma_\psi(t) \\ \gamma_r(t) \end{bmatrix} = \left[\begin{array}{cccc|ccc|c} 0 & 1 & 0 & 0 & 0 & 0 & 0 & 0 \\ 0 & 0 & 1 & 0 & 0 & 0 & 0 & 0 \\ 0 & 0 & 0 & 1 & 0 & 0 & 0 & 0 \\ 0 & 0 & k_1 & k_2 & 0 & 0 & k_w & 1 \\ \hline -k_\psi K & -k_\psi K_d & -k_\psi m & 0 & 0 & 0 & 0 & 0 \\ 0 & -k_r K & -k_r K_d & -k_r m & 0 & 0 & 0 & 0 \\ 0 & 0 & 0 & 0 & 0 & 0 & 0 & k_\tau \\ \hline K & K_d & m & 0 & 1 & 0 & 0 & 0 \\ 0 & K & K_d & m & 0 & 1 & 0 & 0 \end{array}\right] \begin{bmatrix} x_1(t) \\ x_2(t) \\ x_3(t) \\ x_4(t) \\ w_\psi(t) \\ w_r(t) \\ w_\tau(t) \\ \tau(t) \end{bmatrix}$$

$$k_1 = -K_d m^{-1}\beta^{-1}(J - J_R), \;\; k_2 = -K m^{-1}\beta^{-1}(J - J_R) \tag{2.6}$$

2.2.2 The CI-based design mechanism

The CI mechanism was already seen in the Fig. 2.6. Performance indexes (rise and settling time, overshoot, and amplitude of the actuation signal $\tau(t)$) are obtained from the unit step response of the control systems formed with each individual (Fig. 2.8), and evaluated with a cost function implemented with a fuzzy system where those specifications are stored.

2.2.2.1 GA characteristics

The main characteristics of the GA are: 10 binary bits per gene of each individual[2]; 10 individuals per generation; mutation rate of 10%. Each run has a minimum of 5 and a maximum of 20 generations. In order to assure high population diversity, for each new run and depending on the rating, part of the population is recreated randomly. Each run is finished by a stop criterion (supplied by the ratings of the generations) and is followed by a new run; this batch of runs also terminates if the collective rating meets that same criterion. The stop criterion is based on the standard deviation of the last n ratings ($< 0.1\%$). The roulette wheel is used for reproduction based on the logarithmic function $log_{10}(rating - min.rating + 1)$. Only

[2]The PD controller is composed of two gains $K_1 = a_1/a_2$ and $K_2 = b_1/b_2$ or 4 genes, so 40 binary bits are required for each individual.

the first bit (most significative) of each gene is not used for mutation operations. The fitness function is a fuzzy system, as will be seen next.

2.2.2.2 FS characteristics

The FS is Mamdani-type, where the linguistic input variables are the performance indexes (rise and settling time, overshoot, and amplitude of the actuation signal $\tau(t)$) and the linguistic output variable is *Rating*. The linguistic values are expressed as: (i) a Gaussian function f_G, given by the pair $\langle \sigma, c \rangle$ according to the Eq. 2.7a; (ii) a z-polynomial function f_Z, given by the pair $\langle a, b \rangle$ according to the Eq. 2.7c; (iii) a triangular function f_T, given by the triple $\langle a, b, c \rangle$ according to the Eq. 2.7b. The FS premises (Fig. 2.10) and respective universes of discourse are defined as follows:

- The linguistic variable t_r is associated with the rise time of the control system step response, where its universe of discourse is [0, 600] [s]. The linguistic value $\{small\}$ is defined as $f_G(x; 200, 0)$.

- The linguistic variable t_s is associated with the settling time of the control system step response, where its universe of discourse is [0, 600] [s]. The linguistic value $\{large\}$ is defined as $f_G(x; 200, 600)$.

- The linguistic variable M_p is associated with the overshoot size of the control system step response, where its universe of discourse is [0, 100] [%]. The linguistic value $\{satisfactory\}$ is defined as $f_Z(x; 20, 50)$.

- The linguistic variable u_{max} is associated with the maximum actuation signal of the control system step response, where its universe of discourse is [0, 2] [Nm]. The linguistic value $\{small\}$ is defined as $f_G(x; 0.5, 0)$.

- The linguistic variable *Rating* is associated with the total score, where its universe of discourse is [-100, 100]. The linguistic values $\{$*bad, regular, good*$\}$ are defined respectively as $f_T(x; -100, -100, 20)$, $f_T(x; -40, 0, 40)$ and $f_T(x; -20, 100, 100)$.

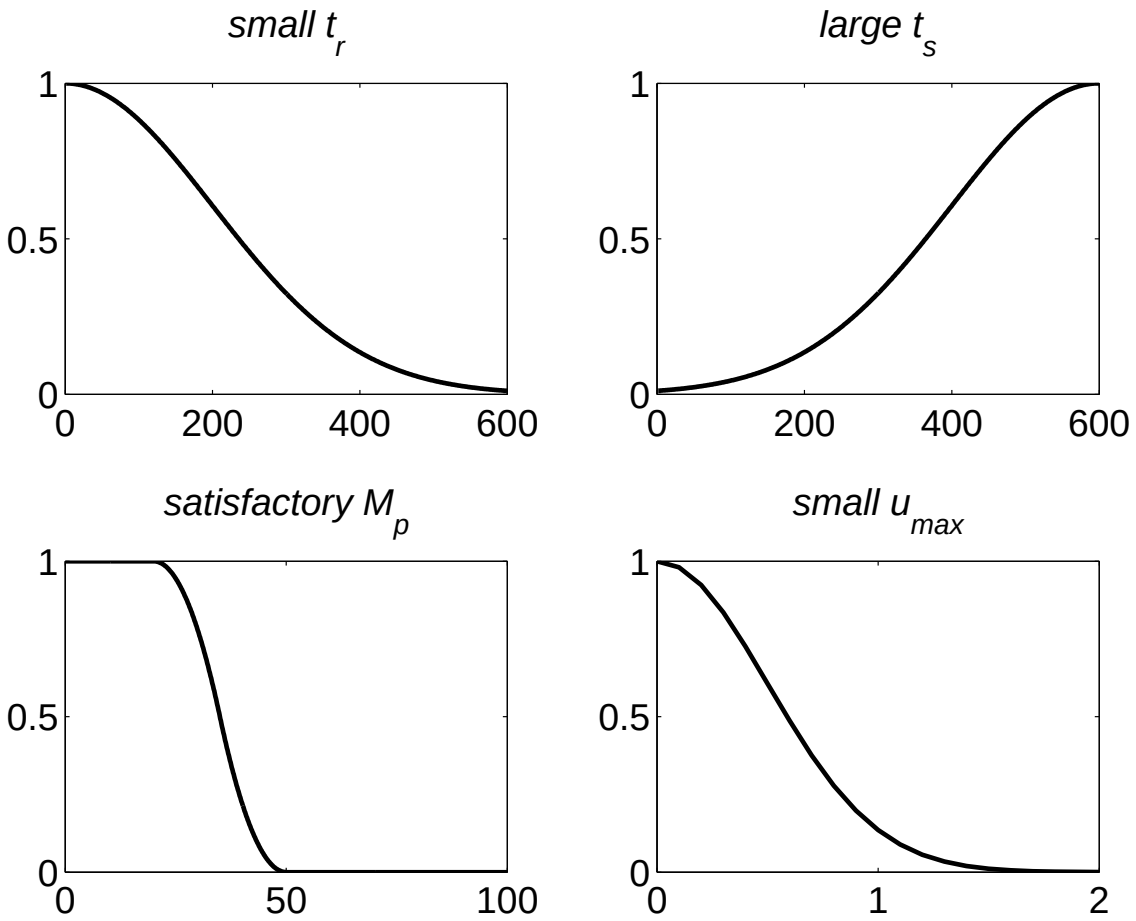

Figure 2.10 - Fuzzy system premises of the satellite CSDA example.

$$f_G(x;\sigma,c) = e^{\left[\frac{-(x-c)^2}{2\ \sigma^2}\right]} \tag{2.7a}$$

$$f_T(x;a,b,c) = max\left(min\left(\frac{x-a}{b-a}, \frac{c-x}{c-b}\right), 0\right) \tag{2.7b}$$

$$f_Z(x;a,b) = \begin{cases} 1, x \leq a \\ 1 - 2\left[(x-a)/(b-a)\right]^2, a < x \leq (a+b)/2 \\ 2\left[(b-x)/(b-a)\right]^2, (a+b)/2 < x \leq b \\ 0, x > b \end{cases} \tag{2.7c}$$

The fuzzy system rules are given by the Eq. 2.8.

R_1: IF (t_s IS *large*) OR (u_{max} IS NOT *small*) THEN (*Rating* IS *bad*)
R_2: IF (t_r IS NOT *small*) AND (t_s IS NOT *large*)AND (M_p IS NOT *satisfactory*)
AND (u_{max} IS *small*) THEN (*Rating* IS *regular*)
R_3: IF (t_r IS *small*) AND (t_s IS NOT *large*)AND (M_p IS *satisfactory*)
AND (u_{max} IS *small*) THEN (*Rating* IS *good*)
(2.8)

Regarding the controller candidates, when the resulting control system is unstable the candidate is immediately assigned the worst rating, thus avoiding time wasting to calculate the step response and fuzzy system cost.

2.2.3 Design comparison

For comparison purposes, the hypothetical case FireSat (LARSON; WERTZ, 1992) is useful to devise the requirements associated with a satellite with appendages, where its mission is Earth-looking, except one optional manoeuvre per month to a chosen target, when it must rotate up to 30^o in less than 10 minutes. The actuation element is a reaction wheel; its choice is dependent of the maximum amplitude on the actuation signal required by the designed controller. Commercial models are available with torque output ranges of 0.01-1.0 [Nm], influencing weight (2-20 [kg]) and power consumption (10-110 [W]); therefore, the smaller the required actuation torque, the most attractive the controller.

Table 2.1 - Comparison between the four automated designs.

Tech.	**Genes** (a/b)	**Design Time** [s]	**Controller**	$\mathbf{t_r}$ [s]	$\mathbf{t_s}$ [s]	$\mathbf{M_p}$ [%]	**Ac** [Nm] (max.)	**Rating**
PD	$\{K_1, K_2\}$	195	$-\,[0.4050\ 27.4048]$	103.8	156.4	2	0.210	47.1
DISO	$\{a, b, c\}$	143	$-\left[\begin{array}{c}\frac{0.1675}{s+0.4185}\\ \frac{11.3856}{s+0.4185}\end{array}\right]^T$	108.5	143.9	2	0.177	48.6
LQ	$\{Q_{11}, \cdots, Q_{44}, R\}$	123	$-\left[\begin{array}{c}0.5477\\ 0.0500\\ 30.8491\\ 2.2371\end{array}\right]^T$	86.0	211.3	3	0.289	38.2
H_2	$\{k_\psi, k_r, k_w, k_\tau\}$ $\{m\}$ = multiplier	181	$\left[\begin{array}{cc}\frac{\sum_{i=0}^{3} a_i s^i}{\sum_{i=0}^{4} b_i s^i} & \frac{\sum_{i=0}^{3} c_i s^i}{\sum_{i=0}^{4} b_i s^i}\end{array}\right]$	126.5	191.5	2	0.238	41.2

Table 2.1 presents the results of the design automation based on the four controllers. The numerical data of the model (SOUZA, 2006) is: $J_0 = 720[\text{kg m}^2], J_P = 40[\text{kg m}^2], K = 320[\text{kg rad}^2/s^2], K_d = 0.48[\text{kg rad}^2/s], L = \sqrt{2}[\text{m}]$, e $m = 20[\text{kg}]$. NOTES: *(i)* the number of genes is different for each technique, where PD has the smallest one (4), LQ and H_2 the biggest ones (10); *(ii)* PD and DISO do not require gain calculation (differently from LQ and H_2 techniques), but only the transformation from binary digits to decimal values; *(iii)* PD and LQ techniques produce scalar controllers, whilst DISO produces first order ones and H_2 fourth order ones (both strictly proper); *(iv)* the design was run five times for each technique, and those results with the best ratings were chosen; *(v)* description of the computing environment: MATLAB v. 7.1 (Release 14), running on AMD SEMPRON 2800+ processor (core speed 1596 [MHz]) and 1 [GByte] of RAM memory (bus speed of 199.6 [MHz]).

It can be seen that all results comply with FireSat specifications, that is, the settling time t_s is always under 10 minutes (even adding it to the design time, allowing online use), and the maximum actuation signal is well below 1 [Nm]; furthermore, the overshoot is negligible.

Despite the PD technique being the most promissory due to the fewer genes (resulting in a smaller search set), it ranked second, yet the first place (DISO) shares the same condition; one questions if the inferior ratings associated with the other two techniques are explained by the higher number of genes or by the techniques themselves. It is important to note that the design specifications do not include stability margins nor robustness, but LQ and H_2 techniques embed somewhat these factors, contrary to the other two; therefore, even admitting that the DISO technique presented the best results regarding the most important requirements, namely t_s and u_{max}, and possessing a simple structure (first-order transfer functions), it must be stressed that additional analysis is required to gather confidence on such technique.

The LQ technique presented the best design and rise times, but scored last to the other indexes. However, most batch runs presented low variation on design times (63 - 123 [s]) and ratings (36.2 - 38.2), and a good LQ controller could be chosen even in the first run, taking around 6 seconds (already considering code initialization); by the other side, this work does not intend to suggest any solution to the proposed problem but rather illustrate the CI embedding in the design.

2.3 Conclusion

CSD is not a pure creative process, it may (and generally does) rely on repetitive and exploratory tasks as well. As machines are best suited to such tasks, CSDA is appealing to human designers. In order to achieve automation, CI-based mechanisms must be built; in this chapter, an *ad-hoc* one was presented, composed of a genetic algorithm to explore the search space, and a fuzzy system to store the design specifications. A simple CSD problem based on a satellite model was stated in order to demonstrate the possibilities of such mechanism. However, in order to justify CSDA even more, one intends to increase the design complexity far beyond, by considering the observer-based realization (OBR) of a given controller, which is introduced in the next chapter.

3 The observer-based realization of a controller

In this section, one presents the Observer-Based Realization (OBR) technique and how CI can be used for closed-loop combinatorics search. It will be shown that most controllers may be represented by three distinct dynamics, namely estimation, feedback and Youla ones. In such sense, the real physical variables of the plant (on which the controller OBR relies) can be estimated, together with other variables of interest such as disturbances, faults, etc. . However, the closed-loop combinatoric must be appropriately chosen, so that the quality of estimation (*i.e.* noise and error characteristics of the estimated variable) is the best one. Such special combinatoric is not always easy to find according to the number of c.l.-poles and estimations; thus, CSDA is again an appealing resource for its search.

3.1 Introduction

For aerospace applications, control system design is not only a matter of satisfying important requirements such as stability, performance, robustness to parameter variations and external disturbances, and so on, but there are also practical issues (as on-board implementation) which draw the attention of the control engineer; it would not be surprising if complexity, flexibility, and memory storage could influence and even decide the choice between rivalling structures. In such aspect, linear quadratic or PID controllers, which rely on single sets of scalar gains, would be preferable to H_∞ controllers, the latter ones typically possessing the same order than the plant model used for design (normally a simplified version of a even more complex validation model). By the other side, one may argue if and what additional features and benefits can be uncovered when using these larger realizations. Fortunately, as wrote by (LUENBERGER, 1971), "almost any system is an observer"; it can be shown that a given controller may have an observer-based realization, as demonstrated by the deterministic separation principle (SCHUMACHER, 1980). By that principle, controller states can be made to correspond to the plant states; in other words, the controller is also an observer and provides the estimates of the plant state vector, and maybe other desired estimates as external disturbances and faults, thus supplying additional elements which could be employed for fault tolerance, for example. One briefly presents now a new technique which allows to redesign a given controller into its observer-based form, without changing the controller dynamics.

3.2 OBR theory

In this section, one presents the resumed procedure ((ALAZARD et al., 1999), (ALAZARD; APKARIAN, 1999)) to compute the observer-based realization of a given controller (that is: the state feedback gain $\mathbf{K_c}$, the state estimator gain $\mathbf{K_f}$ and the YOULA parameter $\mathbf{Q}$).

3.2.1 Observer-based structure with Youla parameter

The general block diagram of the closed-loop system involving an observer-based controller is shown in the Fig. 3.1, which corresponds to the Youla parametrization of all stabilizing controllers built under the LQG structure; from this representation, the separation principle between estimation and control is straightforward. According to (ALAZARD et al., 1999), the principle of Youla parametrization is based on the fact that the closed-loop transfer function between the input e and the inovation $\epsilon_{\mathbf{y}} = \mathbf{y} - \mathbf{C}\,\hat{\mathbf{x}}$ is null (LUENBERGER, 1971). Consequently, changes in $\mathbf{Q}(s)$ imply variations on the equivalent controller but do not affect the c.-l. t. f. .

NOTES:

a) The order n corresponds, at first, to the plant model $\mathbf{G}(s)$ of order n_P and state-space matrices $\mathbf{A_P}$, $\mathbf{B_P}$ and $\mathbf{C_P}$, but it is later extended to the on-board model $\mathbf{G_O}(s)$ of order n_O and state-space matrices $\mathbf{A_O}$, $\mathbf{B_O}$ and $\mathbf{C_O}$.

b) At first, the inputs $\mathbf{u_d}$ (representing external disturbances and actuator misalignments or faults) and $\mathbf{y_d}$ (representing sensor bias or faults) seen in the Fig. 3.1 are not considered, so that $\mathbf{B_P} = \mathbf{B_{Pu}}$ and $\mathbf{C_P} = \mathbf{C_{Py}}$.

c) One must recall the following definitions: *(i)* eigenvalues are the set of solutions λ_i to the characteristic equation $|\mathbf{A} - \lambda\mathbf{I}| = 0$ associated with a given matrix $\mathbf{A}$; *(ii)* poles are the subset of λ_i composed solely of controllable and observable eigenvalues.

Consider the Eq. 3.1, respectively the state-space realization $\{\mathbf{A_P},\ \mathbf{B_P},\ \mathbf{C_P}\}$ (or $\{\mathbf{A},\ \mathbf{B},\ \mathbf{C}\}$ in the following discussion) of the stabilizable and detectable n_P^{th} order (or n^{th} order in the following discussion) plant model $\mathbf{G}(s)$ (n_i inputs and n_m measurements), and the minimal state-space realization of the respective stabilizing n_K^{th}

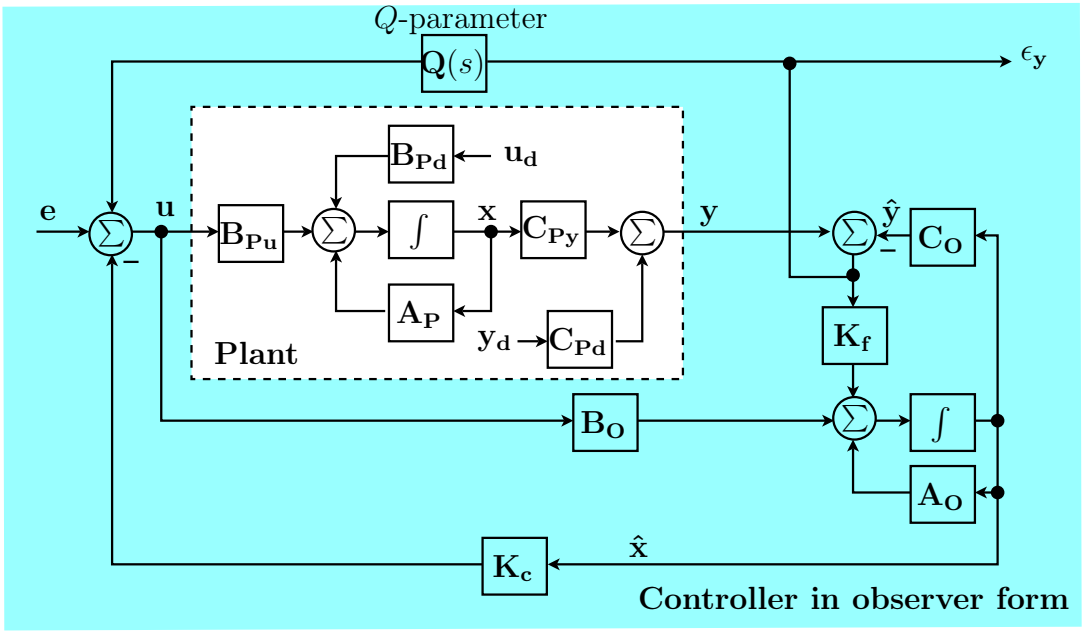

Figure 3.1 - Observer-based structure using YOULA parametrization.

order controller $\mathbf{K}(s)$:

$$\begin{bmatrix} \dot{\mathbf{x}} \\ \mathbf{y} \end{bmatrix} = \begin{bmatrix} \mathbf{A} & \mathbf{B} \\ \mathbf{C} & \mathbf{0} \end{bmatrix} \begin{bmatrix} \mathbf{x} \\ \mathbf{u} \end{bmatrix} \ (a), \quad \begin{bmatrix} \dot{\mathbf{x}}_\mathbf{K} \\ \mathbf{u} \end{bmatrix} \begin{bmatrix} \mathbf{A}_\mathbf{K} & \mathbf{B}_\mathbf{K} \\ \mathbf{C}_\mathbf{K} & \mathbf{D}_\mathbf{K} \end{bmatrix} \begin{bmatrix} \mathbf{x}_\mathbf{K} \\ \mathbf{y} \end{bmatrix} \ (b). \tag{3.1}$$

The key idea is to express the controller as a LUENBERGER observer with a state vector $\mathbf{z} = \mathbf{T}\mathbf{x}$ and thus, we will denote $\mathbf{x_K} = \widehat{\mathbf{z}} = \widehat{\mathbf{T}\mathbf{x}} = \mathbf{T}\hat{\mathbf{x}}$. It can be shown (ALAZARD et al., 1999) that $\mathbf{T}$ is the solution to the generalized non-symmetric RICCATI Eq. (3.2):

$$[-\mathbf{T}\ \mathbf{I}] \overbrace{\begin{bmatrix} \mathbf{A}+\mathbf{B}\mathbf{D}_\mathbf{K}\mathbf{C} & \mathbf{B}\mathbf{C}_\mathbf{K} \\ \mathbf{B}_\mathbf{K}\mathbf{C} & \mathbf{A}_\mathbf{K} \end{bmatrix}}^{\mathbf{A_{cl}}} \begin{bmatrix} \mathbf{I} \\ \mathbf{T} \end{bmatrix} = \mathbf{0}. \tag{3.2}$$

The characteristic matrix $\mathbf{A_{cl}}$ associated with the RICCATI Eq. (3.2) is nothing else than the closed-loop (c.-l.) dynamic matrix built on the state vector $[\mathbf{x}^T\ \mathbf{x_K}^T]^T$. Such a RICCATI equation can then be solved in $\mathbf{T} \in \mathbb{R}^{n_k \times n}$ by standard subspace decomposition techniques, that is :

- computing an invariant subspace associated with the set of n eigenvalues $\mathrm{spec}(\mathbf{\Gamma_n})$ (where $\mathrm{spec}(\mathbf{A})$ is the set of eigenvalues of the matrix $\mathbf{A}$), chosen among $n + n_K$ eigenvalues in $\mathrm{spec}(\mathbf{A_{cl}})$, that is, $\mathbf{A_{cl}} \left[\mathbf{U_1}^T\ \mathbf{U_2}^T\right]^T =$

$\left[\mathbf{U_1}^T\ \mathbf{U_2}^T\right]^T \mathbf{\Gamma_n}$, where $\mathbf{U_1} \in \mathbb{R}^{n\times n}$ and $\mathbf{U_2} \in \mathbb{R}^{n_K\times n}$. Such subspaces are easily computed using SCHUR decompositions of $\mathbf{A_{cl}}$.

- computing the solution $\mathbf{T} = \mathbf{U_2}\ \mathbf{U_1}^{-1}$.

3.2.2 Controller order

One can find three possible cases:

- *Full-order controller ($n_K = n$) :* one can compute a state feedback gain $\mathbf{K_c} = -\mathbf{C_K}\ \mathbf{T} - \mathbf{D_K}\ \mathbf{C}$, a state estimation gain $\mathbf{K_f} = \mathbf{T}^{-1}\mathbf{B_K} - \mathbf{B}\ \mathbf{D_K}$ and a static YOULA parameter $\mathbf{Q(s)} = \mathbf{D_K}$ such that the observer-based structure fitted with the YOULA parameter (Fig. 3.1) is equivalent to the initial controller form according to its input-output behaviour.

- *Augmented-order controller ($n_K > n$) :* the YOULA parameter becomes a dynamic transfer of order $n - n_K$.

- *Reduced-order controller ($n_K < n$) :* in this case, the LQG structure shown in the Fig. 3.1 is no longer valid. However, if $n_K \geq n - n_m$ (n_m stands for the number of plant measurements), one can built a reduced-order estimator with a static YOULA parameter, involving an estimate $\hat{\mathbf{x}} = \mathbf{H_1}\hat{\mathbf{z}} + \mathbf{H_2}\ \mathbf{y}$ by a linear function of the controller state $\hat{\mathbf{z}}$ and the plant output $\mathbf{y}$, with the constraint $\mathbf{H_1}\ \mathbf{T} + \mathbf{H_2}\ \mathbf{C} = \mathbf{I_n}$. Otherwise, if $n_K < n - n_m$, a model reduction is required to built a (partial) state-observer realization.

One can define a general expression $\hat{\mathbf{x}} = \mathbf{H_1}\hat{\mathbf{z}} + \mathbf{H_2}\ \mathbf{y}$ for computing the estimates for all the three cases, where $\mathbf{H_2} = \mathbf{0}$ and $\mathbf{H_1} = \mathbf{T^{-1}}$ when $n_k \geq n$.

3.2.3 Closed-loop combinatoric set

The separation principle of the observer based realization allows to state that :

- The c.-l. eigenvalues can be separated into c.-l. state-feedback eigenvalues ($\text{spec}(\mathbf{A} - \mathbf{BK_c})$), c.-l. state-estimator eigenvalues ($\text{spec}(\mathbf{A} - \mathbf{K_f C})$) and the YOULA parameter eigenvalues ($\text{spec}(\mathbf{A_Q})$).

- The c.-l. state-estimator eigenvalues and the YOULA parameter eigenvalues are uncontrollable by $\mathbf{e}$.

- The c.-l. state-feedback eigenvalues and the YOULA parameter eigenvalues are unobservable from $\varepsilon_{\mathbf{y}}$. The transfer function from $\mathbf{e}$ to $\varepsilon_{\mathbf{y}}$ always vanishes.

Note that there is a combinatoric set of solutions according to the choice of n auto-conjugate eigenvalues among $n + n_K$ c.-l. eigenvalues. The range of solutions can be reduced according to the following considerations :

- A set of auto-conjugated eigenvalues[1] must be chosen in order to find a real parametrization.
- Uncontrollable eigenvalues and unobservable eigenvalues must be selected to the state-feedback and the state-estimation dynamics respectively.
- The state-estimation dynamics (spec($\mathbf{A} - \mathbf{K_f C}$)) is usually chosen faster than the state-feedback dynamics (spec($\mathbf{A} - \mathbf{B K_c}$)).

3.2.4 Complementary topics

On-board model. The initial plant model $\mathbf{G}(s)$ can be further extended as an on-board model. The n_O^{th} order on-board model composed by the state-space matrices $\mathbf{A_O}, \mathbf{B_O}$ and $\mathbf{C_O}$ is required in the computation of the observer form and is built upon the original plant model where other variables of interest (such as disturbances and faults, represented by the variables $\mathbf{u_d}$ and $\mathbf{y_d}$ in the Fig. 3.1) may also be included as states to be estimated. Therefore, n is replaced by n_O and $\{\mathbf{A},\ \mathbf{B},\ \mathbf{C}\}$ by $\{\mathbf{A_O},\ \mathbf{B_O},\ \mathbf{C_O}\}$ in the previous discussion. For example, on considering the original plant model (Eq. 3.1(a)) and a bias term y_b associated with a single output, the correspondent on-board model could be given by the Eq. (3.3).

$$\left[\begin{array}{c} \dot{\mathbf{x}} \\ \hline \dot{y}_b \\ \hline y \end{array}\right] = \left[\begin{array}{cc|c} \mathbf{A_P} & \mathbf{0} & \mathbf{B_P} \\ \hline \mathbf{0} & \lambda_y & \mathbf{0} \\ \hline \mathbf{C_P} & 1 & \mathbf{0} \end{array}\right] \left[\begin{array}{c} \mathbf{x} \\ \hline y_b \\ \hline \mathbf{u} \end{array}\right] = \left[\begin{array}{c|c} \mathbf{A_O} & \mathbf{B_O} \\ \hline \mathbf{C_O} & \mathbf{0} \end{array}\right] \left[\begin{array}{c} \mathbf{x} \\ \hline y_b \\ \hline \mathbf{u} \end{array}\right] \tag{3.3}$$

Balanced realizations. To prevent numerical problems when solving in $\mathbf{T}$ the RICCATI Eq. 3.2 required to compute the OBR, it is recommended to balance both

[1] If $\boldsymbol{\lambda}$ is a set of auto-conjugated values, then $\boldsymbol{\lambda} = \bar{\boldsymbol{\lambda}}$.

realizations: the on-board model $\mathbf{G_O}$ and the original controller $\mathbf{K}$. If $\breve{\mathbf{x}}$ denotes the state vector of the on-board model as a balanced realization and $\mathbf{M}$ the transformation with initial meaningful state $\mathbf{x}$ (i.e. $\breve{\mathbf{x}} = \mathbf{M}\ \mathbf{x}$), then the application of the OBR theory will provide an observed-based realization $\breve{\mathbf{K}}_\mathbf{f}$ and $\breve{\mathbf{K}}_\mathbf{c}$ involving the balanced state vector $\widehat{\breve{\mathbf{x}}}$. Then, it is possible to keep the original meaningful state-space matrices and states by recalculating the state feedback and the state estimator gains such that $\mathbf{K_c} = \breve{\mathbf{K}}_\mathbf{c}\ \mathbf{M}$ and $\mathbf{K_f} = \mathbf{M^{-1}}\ \breve{\mathbf{K}}_\mathbf{f}$.

Exact controller dynamics. It is obvious from the computation of the gains $\mathbf{K_c}$, $\mathbf{K_f}$ and $\mathbf{Q}$ (when $n_K \geq n$), that the resultant controller obtained from the observer-based realization (darker area in the Fig. 3.1) may have not the same dynamics of the original controller, due to numerical inaccuracy. However, the estimations can be obtained by computing $\mathbf{T^{-1}}\ \mathbf{x_K}$ while keeping the existent controller (as it was done using $\mathbf{H_1}$ and $\mathbf{H_2}$ matrices when $n_K < n$).

Reference inputs. When dealing with reference inputs in the control system, the controller structure to be used is shown in the Eq. 3.4; such arrangement is adopted for adapting the non-linear digital simulation code used in the case study no. 2 (chapter 5) in order to replace the original linear-quadratic controller by an OBR H_∞ one.

$$\begin{cases} \dot{\hat{\mathbf{z}}} = \mathbf{A_K}\ \hat{\mathbf{z}} + \mathbf{B_K}\ \mathbf{y} + \mathbf{T}\ \mathbf{B_O}\ \mathbf{K_c}\ \mathbf{x_{ref}} \\ \mathbf{u} = \mathbf{C_K}\ \hat{\mathbf{z}} + \mathbf{D_K}\ \mathbf{y} + \mathbf{K_c}\ \mathbf{x_{ref}} \end{cases} \quad \text{with } \mathbf{K_c} = -\mathbf{C_K}\ \mathbf{T} - \mathbf{D_K}\ \mathbf{C_O}. \tag{3.4}$$

Combinatoric of combinatorics. Given the estimations comprised by the on-board model, the best combinatoric for all of them at the same time may not exist, that is, a single closed-loop eigenvalues distribution between the three dynamics (state-estimation, state-feedback and Youla) which produces the best estimations for all estimated variables according to noise and error criteria. It is advisable that a search be made in order to find the best combinatoric individually for each estimation; for example, assuming that $n_K \leq n$ and two estimations $\hat{\alpha} = \mathbf{H_{\alpha 1}}\ \hat{z} + \mathbf{H_{\alpha 2}}\ y$ and $\hat{b}_q = \mathbf{H_{q1}}\ \hat{z} + \mathbf{H_{q2}}\ y$, then we could compute independent matrices $\mathbf{H_{\alpha i}}$ and $\mathbf{H_{qi}}$ to each estimated variable respectively.

Persistent excitation. Observers are subject to certain requirements related to system identification theory such as persistent excitation, that is (in a general sense), in order to obtain good estimations, the system input signals have to be rich enough

over the range of the signal or parameter to be estimated. For aerospace systems, one can consider as sources of excitation the time-varying nature of the model, the bending and torsional modes, the external disturbances (*e.g.* wind gust), attitude references, controller interpolation, sampling, quantization and sensor noise. In the two case studies presented in this work, all these sources are present, and one primarily assumes (due to time restrictions) that the excitation is persistent; available mathematical expressions (TAO, 2003) used to determine if a given excitation is persistent will be considered for future research.

3.3 CI-based combinatoric search and selection

One wants to show in this work the beneficial synergy of CI and control system design. Now, it is possible to justify even more such synergy by considering the search of the combinatorics associated with the OBR technique: the $n + n_K$ closed-loop eigenvalues must be divided among three dynamics, so that each combination is evaluated according to noise and error criteria. For example, k real closed-loop poles (that is, all eigenvalues but the uncontrollable and observable ones) yield $2^k - d$ combinations (assuming $n = n_K$, that is, static Youla parameter - no poles assigned to it), where d is the number of discarded combinations (when the number of c.l.-poles allocated to the state-feedback, state-feedback or Youla dynamics are inappropriate). Depending on the effective number of combinations, a CI-based method would be advisable for that search.

3.4 Example: OBR of a launch vehicle controller

This example (RAMOS; ALAZARD, 2009b) illustrates, for a launch vehicle control system, the construction of an on-board model embedding the estimation of the angle-of-attack, and the choice of the best closed-loop combinatoric based on noise and error criteria applied to the estimations.

3.4.1 Design technique and models

The H_∞ General Standard Model (GSM) shown in the Figure 3.2 (where $k_{\bullet\bullet}$ are scalar weightings) is used in the computation of the H_∞ controller to be posteriorly converted into its observer form. It is built upon the full pitch plane decoupled dynamics (G_L or equation (3.5), comprising the rigid body and the first two bending modes) of the Brazilian launch vehicle VLS, obtained from its non-linear set of equations (see Appendix A). The model G_L is associated with a vector of state variables which has physical meaning as well.

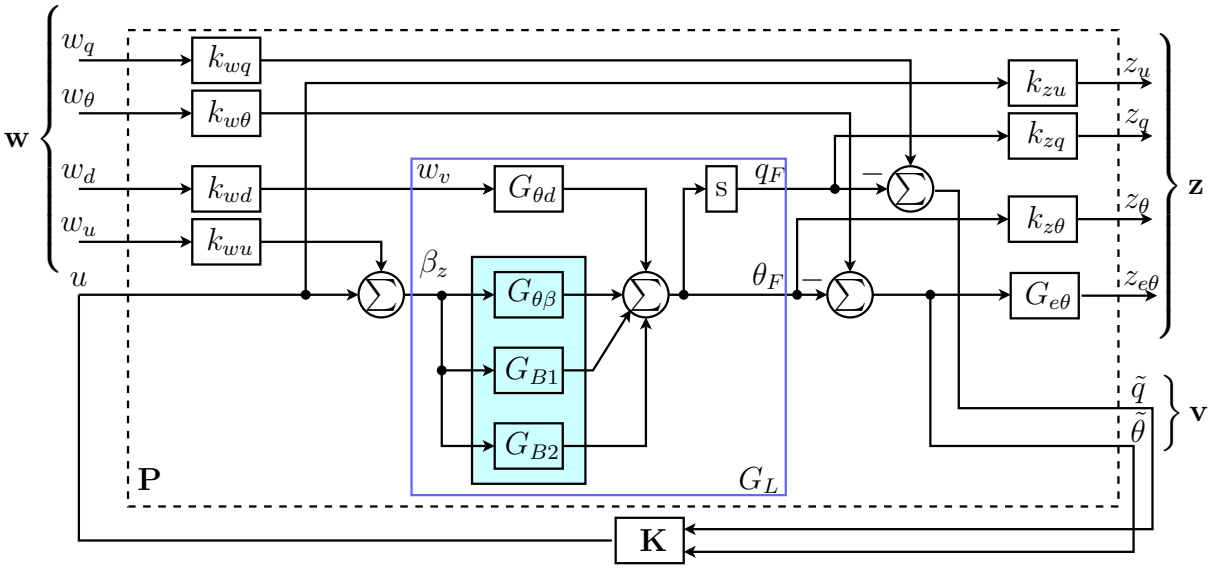

Figure 3.2 - H_∞ general standard model of the VLS launch vehicle.

$$\begin{bmatrix} \dot{w} \\ \dot{q} \\ \dot{\theta} \\ \dot{\theta}_{B11} \\ \dot{\theta}_{B12} \\ \dot{\theta}_{B21} \\ \dot{\theta}_{B22} \end{bmatrix} \approx \begin{bmatrix} -\frac{\bar{Z}_\alpha}{\bar{U}} & A_{12} & A_{13} & 0 & 0 & 0 & 0 \\ \frac{\bar{M}_\alpha}{\bar{U}} & -\bar{M}_q & 0 & 0 & 0 & 0 & 0 \\ 0 & 1 & 0 & 0 & 0 & 0 & 0 \\ 0 & 0 & 0 & 0 & 1 & 0 & 0 \\ 0 & 0 & 0 & -\bar{\omega}_{B,1}^2 & A_{55} & 0 & 0 \\ 0 & 0 & 0 & 0 & 0 & 0 & 1 \\ 0 & 0 & 0 & 0 & 0 & -\bar{\omega}_{B,2}^2 & A_{77} \end{bmatrix} \begin{bmatrix} w \\ q \\ \theta \\ \theta_{B11} \\ \theta_{B12} \\ \theta_{B21} \\ \theta_{B22} \end{bmatrix} + \begin{bmatrix} \bar{Z}_{\beta z} \\ -\bar{M}_{\beta z} \\ 0 \\ 0 \\ K_{B,1} \\ 0 \\ K_{B,2} \end{bmatrix} \beta_z + \begin{bmatrix} \frac{\bar{Z}_\alpha}{\bar{U}} \\ -\frac{\bar{M}_\alpha}{\bar{U}} \\ 0 \\ 0 \\ 0 \\ 0 \\ 0 \end{bmatrix} w_v \tag{3.5}$$

$$\begin{bmatrix} q_F \\ \theta_F \end{bmatrix} = \begin{bmatrix} 0 & 1 & 0 & 0 & 1 & 0 & 1 \\ 0 & 0 & 1 & 1 & 0 & 1 & 0 \end{bmatrix} \begin{bmatrix} w \\ q \\ \theta \\ \theta_{B11} \\ \theta_{B12} \\ \theta_{B21} \\ \theta_{B22} \end{bmatrix} + \begin{bmatrix} 0 \\ 0 \end{bmatrix} \beta_z + \begin{bmatrix} 0 \\ 0 \end{bmatrix} w_v$$

where: $A_{12} = (2\ \bar{\dot{m}}\ \bar{x}_e)/\bar{m} + \bar{U}$, $A_{13} = -\bar{g}\cos(\bar{\theta})$, $A_{55} = -2\zeta_{B,1}\ \bar{\omega}_{B,1}$ and $A_{77} = -2\zeta_{B,2}\ \bar{\omega}_{B,2}$, associated with the parameters (shown with a top bar, as $\bar{g}$) and variables identified in the Appendix A.

The following transfer functions are considered:

a) $G_{\theta\beta}$ and $G_{\theta d}$ are the transfer functions of the pitch plane decoupled model with respect to the control input β_z and disturbance input w_v, given by the equations:

$$G_{\theta\beta}(s) = \frac{-\bar{M}_{\beta z}s + \frac{1}{\bar{U}}\left(\bar{M}_\alpha \bar{Z}_{\beta z} - \bar{Z}_\alpha \bar{M}_{\beta z}\right)}{s^3 + \left(\frac{\bar{Z}_\alpha}{\bar{U}} + \bar{M}_q\right)s^2 + \left[\frac{\bar{Z}_\alpha \bar{M}_q}{\bar{U}} - \bar{M}_\alpha\left(\frac{2\bar{m}\bar{x}_e}{\bar{m}\bar{U}} + 1\right)\right]s + \frac{\bar{M}_\alpha \bar{g}\cos(\bar{\theta})}{\bar{U}}} \tag{3.6}$$

$$G_{\theta d}(s) = \frac{-\frac{\bar{M}_\alpha}{\bar{U}}s}{s^3 + \left(\frac{\bar{Z}_\alpha}{\bar{U}} + \bar{M}_q\right)s^2 + \left[\frac{\bar{Z}_\alpha \bar{M}_q}{\bar{U}} - \bar{M}_\alpha\left(\frac{2\bar{m}\bar{x}_e}{\bar{m}\bar{U}} + 1\right)\right]s + \frac{\bar{M}_\alpha \bar{g}\cos(\bar{\theta})}{\bar{U}}} \tag{3.7}$$

b) G_{B1} and G_{B2} are the transfer functions of the 1^{st} and 2^{nd} bending modes, given by the equation:

$$G_{Bi}(s) = \frac{\bar{K}_{Fi}}{s^2 + 2\ \zeta_M\ \bar{\omega}_{B,i}\ s + \bar{\omega}_{B,i}^2},\ i = 1, 2 \tag{3.8}$$

c) $G_{e\theta}$ is the transfer function representing the (approximated) integral of the error signal $k_{w\theta}\, w_\theta - \theta$:

$$G_{e\theta}(s) = \frac{1}{s + \epsilon_{e\theta}} \tag{3.9}$$

This transfer function behaves approximately as an integrator and is required to reduce the steady-state error to a step function at input w_θ (or otherwise reference input θ_{ref}). The parameter $\epsilon_{e\theta}$ is necessary to comply with the properties required by the GSP.

The GSM depicted in the Figure 3.2 is of 8^{th} order (seven from the model $G_L(s)$ plus one due to the weight $G_{e\theta}(s)$), thus producing an 8^{th} order controller. The various weights $k_{\bullet\bullet}$ on exogenous inputs (w's) and outputs (z's) allows to satisfy the main specifications required for the attitude control loop: rise time - t_r, settling time - t_s, overshoot - M_p, maximum amplitude of the control signal - u_{max}, gain margin - m_g and phase margin - m_p. The tuning of the weights to meet good trade-off between these specifications is left to a CI-based mechanism.

3.4.2 On-board model

In our application the nominal model G_L (equation 3.5) is of 7^{th} order with 2 measurements ($n_m = 2$), and the controller at the end of the CI design is of 8^{th}

order. That means one can add up to three extra states in the on-board model ($n = n_K + n_m = 8 + 2 = 10$). In this example, only the full order controller case is considered ($n_K = n$); thus, a single extra state will be added in the on-board model to take into account a first order wind model for disturbance estimation.

Let us denote the nominal 7^{th} order model G_L in the following way:

$$\left[\begin{array}{c} \dot{\mathbf{x}}_L \\ \hline \mathbf{y} \end{array}\right] = \left[\begin{array}{c|cc} \mathbf{A}_L & \mathbf{B}_{1L} & \mathbf{B}_{2L} \\ \hline \mathbf{C}_L & \mathbf{D}_{1L} & \mathbf{D}_{2L} \end{array}\right] \left[\begin{array}{c} \mathbf{x}_L \\ \hline d \\ u \end{array}\right] \tag{3.10}$$

with: $\mathbf{x}_L = [w,\ q,\ \theta,\ \theta_{B11},\ \theta_{B12},\ \theta_{B21},\ \theta_{B22}]^T$ the state vector, $\mathbf{y} = [q_F,\ \theta_F]^T$ the output, $d = w_v$ the external disturbance (wind) and $u = \beta_z$ the control signal (thruster deflection).

The on-board model $G_O(s)$, which will be used to compute the OBR of the 8^{th} order H_∞ controller, is presented in the Eq. 3.11.

$$\left[\begin{array}{c} \dot{\mathbf{x}}_L \\ \dot{d} \\ \hline \mathbf{y} \end{array}\right] = \left[\begin{array}{cc|c} \mathbf{A}_L & \mathbf{B}_{1L} & \mathbf{B}_{2L} \\ \mathbf{0} & \lambda & 0 \\ \hline \mathbf{C}_L & \mathbf{D}_{1L} & \mathbf{D}_{2L} \end{array}\right] \left[\begin{array}{c} \mathbf{x}_L \\ d \\ \hline u \end{array}\right], \quad i.e.: \left[\begin{array}{c} \dot{\mathbf{x}}_O \\ \hline \mathbf{y}_O \end{array}\right] = \left[\begin{array}{c|c} \mathbf{A}_O & \mathbf{B}_O \\ \hline \mathbf{C}_O & \mathbf{D}_O \end{array}\right] \left[\begin{array}{c} \mathbf{x}_O \\ \hline u \end{array}\right] \tag{3.11}$$

3.4.3 Choice of the disturbance estimation dynamics

The realistic wind profile w_v used in the simulation is depicted in the Figure 3.4. The steady state of w_v cannot be observed, according to the transfer function $G_{\theta d}$ (Eq. 3.7, there is a zero at $s = 0$). By the other side, if one replaces the state variable w in the equation 3.5 by the expression $\bar{U}\alpha + w_v$ (where α is the angle-of-attack), then one realises that the steady state of w_v has no effect on α, θ and q (equation

3.12), only its time derivative.

$$\begin{bmatrix} \dot{\alpha} \\ \dot{q} \\ \dot{\theta} \end{bmatrix} = \begin{bmatrix} -\frac{\bar{Z}_\alpha}{\bar{U}} & \frac{A_{12}}{\bar{U}} & \frac{A_{13}}{\bar{U}} \\ \bar{M}_\alpha & -\bar{M}_q & 0 \\ 0 & 1 & 0 \end{bmatrix} \begin{bmatrix} \alpha \\ q \\ \theta \end{bmatrix} + \begin{bmatrix} \frac{\bar{Z}_{\beta z}}{\bar{U}} \\ -\bar{M}_{\beta z} \\ 0 \end{bmatrix} \beta_z + \begin{bmatrix} -\frac{1}{\bar{U}} \\ 0 \\ 0 \end{bmatrix} \dot{w}_v \tag{3.12}$$

Therefore, these variables can be observed even if the steady state of the disturbance is not observable (clearly, $\hat{w}$ alone is not reliable at this level of the attitude control loop due to the unobservable effect of the disturbance w_v, but could be observed at the level of the guidance loop taking into account other measurements). Assigning $\lambda = 0$ means to follow a constant steady state of the disturbance w_v, which is not only unobservable, as noted before, but also uncontrollable. Therefore, this choice is prohibited as the resulting on-board model would have an unobservable and uncontrollable eigenvalue and it would not possible to affect it to the state-feedback dynamics and the state-estimator dynamics at the same time; as $\lambda \neq 0$, one chooses $\lambda = -1$. Furthermore, it is worth to estimate the angle-of-attack $\hat{\alpha} = (\hat{w} - \hat{w}_v)\, \bar{U}^{-1}$ from the state variables of the on-board model[2].

3.4.4 Observer-based realization

According to the distribution of the 16 closed-loop eigenvalues between the 8 eigenvalues for the state feedback dynamics and the 8 eigenvalues for the state estimation dynamics, two options are considered:

- for option "B" (table 3.2), the 8 closed-loop eigenvalues which are closest, in the complex plane, to the 8 eigenvalues of the open-loop on-board model are allocated to the state feedback dynamics. Thus the state estimation dynamics is very fast.
- for option "A" (table 3.1), the eigenvalue at -1.1197 is allocated to the state estimation dynamics instead of the eigenvalue located at -27.9539 (now allocated to the state-feedback dynamics).

[2]Notice that $\hat{\alpha}$ is not included in the on-board model.

Table 3.1 - Closed-loop distribution, option “A”.

Eigenvalues	$\in \text{spec}(A - B\ K_c)$	$\in \text{spec}(A - K_f\ C)$
-0.0833	*	
-0.0922	*	
-1.0000	*	
-1.1197		*
-1.6765		*
-5.3022		*
-5.8861		*
-27.9539	*	
$-4.3150 \pm 80.7212i$	*	
$-5.4127 \pm 29.6802i$	*	
$-44.9965 \pm 15.3888i$		*
$-81.796e \pm 105.17i$		*

Table 3.2 - Closed-loop distribution, option “B”.

Eigenvalues	$\in \text{spec}(A - B\ K_c)$	$\in \text{spec}(A - K_f\ C)$
-0.0833	*	
-0.0922	*	
-1.0000	*	
-1.1197	*	
-1.6765		*
-5.3022		*
-5.8861		*
-27.9539		*
$-4.3150 \pm 80.7212i$	*	
$-5.4127 \pm 29.6802i$	*	
$-44.9965 \pm 15.3888i$		*
$-81.796e \pm 105.17i$		*

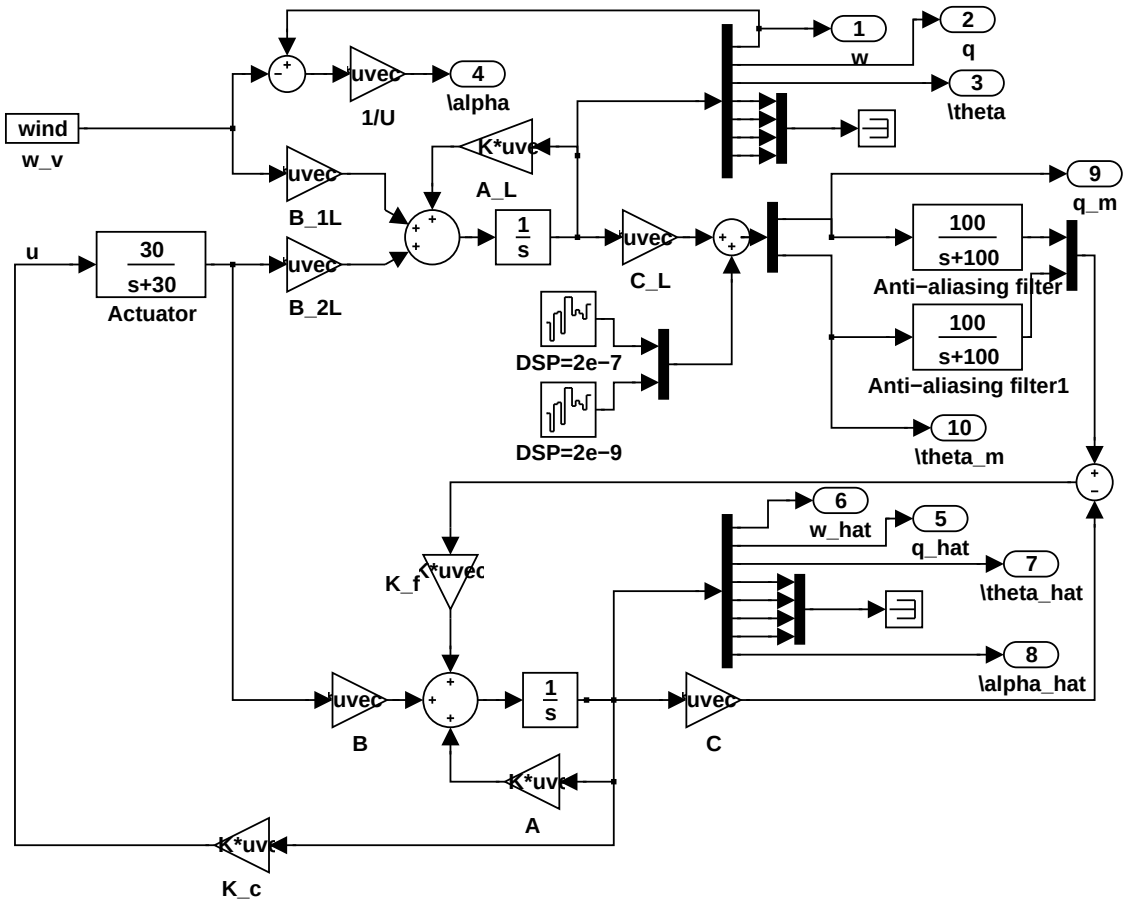

Figure 3.3 - Simulation schema comprising the attack angle estimate $\hat{\alpha}$.

3.4.5 Simulations results

The general simulation schema is depicted in the Figure 3.3. The simulation model of the launch vehicle includes actuator dynamics, anti-aliasing filter on both measurements and various disturbing signals:

- an external disturbance given by a wind profile (Figure 3.4) is always applied to the input w_v throughout the examples seen in this section,
- measurement noises can be also taken into account on measurements of pitch attitude θ and rate q, respectively.

a) *Estimation of the state variables without measurement noise.* The Figure 3.5 shows the time histories of the state variables when the only excitation

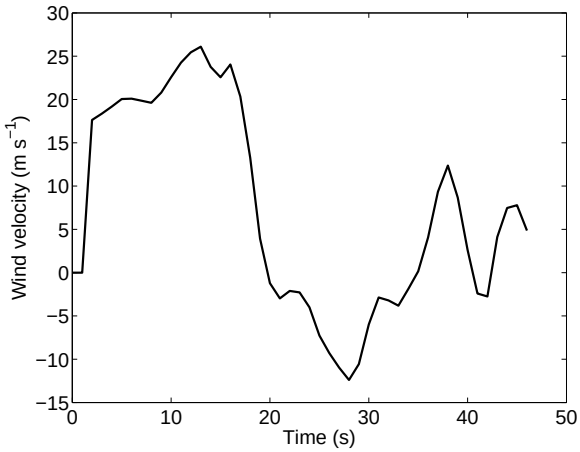

Figure 3.4 - Wind profile used as an external disturbance at the input w_v of the model.

on the closed-loop system is the external disturbance (*i.e.*, wind profile only, no noise). One can see that most graphs present superimposition of the real and the estimated signals except the linear velocity w as it was mentioned in section 3.4.3. It can be also noticed that the angle-of-attack estimation is better using option "B"; estimation errors $\alpha - \alpha_{hat}$ plotted in the Figure 3.7 confirm this result: this is the direct consequence of the state-estimation dynamics which is faster for option "B" than option "A".

b) *Estimation of the state variables with measurement noise.* When measurement noises are taken into account (Figure 3.6) the state estimation provided by option "B" is too much noisy while the angle-of-attack estimation is quite good using option "A" (see also the Figure 3.8). It can be also noticed in the Figure 3.6 that the measurement noise on θ is filtered using option "A" and so, θ_{hat} is a better estimate of θ than the direct measurement θ_m (it is not the case for q where the green and grey plots are superposed).

3.4.6 Response to parameter variation

The mission profile of the VLS assumes ideally a previously known trajectory and the respective model parameters as functions of the flight time. However, in practice some variation due to the real thrust force supplied by the solid-propellant engines related to the nominal levels is admissible. Therefore, it is worth to evaluate the control system with the nominal controller and plant models corresponding to different instants of flight around the linearisation point: the results are presented in

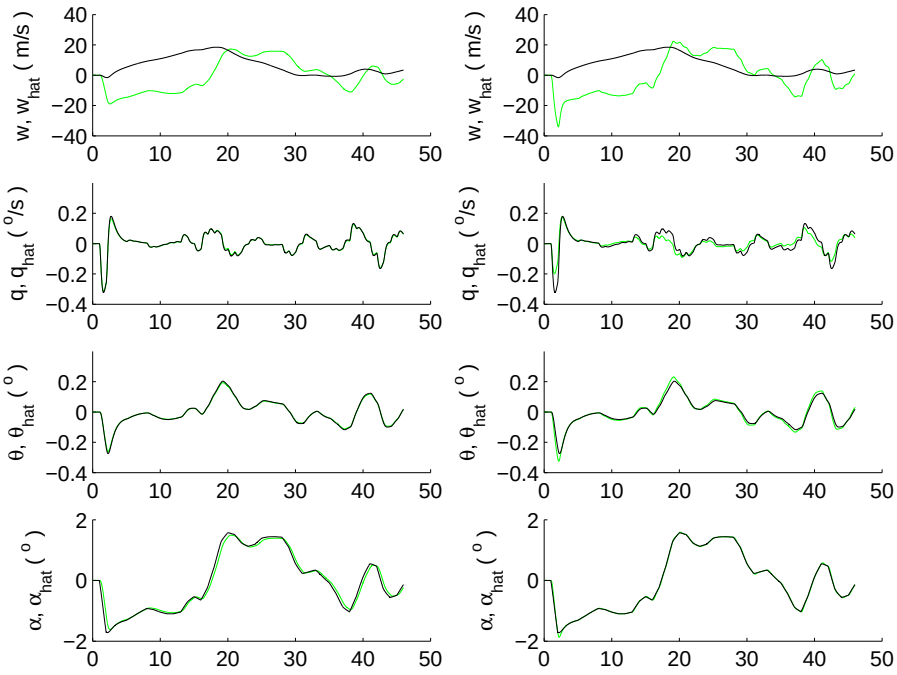

Figure 3.5 - Variables w, q, θ and α: comparison between real (black) and estimated (green) ones for options "A" (left) and "B" (right).

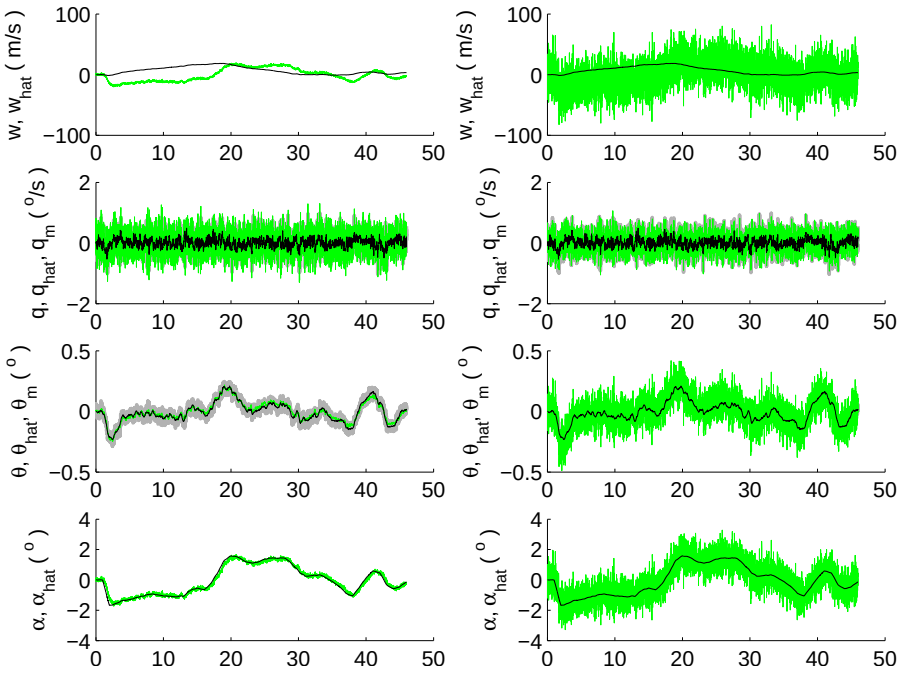

Figure 3.6 - Variables w, q, θ and α: comparison between real (black), estimated (green) and measured (gray; only for q_m and θ_m) ones, with noise added to the sensor outputs, for options "A" (left) and "B" (right).

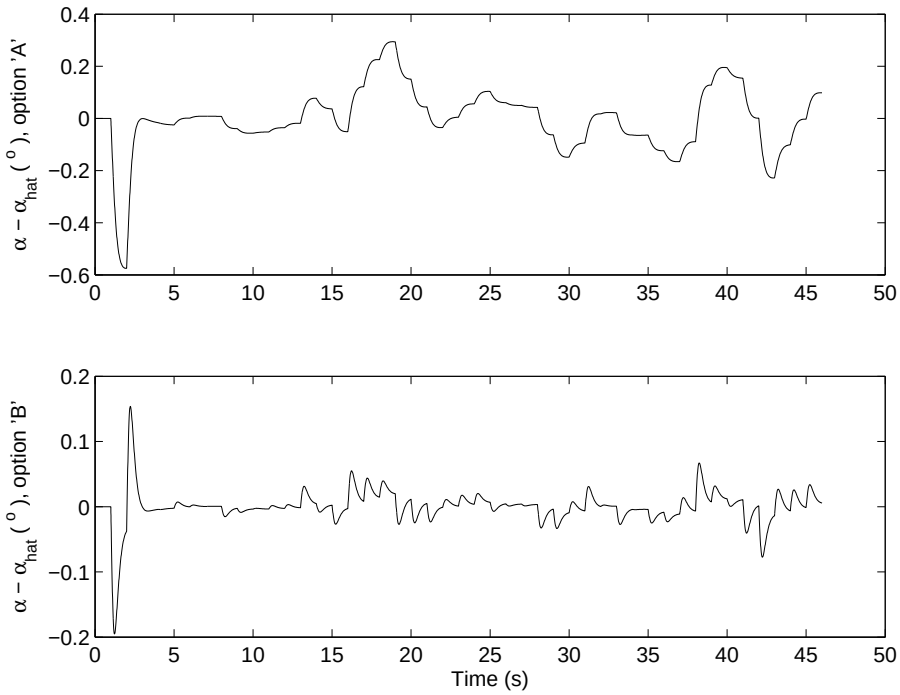

Figure 3.7 - Error between real (α) and estimated (α_{hat}) angles-of-attack (options "A" and "B").

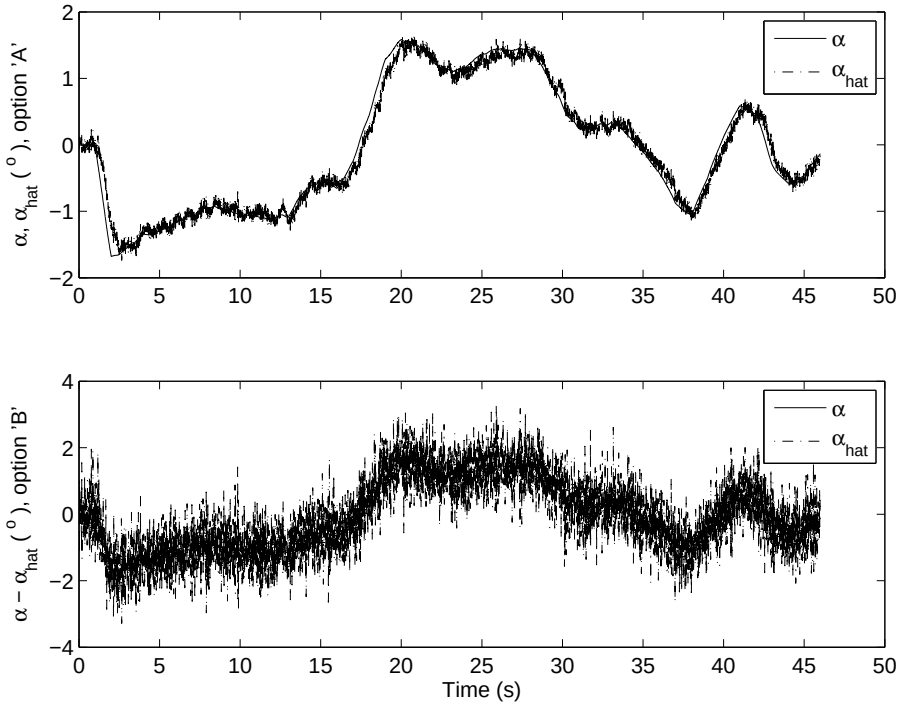

Figure 3.8 - Real (α) and estimated (α_{hat}) angles-of-attack, when measurement noises are taken into account (options "A" and "B").

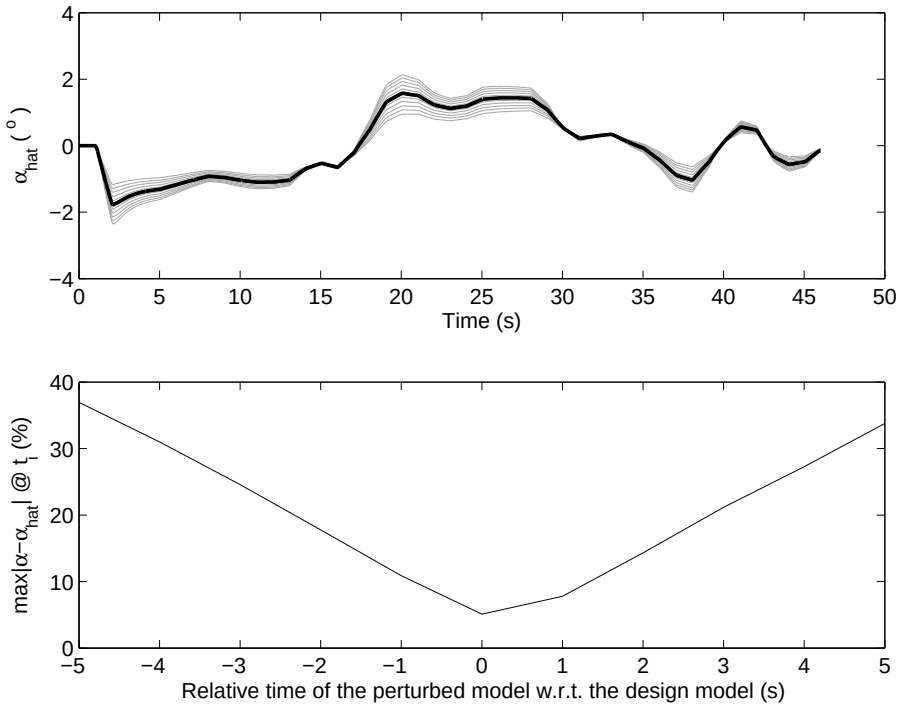

Figure 3.9 - Variation of the estimated angle-of-attack when the parameters of the plant correspond to different linearisation points of the launch vehicle trajectory. (Top sub-figure, black line: nominal condition.)

the Figure 3.9 (option"A"- without noise measurements). It can be noticed that the controller is robust to these parametric variations (it is always stable) and the monitoring of the angle-of-attack is quite representative in spite of parametric errors in the on-board model.

3.5 Conclusion

It was shown that, for order-compatible models of plant and controller, an observer-based realization of the latter one can be found, where a specific closed-loop combinatoric must be selected accordingly. Besides, the respective on-board model may include not only the plant variables but another ones such as disturbances and faults to be estimated. The presented technique was proven successful when applied to an attitude control system based on a launch vehicle model, where its attack angle was estimated. For the same case, parametric variation of the vehicle model implied proportional degradation of the same estimation but in an reasonable way; at the same time, the OBR controller is robust to these variations (it is always stable). However, sometimes it must be robust also to the time-varying nature of the plant.

While that can be achieved by designing "smooth" gain-scheduled controllers, one will propose a special metric in the next chapter that allows to μ-analyse a given closed-loop system where some of this state-space elements have an exponential-like time behaviour.

4 New robustness metric for LTV systems

This chapter presents a new metric for robustness evaluation taking into account a specific time-varying behaviour of the plant, relying on the insertion of an unstable initial condition in the original LTI model as an additional input. The purpose of such adaptation is to allow for μ-analysis, a popular technique available in the robust control area. A simple example illustrates the effectiveness of the approach.

4.1 Introduction

In this work, one intends to design robust controllers according a gain-scheduled approach. As the stability analysis is not performed in the same way for LTI and LTV systems, it is advisable to consider some form of robust stability evaluation taking into account such time-variation, which is proposed now with a new metric.

4.1.1 Brief history of robust control and general overview

We start with the following definitions:
Definition 4.1.1. *"The model of a system is a set of mathematic relationships describing the real system in a reasonable degree." (Adapted from (FRANKLIN et al., 1994)).*
Definition 4.1.2. *"A control system is robust if it is insensitive to differences between the actual system and the model of the system which was used to design the controller." (SKOGESTAD; POSTLETHWAITE, 2005).*

The Robust Control history can be divided in three periods (see the Fig. 4.1):

- Classic, starting with the studies of H. S. Black proposing feedback in the design of a precise vacuum-tube system, given significant plant uncertainties, followed by H. Nyquist (stability), H. W. Bode and I. Horowitz (differential sensitivity).
- State variable, with the contributions of K. E. Kalman (controllability, observabillity, Kalman filtering), J. B. Cruz Jr. and W. R. Perkins (system sensitivity).
- Modern Robust Control, represented by two publications (*IEEE Transactions on Automatic Control* and *IEE Proceedings*) presenting the state-of-the-art of the multivariable systems theory, concepts such as singular va-

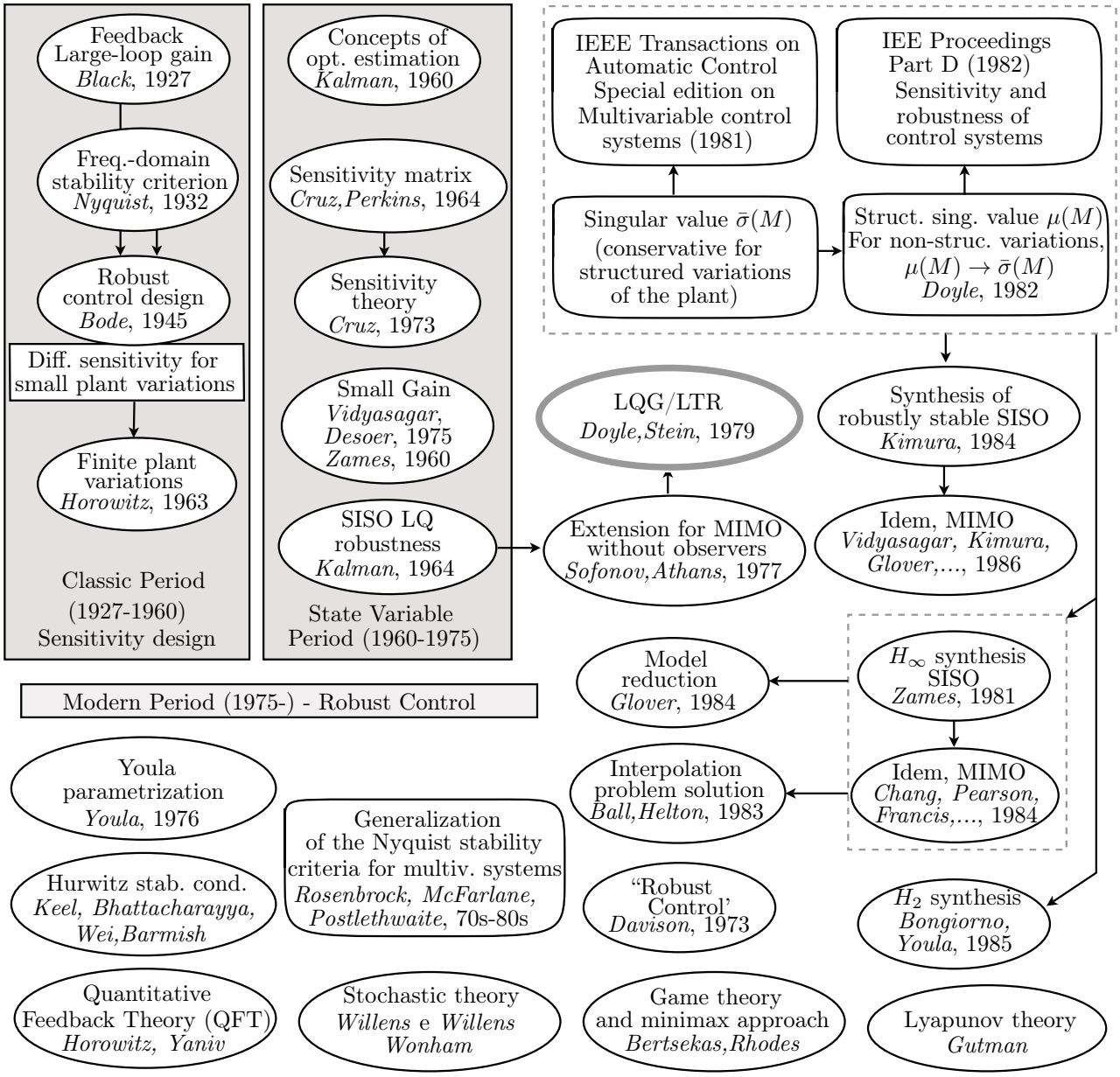

Figure 4.1 - Development of the robust control area.
Source: based on (DORATO, 1987).

lues, Nyquist stability criterion, Youla parametrization, new approachs of the H_2 and H_∞ norms, and synthesis techniques of robustly stable Single-Input-Single-Output (SISO) and Multiple-Input-Multiple-Output (MIMO) controllers (posteriorly, other techniques emerged, such as the Qualitative Feedback Theory (QFT), the Robust Stochastic Theory, the Robust Lyapunov Theory and the Linear Quadratic Gaussian - Loop Transfer Recovery (LQG/LTR)).

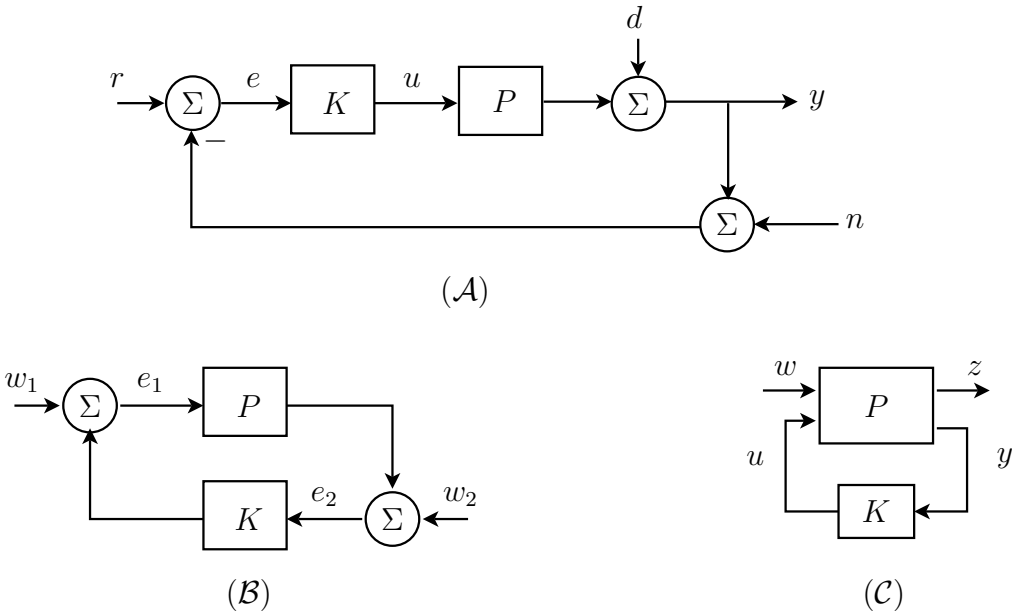

Figure 4.2 - Block diagrams used for control system analysis.

The modern robust control put more focus on MIMO systems, because they must be normally designed and analysed differently of SISO ones; that was the reason for the creation of the singular value concept and the internal stability condition (see Fig. (4.2, $\mathcal{B}$)), which depends on if the matrix $\begin{bmatrix} I & -K \\ -P & I \end{bmatrix}^{-1}$ is stable or not. An important factor in MIMO problems are the plant's uncertainties, which can affect stability and performance more than in the SISO case (see examples in (SKOGESTAD; POSTLETHWAITE, 2005)); thus, the concepts "nominal stability", "robust stability", "nominal performance" and "robust performance" were coined. Robustness analysis is achieved primarly by means of two of the twelve point-to-point functions associated

with the Fig. (4.2, $\mathcal{A}$), named sensitivity ($S = (I + PK)^{-1}$, from d to y) and complementary sensitivity ($T = (I + PK)^{-1}PK$, from r to y). Furthermore, the so-called general standard problem (Fig. 4.2, $\mathcal{C}$), associated with the linear fractional transformation (LFT) and the Youla parametrization, served as the base for the development of many techniques in the robust control area, such as the syntheses μ, H_2 and H_∞, including mixed approaches.

Until now we implicitly assumed linear time-invariant (LTI) systems. By the other side, stable frozen versions of LTV systems may exhibit unstable behaviour when subject to real conditions (ROSENBROCK, 1963), except for slow variations of their parameters; that was the question which led many authors to propose stability bounds regarding the rate of the variation, normally based on Lyapunov functions and frozen system configurations (MULLHAUPT et al., 2007). An example of this type of problem is found in the aerospace area, for the attitude control system design of launch vehicles (CLÉMENT; MAUFFREY, 2005), associated with gain scheduling, where the controller interpolation must obey a given criterion. A survey of both gain-scheduling and interpolation schemes is presented by (LEITH; LEITHEAD, 2000) and (PELLANDA; APKARIAN, 2002), where one can verify that the popular way is to interpolate the controller state-space matrices or transfer functions, assuming that the rate of variation of the elements of the controller and plant realizations is sufficiently slow. For observer-based realizations, interpolation of the gains $\mathbf{K_c}$, $\mathbf{K_f}$ and $\mathbf{Q}$ (state-feedback, state-estimation and Youla parameter) is also suggested.

4.1.2 μ-analysis

Let us consider a system composed of a controller $\mathbf{K}$, a plant $\mathbf{P}$ and its associated structured uncertainty $\mathbf{\Delta} = \text{diag}\{\Delta_i\}$, $\bar{\sigma}(\mathbf{\Delta}) \leq 1$. One can obtain an $\mathbf{M\Delta}$-structure (useful for robust stability analysis) by applying the lower linear fractional transformation on $\mathbf{P}$ and $\mathbf{K}$ to produce $\mathbf{N}$, where $\mathbf{N} = F_\ell(\mathbf{P}, \mathbf{K}) \triangleq \mathbf{P_{11}} + \mathbf{P_{12}K}(\mathbf{I} - \mathbf{P_{22}K})^{-1}\mathbf{P_{21}}$ and $\mathbf{M} = \mathbf{N_{11}}$.

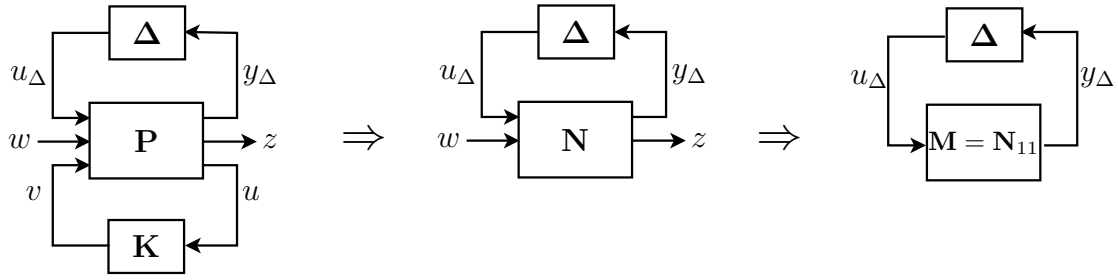

Then, a system is robustly stable if $\mu_{\mathbf{\Delta}}(\mathbf{M}) < 1$, where $\mu_{\mathbf{\Delta}}$ is the structured singular value, given by:

$$\mu_{\mathbf{\Delta}}(\mathbf{M}) \triangleq \frac{1}{min\left\{k_m | det(\mathbf{I} - k_m \mathbf{M}\mathbf{\Delta}) = 0, \mathbf{\Delta} \text{ structured}, \bar{\sigma}(\mathbf{\Delta}) \leq 1\right\}}$$

The smaller the value of $\mu_{\mathbf{\Delta}}(\mathbf{M})$ the better, that is, a larger perturbation is required to make the system loose stability.

Here, one intends to propose a simple approach based on an exponential behaviour of one or some of the coefficients of the plant model, and then computing the robust stability tolerances using μ-analysis. μ-analysis is one of the most known techniques available today for robustness evaluation, being part of the Robust Control toolbox of the MATLAB®ambient (BALAS et al., 2004); the next sections provide a deeper understanding on the proposed metric.

4.2 New metric for exponential uncertainty

In order to perform the μ-analysis, one must have a convenient description of the system to be evaluated. As the direct inclusion of time-varying coefficients into the state-space matrices is not possible, one will consider a different approach.

4.2.1 Invariant x time-varying systems

Suppose for instance the LTV system described by the Eq. 4.1:

$$\dot{\mathbf{x}}(t) = \begin{bmatrix} -1 & e^{kt} \\ 0 & -1 \end{bmatrix} \mathbf{x}(t) = \mathbf{A}(t)\ \mathbf{x}(t) \tag{4.1}$$

The associated eigenvalues are $\{-1, -1\}$; however, that system is stable only if $k \leq 1$, according to the respective state transition matrix[1]:

[1]Note that $\mathbf{A}(t)$ and $\int_{t_0}^{t} \mathbf{A}(\tau)d\tau$ commute.

$$\mathbf{x}(t) = \mathbf{\Phi}(t,\ t_0)\ \mathbf{x}(t_0),\ \ \mathbf{\Phi}(t,\ t_0)\ = \begin{cases} \begin{bmatrix} e^{-(t-t_0)} & k^{-1}\left(e^{k\ t} - e^{k\ t_0}\right) e^{-(t-t_0)} \\ 0 & e^{-(t-t_0)} \end{bmatrix}, \ k \in \Re,\ k \neq 0 \\ \text{or otherwise} \begin{bmatrix} e^{-(t-t_0)} & (t-t_0)\ e^{-(t-t_0)} \\ 0 & e^{-(t-t_0)} \end{bmatrix} \end{cases} \tag{4.2}$$

Replacing the exponential function by t^k, the system is stable for all k. Furthermore, modifying slightly the original system, one can show that bounded external signals can also change the destabilizing point. After Laplace transforming the Eq. 4.3 (where $u_h(t)$ is the Heaviside function or unit step function), the new system is found unstable for $k > 0$. Once again replacing the exponential function by t^k leads the system to be marginally stable.

$$\dot{\mathbf{x}}(t) = \begin{bmatrix} -1 & e^{kt} \\ 0 & -1 \end{bmatrix} \mathbf{x}(t) + \begin{bmatrix} 0 \\ 1 \end{bmatrix} u_h(t) \tag{4.3}$$

4.2.2 Time-varying systems and Laplace transformation

Consider now the system presented in the Eq. 4.4:

$$\begin{bmatrix} \dot{x}_1(t) \\ \dot{x}_2(t) \end{bmatrix} = \begin{bmatrix} a_{11} & a_{12}\ e^{kt} \\ a_{21} & a_{22} \end{bmatrix} \begin{bmatrix} x_1(t) \\ x_2(t) \end{bmatrix} \tag{4.4}$$

After Laplace transforming and equation solving, one finds

$$X_1(s) = (s - a_{11})^{-1} \left\{ x_1(0) + a_{12}\ (s - k - a_{22})^{-1} \left[x_2(0) + a_{21} X_1(s-k) \right] \right\} \tag{4.5}$$

The unstable condition found in the system given by the previous Eq. 4.1 is confirmed by the pole $(s - k - a_{22})$, and is associated with both the initial condition $x_2(0)$ and the shifted function $X_1(s-k)$. One will concentrate on the former in order to modify the original system by transforming the effect of the initial condition into an additional input, as shown in the Eq. 4.6, since $x_2(0)$ cannot compose directly the

model used for μ-analysis.

$$\begin{bmatrix} \dot{x}_1(t) \\ \dot{x}_2(t) \end{bmatrix} = \begin{bmatrix} a_{11} & a_{12}\ e^{kt} \\ a_{21} & a_{22} \end{bmatrix} \begin{bmatrix} x_1(t) \\ x_2(t) \end{bmatrix} + \begin{bmatrix} 0 \\ e^{-kt} \end{bmatrix} \alpha(t) \tag{4.6}$$

With $x_2(0) = 0$, one arrives at the same Eq. 4.5 with $x_2(0)$ replaced by $\alpha(s)$. One may include the term $(s - k - a_{22})^{-1}\ \alpha(s)$ in the LTI form of the Eq. 4.4 ($k = 0$) by redefining $\alpha(s) = (s - a_{22})(s - k - a_{22})^{-1}U_0(s)$, so that the original pole is replaced by the unstable one, producing the desired effect observed in the time-varying model due to the initial condition $x_2(0)$. However, note that the effect of the shifted function $X_1(s-k)$ is not present in the LTI-adapted system; thus, the results obtained with this approach are preliminary in the sense that the bound on k of the exponentially-varying function e^{kt} obtained with μ-analysis of the LTI-adapted system is not necessarily minimum.

4.2.3 Required procedure for the new metric

Suppose a given system where two of your state variables $\{x_i,\ x_j\}$ (with $\mathbf{x} = [x_1\ x_2\ \cdots x_m]$) are expressed according with the Eq. 4.7.

$$\begin{cases} \dot{x}_i = a_{i1}\ x_1 + a_{i2}\ x_2 + \cdots + a_{ij}\ x_j + \cdots + a_{im}\ x_m \\ \dot{x}_j = a_{j1}\ x_1 + a_{j2}\ x_2 + \cdots + a_{jj}\ x_j + \cdots + a_{jm}\ x_m \end{cases} \tag{4.7}$$

One knows that the element a_{ij} is time-varying, where its rate of variation can be approximated to an exponential function e^{kt}. In order to include this behaviour in the original system, one adds an extra state x_{m+1} and an extra input u_0 and modifies the original state x_j, arriving at the transformed system shown in the Eq. 4.8, which reflects the replacement of the initial condition $x_j(0)$ by the expression $\alpha(s) = (s - a_{jj})(s - k - a_{jj})^{-1}\ U_0(s)$.

$$\begin{cases} \dot{x}_j = a_{j1}\ x_1 + a_{j2}\ x_2 + \cdots + a_{jj}\ x_j + \cdots + x_{m+1} + u_0 \\ \dot{x}_{m+1} = (k + a_{jj})\ x_{m+1} + k\ u_0 \end{cases} \tag{4.8}$$

4.2.4 Example: LTV system

Applying the procedure to the LTV system given by the Eq. 4.1, and using the MATLAB® script shown below, one finds that the tolerance for the uncertain parameter k is 50% of its bound (=2), which confirms the previous results. Furthermore,

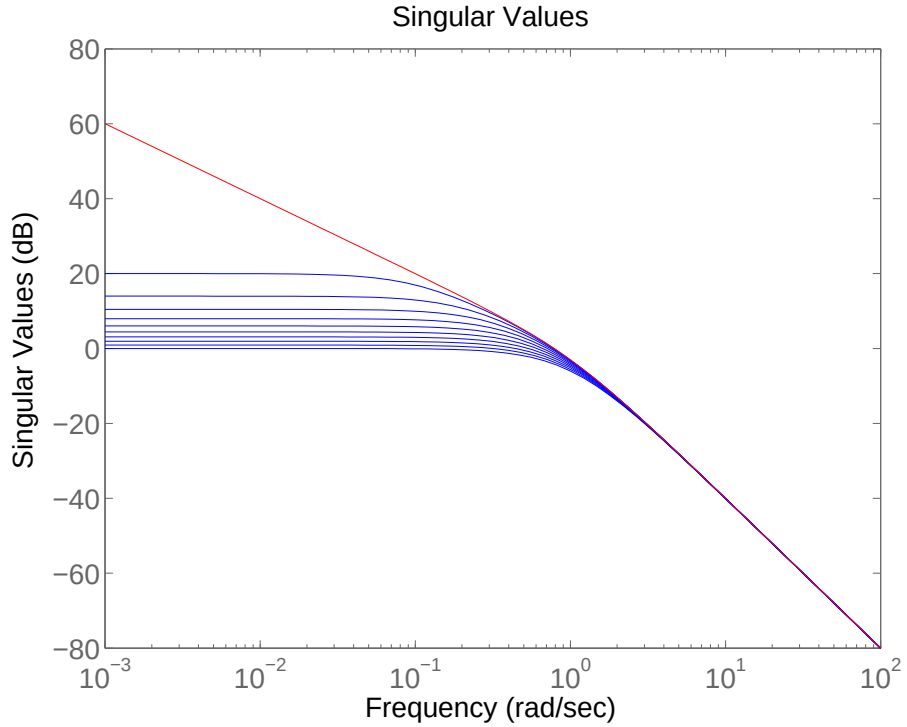

Figure 4.3 - Singular values representing a LTV system with $A(1,2) = e^{kt}$, $k = [0.0,\ 0.1,\ \cdots 1.0]$.

the Fig. 4.3 presents 11 curves of the singular values found with $k = [0.0, 0.1, ...1.0]$, where the red line corresponds to the limit case of stability.

```
k_unc = ultidyn('k',[1 1],'Bound',2);
A_unc = [-1 1 0;0 -1 1;0 0 (k_unc-1)]; B_unc=[0 ;1; k_unc];
Gp_unc = uss(A_unc,B_unc,C,0);
[stabmarg,destabunc,report,info] = robuststab(Gp_unc);
```

Uncertain System is NOT robustly stable to modeled uncertainty.

– It can tolerate up to 50% of modeled uncertainty.

– A destabilizing combination of 50% the modeled uncertainty exists, ...

– Sensitivity with respect to uncertain element ... 'k' is 100%. Increasing 'k' by 25% leads to a 25% decrease in the margin.

4.3 Conclusion

As LTV systems are harder to evaluate regarding robust stability issues (as one saw with state transition matrix computations for a simple model), one aimed here to consider the time variation of the system coefficients as dynamic uncertainties embodied partially as additional inputs, allowing to use μ-analysis. This approach will act as a complimentary validation for the smoothing action provided by the CSDA mechanism adopted in the next chapter, where two case studies based on the same CSD problem will be settled and evaluated.

5 Case studies: CSDA of the VLS launch vehicle control system

In this chapter, one defines two case studies based on the same model (VLS launch vehicle) to which CSDA is to be employed. The first one keeps the original linear-quadratic controller while replaces the frozen-poles strategy by a smoothing optimization of all gain-scheduled controllers. The second one replaces the LQ controller by an H_∞ one, and at the same time finds its OBR vectors used to estimate a bias on the roll angular-velocity output. Improvements supplied by the CSDA mechanism compared to its CSD counterpart are presented for both cases.

5.1 Introduction

The current design technique employed for VLS launch vehicle controller computation is the linear-quadratic one. One intends to *(i)* combine CI with the current design procedure (thus yielding CSDA) in order to optimize the complete trajectory and not only a single instant, and *(ii)* repeat CSDA replacing the linear-quadratic controller by an OBR H_∞ one. In both cases, one considers interpolation constraints.

5.1.1 Overview of the Brazilian space mission

The VLS-1 satellite launch vehicle was first mentioned in 1979, enclosed in the Complete Brazilian Space Mission (Portuguese acronym MECB), and its development started in 1989. Three flight models were built since then; two of them were launched (V01 in 1997 and V02 in 1999), but failures prevented full mission accomplishment. On August 22, 2003, an accident with casualties occurred with the vehicle on the launch pad, and led to an extensive revision of the project, with the cooperation of a Russian institution. A technological model (based on the VLS-1 conception) is expected to be developed and launched from a new launch pad in 2012.

The research and development activities related to the MECB are mainly conducted at the *Instituto de Aeronáutica e Espaço* (IAE) laboratories in São José dos Campos (Brazil), which works " *(...) in fundamental areas of the aerospace field including materials, propulsion, aerodynamics, guidance, control, meteorology, telemetry, sensors, on board software and acoustics.*" (see folder in the Fig. 5.1). Internationally, IAE is the provider of VSB-30 sounding rockets used by the Germany's national Texus sounding-rocket programme (SEIBERT, 2006).

Figure 5.1 - Mission, projects and activities conducted at the Instituto de Aeronáutica e Espaço (IAE).

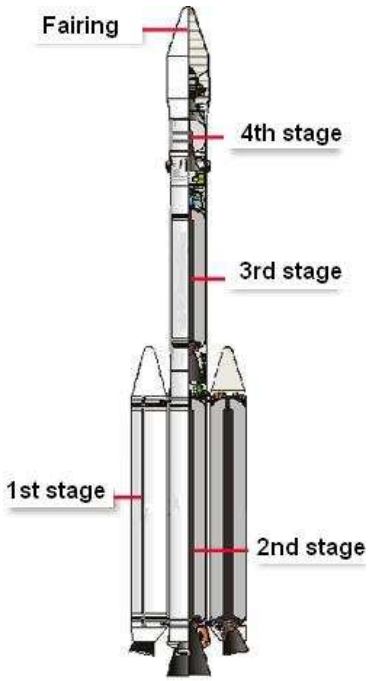

Figure 5.2 - VLS launch vehicle.

The VLS-1 vehicle (Fig. 5.2) has the following main characteristics (approximated values):

- **Physical.** Mass = 50 ton, height = 19m, 4 stages (solid propellant), 1^{st} stage composed of 4 boosters.
- **Mission.** Circular orbit insertion capability: (i) 100-380 [kg], equatorial orbit (200-1200 [km]), and (ii) 75-275 [kg], polar orbit (200-1000 [km]).

More details can be found in (LEITE FILHO; CARRIJO, 1999).

For the real flights of the models V01 and V02, the attitude controller performance was acceptable. However, further efforts are currently being carried to reduce the amplitude of the actuation signal driving the movable nozzle actuators, to minimize the effects of a non-linear phenomenon known as limit-cycle, also associated with the actuators and to lessen the influence of the bending modes on the launcher stability. The design procedure of the attitude control system by movable nozzles regarding the pitch and yaw planes associates gain scheduling with a linear quadratic optimization (Riccati equation) of the control effort, attitude angle and its derivative, and angle

error integral, producing a proportional-integral plus velocity feedback controller. The procedure is given below, according (RAMOS et al., 2003) and (RAMOS et al., 2005):

- The design is based on a particular instant t_d of the vehicle trajectory simulation when the aerodynamic load is maximal.
- The linear quadratic optimization, based on a simplified version of the control system (2^{nd} order plant plus controller), calculated at t_d, produces a closed loop transfer function, from which the poles are identified.
- The controller gains for each of the remaining instants are calculated based on the respective closed loop transfer functions, maintaining the *frozen* poles identified in the previous step.

It is important to observe that, despite the linear quadratic technique being employed in the design, only a particular instant is optimized. The remaining ones just mirror the poles of the original closed loop transfer function, but are not optimized. Therefore, the interpolation strategy is based on frozen closed-loop poles (although is popularly based on controller smoothing). For the control system analysis, the specifications to be met are mainly related to stability and performance, regarding a linear detailed system composed of a 3^{rd} order plant, 2 bending modes, actuator, notch filter (for rejection of the 1^{st} bending mode) and controller. Scenarios are defined where engine configuration, bending mode frequency tolerances and synthetic wind profiles are also considered.

Additionally, non-linear digital simulations are performed in order to verify stability under parameter variation, taking into account:

- A launch vehicle model with six degrees of freedom.
- Discrete implementations of the designed controllers.
- Movable nozzles actuators' saturation and delay effects.
- Roll controller parameters for Roll Control System (RCS) of the 2nd and 3rd stages.
- Asymmetries and misalignments of the movable nozzles.

Figure 5.3 - Elements of the VLS hardware-in-the-loop simulation complex.

① Contraves-Goerz three-axis motion controller; ② vehicle dynamics simulator PC; ③ on-board computer; ④ + ⑤ interface of the on-board inertial measurement sensors; ⑥ set of movable nozzle and pitch+yaw actuators used for the 2^{nd} and 3^{rd} stages; ⑦ 1^{st} stage actuators; ⑧ Contraves-Goerz three-axis table.

- A/Ds and D/As characteristics for navigation sensors signal acquisition by the on-board computer.

- True trajectory profiles, controllers and external disturbances (synthetic wind gust).

The final step comprises hardware-in-the-loop simulations, described by (LEITE FILHO; CARRIJO, 1997) (Fig. 5.3), divided in four phases ("A", "B", "C", "D"), where phase "A" is essentially equivalent to the non-linear digital simulation (no hardware).

5.1.2 Cases studied

The Table 5.1 presents a summary of the two case studies associated with gain-scheduling (GS) to be presented from now on. The first one (RAMOS; LEITE FILHO, 2007a) keeps the original linear-quadratic controller of the VLS launch vehicle and extends the optimization to the complete trajectory. The second one replaces the original controller by a H_∞ one and searches for its observer-based realization. In both cases, the interpolation issue is addressed by smoothing the gains of the controller, the eigenvalues of the closed-loop transfer functions or the vectors required to compute the estimations.

Table 5.1 - Case studies characterization of the VLS launch vehicle CSDA.

	Design technique	
	Linear-quadratic	H_∞
Models	*Design*: simplified versions of the Eqs. A.6. *Analysis*: Eqs. A.6 (plus actuator, bending modes, etc.) and *Analysis*: non-linear digital simulations$^{[A,B,C]}$. *Validation*: hardware-in-the-loop simulations$^{[A,B,D]}$. $^{[A]}$Actuator saturation. $^{[B]}$Sensors bias and faults. $^{[C]}$Sensors simulated noise. $^{[D]}$Sensors real noise. *For conventional and OBR purposes.	*Design*: Sec. A.5. *Analysis*: linear models*; non-linear simplified$^{[A,B,C]}$ and
Stability indexes	SISO gain and phase margins.	MIMO gain and phase margins. (BALAS et al., 2007).
Performance indexes	Rise and settling time, maximum overshoot and maximum control effort.	
Robustness indexes	Inherent to the chosen technique.	New metric for LTV systems (see Sec. 4).
Additional indexes	Smoothness of the controller gains.	Smoothness of the closed-loop eigenvalues and OBR estimation vectors, combined with the quality of the OBR estimation.
Main CSDA purposes	Controller smoothing and full trajectory optimization.	Smoothing of the closed-loop eigenvalues and OBR vectors; combinatoric search.
CSDA components	Multi-objective GA.	Multi-objective GA plus FS.
Additional features	-	Computation of the controller OBR.

5.2 VLS CSDA no. 1: GS linear-quadratic controller

The LQ controller is composed of only three gains, which are to be smoothed by the CI-based GS design. The adopted strategy is simple: obtain the elite for a time instant of the vehicle trajectory, and try to mimic its gains at the next instant. However, the second case study will require a different strategy due to the length of the smoothed vector.

5.2.1 GA characterization.

The procedure for the CSDA-LQ is shown in the Fig. 5.4. There, one assumes a system with time variant parameters; thus, a new model is defined for each *time*, upon which the controller gains are calculated for the n-element population (binary representation of each individual), modified through reproduction, cross over and mutation processes (figure 5.5). Then, the controller candidates are rated, based on certain indexes to be given next, where the best one is selected to the elitism process.

The cost function considers the well known indexes in the control engineering community: rise time (t_r), settling time (t_s), overshoot size (M_p), and gain and phase margins (m_g and m_p). Furthermore, a smoothing factor (S_f) is also included, which weights the relative magnitude of the gain vectors, according to the equation 5.1:

$$S_f = \sqrt{\frac{\sum_i [K_i(k+1) - K_i(k)]^2}{\sum_i [K_i(k)]^2}} \tag{5.1}$$

where $\mathbf{K}(k) = [K_1(k)\ K_2(k)\ ...\ K_n(k)]$, $i \leq n$ and k is the design time.

The smoothing factor is necessary because the genetic way to produce the gain vectors does not address directly the relative variation of these vectors for consecutive design times, which is an important issue as shown by (CLÉMENT; MAUFFREY, 2005); in this case, linear interpolation is permitted if the gains are sufficiently closer from each other.

The mapping from the indexes to the cost values is assigned as shown in the Fig. 5.6. These unity values are further scaled to give the final rating points. The Table 5.2 presents the parameters indicated in the Fig. 5.6 for each index.

```
01 procedure gen_alg()
02  Elite = Elite_init
03  for time = initial_time:end_time
04   NewModel = model(parameter(time))
05   Population = {}
06   for generation=1:max_number_gener
07    Data = {Population,Elite}
08    Population = evolute(Data)
09    Data = {Population,NewModel}
10    Rating = evaluate(Data)
11    Elite = Population(max(Rating))
12    if Rating_Steady_Value, break
13   end generation
14   Evolution(time) = Elite
15  end time
16  return Evolution
17 end gen_alg
```

Figure 5.4 - The pseudocode of the main procedure *gen_ alg*.

```
01 procedure evolute(Data)
02  if isempty(Population)
03   Population = randomize()
04   return Population
05  end
06  Population = reproduce(Population)
07  Population = crossover(Population)
08  Population = mutate(Population)
09  Population = elitism(Population,Elite)
10  return Population
11 end evolute
```

```
01 procedure evaluate(Data)
02  for element = 1:size(Population)
03   Individual = Population(element)
04   Gains = lqdesign(Individual,NewModel)
05   [Output Stab]= simulate(Gains,NewModel)
06   Performance = analyse(Output)
07   Data = {Performance, Stab, Gains}
08   Score(element) = cost(Data)
09  end element
10  return Score
11 end evaluate
```

Figure 5.5 - The pseudocode of the procedures *evolute* and *evaluate*.

Table 5.2 - Parameter values of the cost function indexes (N. A. = not applied).

Index	I_0	I_1	I_2	I_3	I_4
t_r	tr_inf	tr_min	tr_opt	tr_max	tr_sup
t_s	tr_min	tr_opt	ts_opt	ts_max	ts_sup
M_p	N. A.	N. A.	0	mp_max	mp_sup
m_g	mg_inf	mg_min	mg_opt	N. A.	N. A.
m_p	mp_inf	mp_min	mp_opt	mp_max	mp_sup
S_f	N. A.	N. A.	0	sf_max	sf_sup

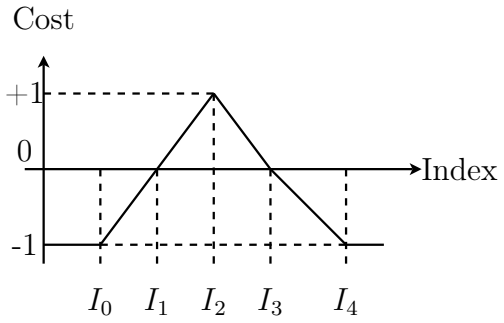

Figure 5.6 - Mapping from constraints and indexes to cost values.

5.2.2 Design comparison with respect to the smoothing issue

This section presents the following design comparisons: (i) LQ-CSDA including or not the gain vector smoothing factor in the genetic algorithm cost function and (ii) LQ-CSDA design with smoothing factor given earlier and the conventional one. The following conditions apply:

- Genetic algorithm characterization: 8 bit representation of each individual, 10 individuals per generation and maximal mutation rate of 5%.
- Performance indexes and robustness margins (see the Table 5.2): `tr_inf` = 0.5 [s], `tr_min` = 0.6 [s], `tr_opt` = 0.65 [s], `tr_max` = 0.8 [s], `tr_sup` = 1.0 [s], `ts_opt` = 5.0 [s], `ts_max` = 8.0 [s], `ts_sup` = 10.0 [s], `Mp_max` = 30 [%], `Mp_sup` = 35 [%], `mg_inf` = 6 [dB], `mg_min` = 9 [dB], `mg_opt` = 12 [dB], `mp_inf` = 15 [^{o}], `mp_min` = 30 [^{o}], `mp_opt` = 60 [^{o}], `mp_max` = 90 [^{o}] and `mp_sup` = 120 [^{o}].

The index-to-cost mapping of S_f (C_{sf}) is redefined as shown in equation 5.2, where `sf_max` = 0.5, S_{sf} is the cost-to-rating scaling factor and P_{max} is the maximum rating which can be obtained with the cost function for all indexes. The new mapping imposes higher penalties to the individuals outside a given region of smoothness, avoiding large discontinuities of the gain vector due to the variation of the aerodynamic coefficients, used for the linear-quadratic design. **Note:** the individuals are gain vectors, each one composed of proportional, integral and velocity feedback gains (K_p, K_i and K_d respectively).

$$C_{sf} = 1 - K_{sf}\left[1 - e^{\left(\frac{-S_f}{S_{f,max}}\right)}\right], K_{sf} = \frac{P_{max}}{S_{sf}} \tag{5.2}$$

The linear-quadratic optimization is now applied over the complete trajectory, from 1^{st} stage ignition to 3^{rd} stage burnout, thus complementing the work of (RAMOS; LEITE FILHO, 2007c). However, there are certain regions of the trajectory (around lift-off and engine burnout) which demand special treatment. For example, during the lift-off when the vehicle is close to the launch pad and hence a collision may occur, the integral action of the controller should be reduced or even disabled. Therefore, after the CSDA-LQ design these regions are modified in order to comply with the imposed restrictions.

Other details of the genetic optimization are:

a) Intervals optimized: from maximal dynamic pressure to (a) 2^{nd} stage burnout and (b) 1^{st} stage ignition; few seconds before 3^{rd} stage burnout to (c) 3^{rd} stage burnout and (d) 3^{rd} stage ignition.

b) The first point of each interval is found with three times more individuals, to assure a better elite, from which the other ones will follow.

Evaluation of the CSDA-LQ design. Observing the Fig. 5.7, it is evident the contribution of the S_f factor to the controller optimization. The CSDA-LQ design presents a gain vector profile even smoother than the conventional design (Fig. 5.8). Moreover, it can be noticed that lower gain values are produced; this is an attractive feature for fault tolerant systems, as concluded by (RAMOS; LEITE FILHO, 2001). (It is important to note the fast variations of the gain vector during lift-off and engine burnout; as was said before, these are regions dealt in a particular manner.)

Figures 5.9 and 5.10 present the comparisons between the performance indexes and the stability margins between the CSDA-LQ design with the smoothing factor and the conventional one. The genetic optimization improved the rise time (since a lower bound is required in order to reduce bending excitation), although the overshoot has increased, but not excessively. For the robustness issue, the gain margin is much higher during the most part of the flight, at the expense of subtracting few degrees of the phase margin.

The most notable result comes from the evaluation of the control signal; as shown in the Fig. 5.11 (obtained from a non-linear digital simulation), the linear quadratic optimization was fully achieved by the CSDA-LQ design, since the maximal control effort was considerably smaller.

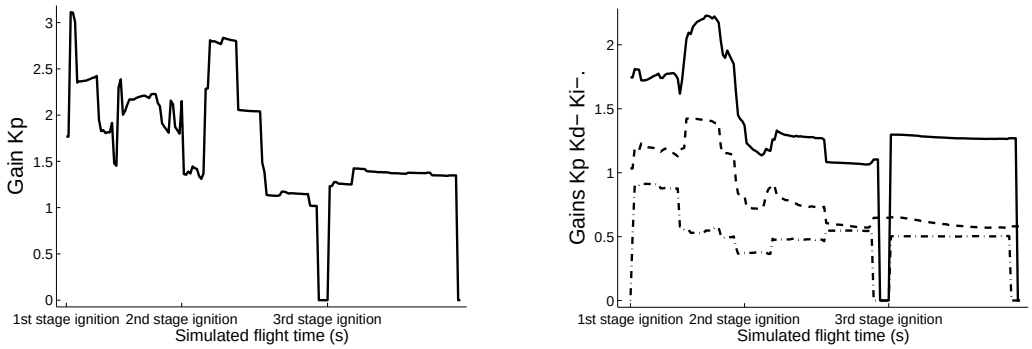

Figure 5.7 - Controller gains obtained by the CSDA-LQ design without (left, proportional gain only) and with a smoothing factor S_f in the cost function.

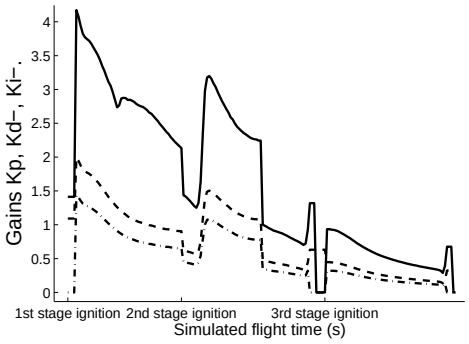

Figure 5.8 - Controller gains obtained by the conventional design.

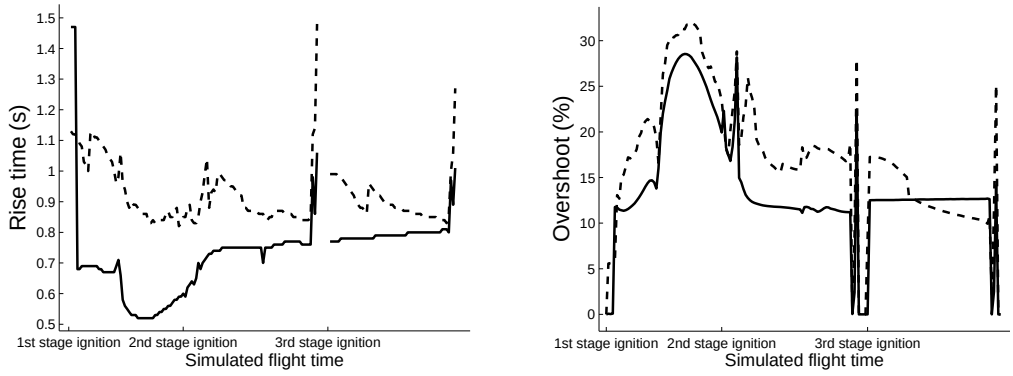

Figure 5.9 - Rise time and overshoot: a comparison between the conventional and the CSDA-LQ (-) designs.

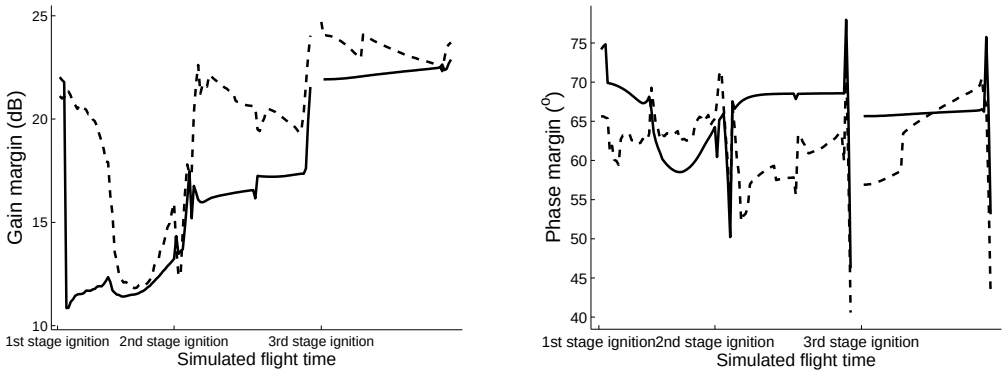

Figure 5.10 - Gain and phase margins: a comparison between the conventional and the CSDA-LQ (-) designs.

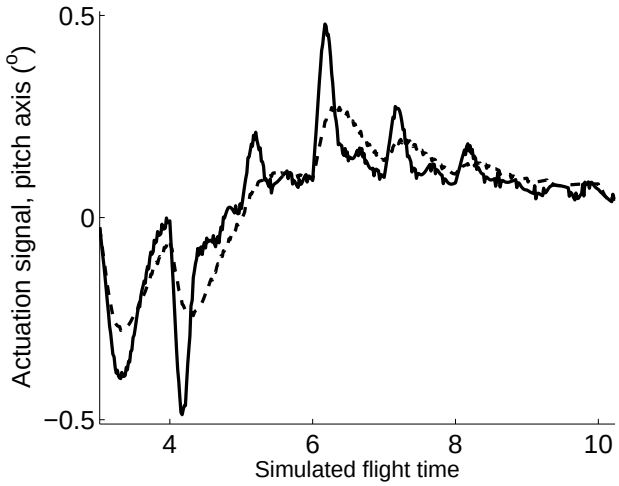

Figure 5.11 - Maximal control effort (pitch axis): a comparison between the conventional and the CSDA-LQ (-) designs (non-linear digital simulation).

5.2.3 Hardware-in-the-loop simulations

This section presents and evaluates the results of the Hardware-in-the-loop (HWIL) simulations, for the nominal case and scenarios. Most of the simulations were executed as phase B ones (see (LEITE FILHO; CARRIJO, 1997)), plus two phase D simulations (with real inertial sensors instead of models), accounting for the nominal cases of conventional and CSDA-LQ designs.

Scenarios for HWIL simulations, phase B. The following scenarios were defined for the phase B HWIL simulations:

a) *(Nominal)* Nominal case for thrust force and bending modes. No external disturbance. Guidance disabled.

b) *(Engine+,Engine-,EngUn)* Engines: all strong, all weak, unbalanced. Nominal case for bending modes. No external disturbance. Guidance disabled.

c) *(Bend+,Bend-)* Bending modes: bending frequencies variation of +15% and -5%. Nominal case for thrust force. No external disturbance. Guidance disabled.

d) *(Wind)* External disturbance: wind synthetic profile. Guidance disabled. Nominal case for thrust force and bending modes.

e) *(Guidance)* Guidance enabled. External disturbance: wind synthetic profile. Nominal case for thrust force and bending modes.

The indexes used to compare both designs (CSDA-LQ and conventional) are:

a) The integral of the squared control signal (ISCS).

b) The maximal amplitude of the 1^{st} and 2^{nd} bending modes (BM1,BM2), according to the Fast Fourier Transform of the pitch axis angular velocity. **Note:** BM2 is negligible during the 3^{rd} stage flight phase.

c) The maximum amplitude associated with the limit-cycle (LCyc) due to the actuator non-linearities, according to the Fast Fourier Transform of the pitch axis angular velocity.

Tables 5.3, 5.4 and 5.5 summarize the results for each flight phase. Regarding the ISCS index, small regions around lift-off and engine ignition and burnout were not taken into account. LCyc, BM1 and BM2 indexes were measured during the maximal dynamic pressure (1^{st} stage) and near engine burnout (2^{nd} and 3^{rd} stages). **Note:** for the 1^{st} stage, only the results of boosters 1A and 1B are presented, since they are representative of the other two. The main comments related to the simulations are:

a) The CSDA-LQ design presents better or equivalent results according to the ISCS index; the conventional design is superior only for *Engine+* and *Wind* scenarios of the 1^{st} stage phase.

b) The results associated with the LCyc index are favourable to the CSDA-LQ design in the 1^{st} and 2^{nd} stage phases and favourable to the conventional design in the 3^{rd} stage phase, considering LCyc amplitudes and frequencies (for both characteristics, smaller values mean better evaluation).

c) The first bending mode is a problem for both designs during the 2^{nd} stage phase. For the *EngUn* and *Bend-* scenarios, the CSDA-LQ design is inferior; however, for scenarios *Engine-* and *Wind*, the conventional design performed even worse, and unsatisfactorily (although stable) for the *Bend+* scenario.

Table 5.3 - Results of the HWIL simulations, phase B, 1^{st} stage.

Scenario	Conventional design				CSDA-LQ design			
	ISCS (1A)	ISCS (1B)	LCyc	BM1, BM2	ISCS (1A)	ISCS (1B)	LCyc	BM1, BM2
Nominal	6.3	11.6	0.4@1.2Hz	3.6,0.3	5.6	11.4	1.2@1.4Hz	0.6,0.1
Engine+	5.2	14.3	0.9@1.1Hz	0.9,0.4	5.4	14.6	0.5@1.0Hz	1.2,0.8
Engine–	5.6	9.3	1.0@1.0Hz	1.6,0.4	5.2	9.1	0.6@1.2Hz	1.8,0.2
EngUn	5.8	18.3	1.0@1.1Hz	0.9,0.4	5.8	18.4	0.3@1.5Hz	0.8,0.1
Bend+	5.1	12.0	1.6@1.1Hz	12.5,0.1	5.1	11.5	0.3@1.5Hz	18.5,0.6
Bend–	5.3	11.7	0.6@1.1Hz	0.4,0.3	5.1	11.6	0.4@1.5Hz	0.2,0.3
Wind	30.1	23.4	1.9@1.2Hz	0.6,0.3	35.9	25.6	1.0@1.5Hz	1.0,0.1

HWIL simulations, phase D (inertial sensors included). Phase D and phase B simulations results agreed, according to the indexes given. Besides, the actuation signals (Fig. 5.12) confirmed the same behaviour seen in the non-linear digital

Table 5.4 - Results of the HWIL simulations, phase B, 2^{nd} stage.

Scenario	Conventional Design				CSDA-LQ design			
	ISCS (Pitch)	ISCS (Yaw)	LCyc	BM1, BM2	ISCS (Pitch)	ISCS (Yaw)	LCyc	BM1, BM2
Nominal	18.8	66.0	1.9@1.1Hz	272.0,0.8	16.9	66.3	0.9@1.4Hz	126.0,0.4
Engine+	16.3	67.5	1.9@1.4Hz	92.6,0.2	16.8	66.4	0.2@1.6Hz	0.4,0.0
Engine–	19.8	71.5	1.7@0.8Hz	930.0,0.5	19.1	71.1	2.2@0.9Hz	30.7,1.4
EngUn	17.9	67.2	0.9@1.2Hz	188.0,0.6	17.4	64.4	0.7@0.9Hz	360.0,0.7
Bend+	33.9	69.2	1.3@1.0Hz	14449.0,0.4	16.7	65.7	2.9@0.9Hz	143.5,1.0
Bend–	17.5	66.5	1.5@1.1Hz	182.6,0.3	17.0	65.4	2.0@0.7Hz	303.0,0.5
Wind	17.9	68.1	3.0@1.4Hz	1420.5,0.9	17.1	66.9	2.6@0.7Hz	5.5,0.4

Table 5.5 - Results of the HWIL simulations, phase B, 3^{rd} stage.

Scenario	Conventional design				CSDA-LQ design			
	ISCS (Pitch)	ISCS (Yaw)	LCyc	BM1	ISCS (Pitch)	ISCS (Yaw)	LCyc	BM1
Nominal	15.5	74.1	22.4@1.0Hz	0.2	15.2	68.9	4.9@1.1Hz	0.2
Engine+	14.9	70.4	0.3@1.1Hz	0.0	14.8	69.7	17.8@1.1Hz	0.2
Engine–	16.2	69.9	7.7@1.1Hz	0.1	15.9	69.9	12.4@1.1Hz	0.3
EngUn	16.0	71.5	7.8@0.7Hz	0.2	15.6	69.0	8.1@0.9Hz	0.1
Bend+	14.6	71.1	14.0@1.2Hz	0.0	14.2	67.7	10.4@0.9Hz	0.0
Bend–	14.4	70.5	7.1@0.7Hz	0.2	14.5	68.2	8.7@1.1Hz	0.3
Guidance	15.3	69.2	1.3@1.1Hz	2.6	15.9	68.0	2.5@1.4Hz	1.0

simulation (Fig. 5.11).

5.3 VLS CSDA no. 2: GS OBR H_∞ controller

Compared with the previous case, this is a more complex one:

- The vector to be smoothed has more elements and variable length, thus it is more difficult to find good matings.
- A new design step, the OBR computation, imposes additional effort to the CSDA-H_∞ mechanism, such as estimation evaluation and combinatoric search.
- The computation time can increase excessively due to the search process and the number of simulation runs, unless some measures are taken.

Those aspects are considered in the following sections.

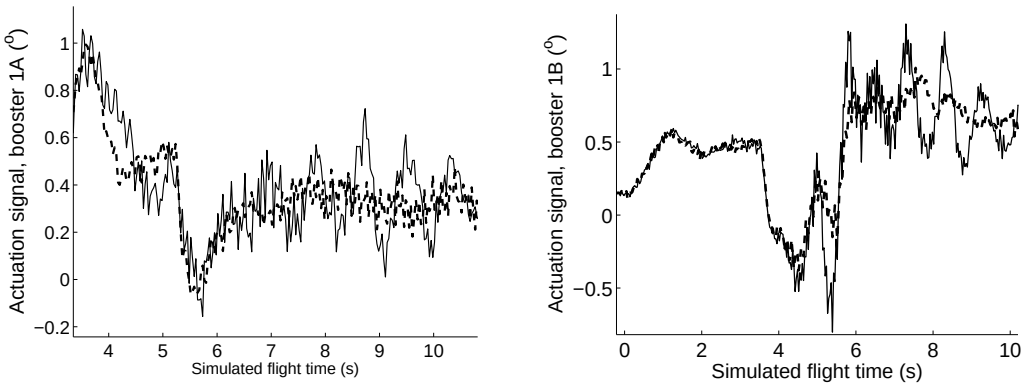

Figure 5.12 - Control effort (boosters A and B of the 1^{st} stage): a comparison between conventional and CSDA-LQ (-) designs, obtained from hardware-in-the-loop phase D simulations, nominal scenario.

5.3.1 Design characterization

In order to reduce the problem size, one applies the CSDA to the roll plane of the VLS launch vehicle, which has less states than the other two. This is a good choice for posterior hardware-in-the-loop simulations, since one may keep the existing pitch/yaw controllers developed with the linear-quadratic technique in order to evaluate the interpolation effects on the OBR estimations to be supplied by the new H_∞ roll plane GS controller presented now. Of course, the final step is to replace the remaining controllers as well, but unfortunately it is beyond the scope of this thesis due to time restrictions.

The GSM used for the H_∞ design is presented in the Fig. 5.13, where G_{LA} refers to the association of the launcher and the actuator models. Most of the weighting values $k_{\bullet\bullet}$ used in the H_∞ design are scalars, although transfer functions would be preferable (and are popularly adopted) in order to achieve a good trade-off between conflicting objectives in various frequency ranges. One chose scalar values to keep the problem simple, but it is surely possible to use transfer functions as well.

Gain and phase margins. The equations used to compute stability (BALAS et al., 2007) are $m_g = 20\ \log_{10}\left(1 + |\mathbf{T}|_\infty^{-1}\right)$ and $m_p = \frac{180}{\pi}\ 2sin^{-1}\left(\left(2\,|\mathbf{T}|_\infty\right)^{-1}\right)$, where $\mathbf{T} = \mathbf{I} - \mathbf{S}$ is the complementary sensitivity function, $\mathbf{S} = (\mathbf{I} + \mathbf{L})^{-1}$ is the sensitivity function, $\mathbf{L} = \mathbf{G_P}\ \mathbf{G_A}\ \mathbf{K}$ is the open-loop function and $\mathbf{G_P},\ \mathbf{G_A},\ \mathbf{K}$ are the models of the plant, actuator and controller respectively.

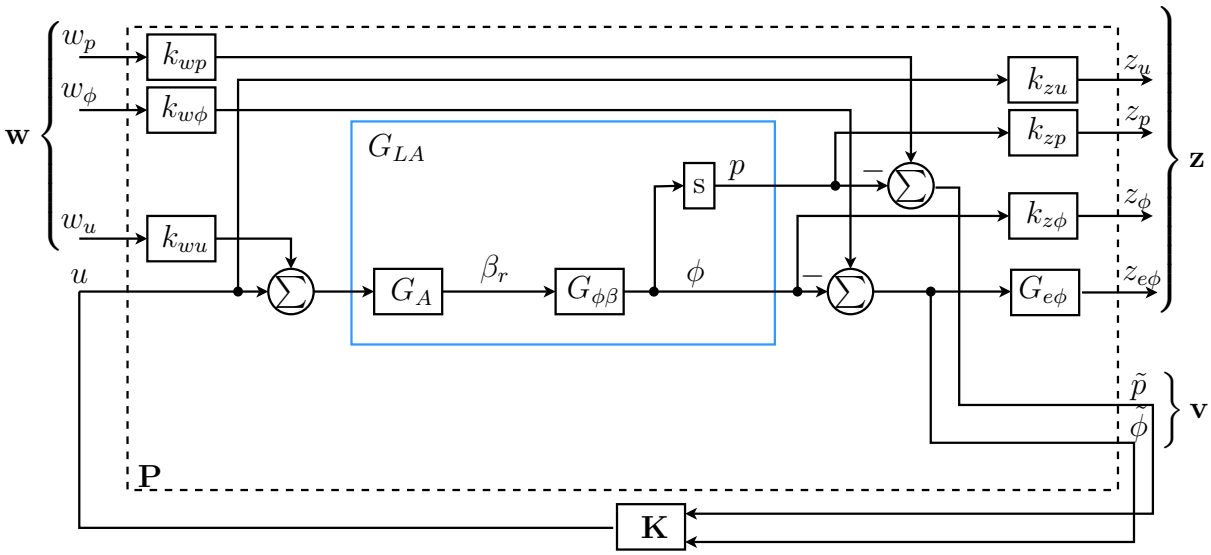

Figure 5.13 - GSM of the VLS launch vehicle (roll plane).

H_∞ design. The H_∞ optimal controller synthesis for LTI plant (available as the `hinfsyn` function of the MATLAB's Robust Control Toolbox) was chosen for the VLS H_∞ CSDA. One limited the maximum H_∞ norm $\|T_{zw}\|$ (see Fig. (4.2, $\mathcal{C}$)) as $\|T_{zw}\| < \gamma_{ref}$, choosing γ_{ref} as small as possible in order to reduce the number of iterations and speed up the CSDA process.

Simulation models. In order to obtain the indexes used to feed the FSs presented later and verify the quality of the estimations under time-varying conditions, two simulation models were built and one adapted:

a) The first one (Fig. 5.14) is composed of the discrete versions of the plant, output-limited controller (reflecting the real VLS on-board implementation) and actuator, where rate-transition blocks are used to connect the controller with the remaining elements with higher sampling rates;

b) The second one produces the OBR estimation quality index, being composed by the plant, actuator and controller with OBR estimation vectors (Fig. 5.15), plus noise (added to plant outputs p and ϕ) and bias (added to the output p).

c) Finally, the non-linear digital simulation program (written in C++) had its original linear-quadratic controller replaced by the GS OBR H_∞ one here produced with state-space matrices interpolated during the simulation.

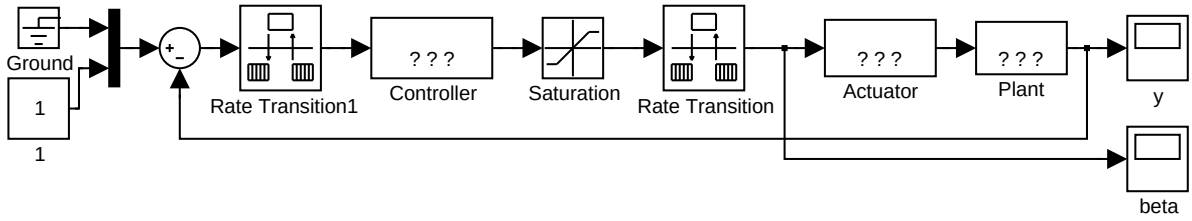

Figure 5.14 - Non-linear simplified simulation model for unit step input response.

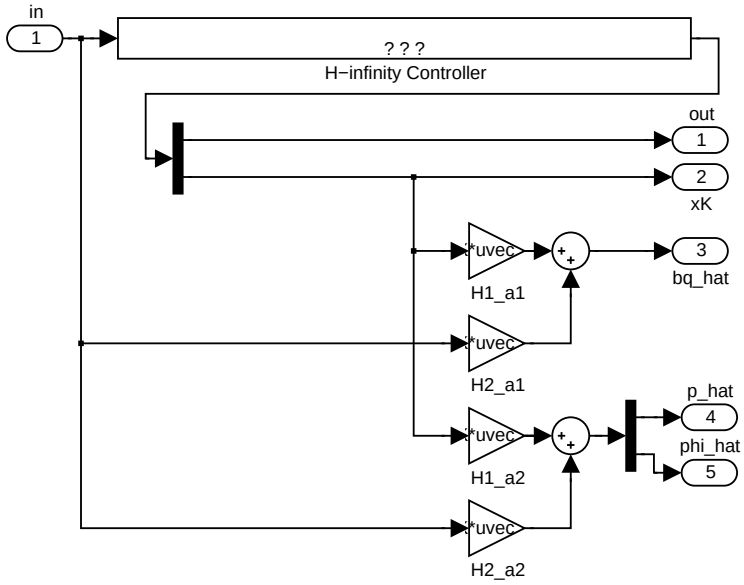

Figure 5.15 - Part of the simulation model used for obtaining the OBR estimation.

5.3.2 OBR characterization

Before defining the on-board model used for the OBR computation, it is worth to present some practical possibilities as the estimations of sensor bias or thrust vector misalignment. In (RAMOS; ALAZARD, 2009a), one considers the former case associated to the pitch plane of the same launch vehicle model used here; the on-board model (Eq. 5.3 and Fig. 3.1) comprises the estimates $\hat{b}_q$ (bias fault at the angular velocity sensor output $\tilde{q}$) and the attack angle $\hat{\alpha} = (\hat{w} - \hat{w}_v)/\bar{U}$ (where $\bar{U}$ is the vehicle longitudinal velocity) by means of the wind disturbance $\hat{w}_v$ (whose steady value cannot be estimated) and the plant's physical estimated variable $\hat{w}$ (from the state vector $\mathbf{x_L}$). The figures 5.16 (attack angle estimate) and 5.17 (sensor bias estimate) depict the simulation results when a realistic wind disturbance, noise

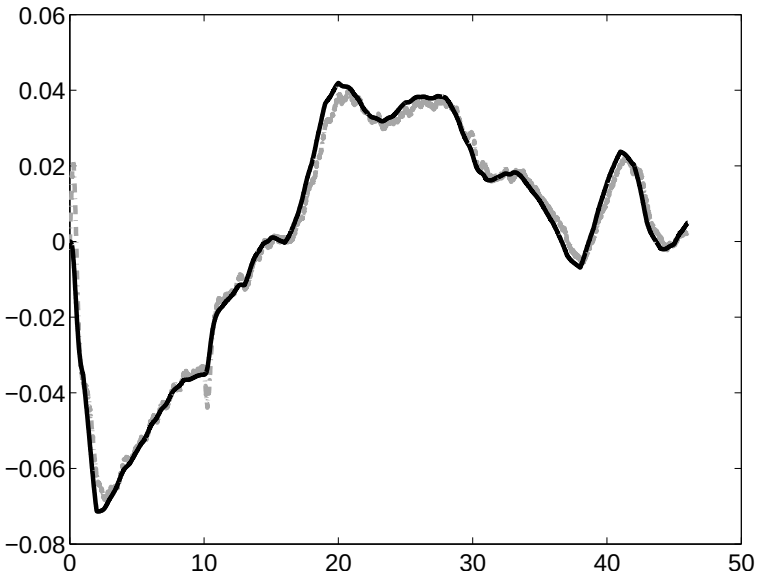

Figure 5.16 - Estimation of the attack angle α.
Simultaneous occurrence of output bias b_q (abrupt variation at 10 seconds) and external disturbance w_v (wind gust profile); noise added to both plant outputs. Black line: real value, gray line: estimated one.

added at both sensor outputs and a bias at the sensor output q are all applied simultaneously in the same simulation model.

$$\begin{bmatrix} \dot{\hat{\mathbf{x}}}_{\mathbf{L}} \\ \dot{\hat{w}}_v \\ \dot{\hat{b}}_q \\ \hline \tilde{q} \\ \tilde{\theta} \end{bmatrix} = \left[\begin{array}{ccc|c} \mathbf{A_P} & \mathbf{B_{Pd}} & \mathbf{0} & \mathbf{B_{Pu}} \\ \mathbf{0} & \lambda_\alpha & 0 & 0 \\ \mathbf{0} & 0 & \lambda_q & 0 \\ \hline \mathbf{C_{Pq}} & D_{Pdq} & 1 & D_{Puq} \\ \mathbf{C_{P\theta}} & D_{Pd\theta} & 0 & D_{Pu\theta} \end{array}\right] \begin{bmatrix} \hat{x_L} \\ \hat{w}_v \\ \hat{b}_q \\ \hline \beta_z \end{bmatrix} \tag{5.3}$$

The second case takes into account the roll plane of the launch vehicle; the on-board model (Eq. 5.4) comprises the estimates of a bias fault b_p at the angular velocity sensor output $\tilde{p}$ and a thrust vector misalignment b_β. Note that the state-space representation of $\mathbf{G}_{\phi\beta}$ (Fig. 5.13) is $\{\mathbf{A_L}, \mathbf{B_L}, \mathbf{C_L}, \mathbf{D_L}\}$ and the actuator model is built upon the state variable β. The estimates produced for fault and misalignment occuring at the same time range (besides the noise added to both sensor outputs)

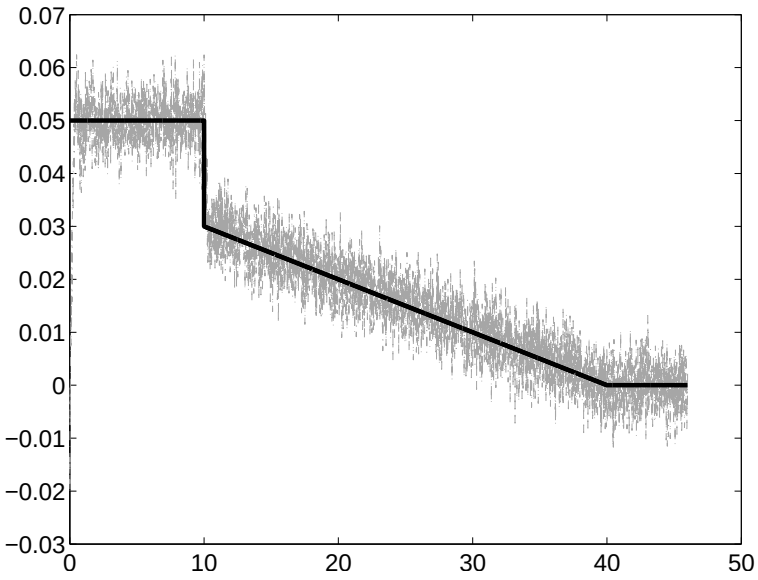

Figure 5.17 - Estimation of the bias b_q.
Simultaneous occurrence of external disturbance w_v (wind gust profile); noise added to both plant outputs. Black line: real value, gray line: estimated one.

are displayed in the Fig. 5.18.

$$\left[\begin{array}{c} \dot{\mathbf{x}}_L \\ \dot{b}_p \\ \dot{\beta} \\ \dot{b}_\beta \\ \hline \tilde{p} \\ \tilde{\phi} \end{array}\right] = \left[\begin{array}{cccc|c} \mathbf{A}_L & \mathbf{0} & \mathbf{B}_L & \mathbf{B}_L & 0 \\ \mathbf{0} & \lambda_p & 0 & 0 & 0 \\ \mathbf{0} & 0 & -\lambda_A & 0 & \lambda_A \\ \mathbf{0} & 0 & 0 & \lambda_\beta & 0 \\ \hline \mathbf{C}_L & \left[\begin{array}{c} 1 \\ 0 \end{array}\right] & \mathbf{D}_L & \mathbf{0} & \mathbf{0} \end{array}\right] \left[\begin{array}{c} \mathbf{x}_L \\ b_p \\ \beta \\ b_\beta \\ \hline u \end{array}\right] \tag{5.4}$$

Given those interesting implementations, one will introduce now the on-board model devised for this second case study. The roll plane nominal model is of order 3 (two states from the vehicle model (A.5c) plus the actuator state), with 2 measurements ($n_m = 2$), and the controller at the end of the CI design is of order 4 ($n_K = 4$, that is: the order of the GSM depicted in the Fig. A.4). Therefore, one can devise an on-board model comprised of the plant model plus up to three extra states ($n_K + n_m = 6 \geq n = n_O = n_P + 3$).

In order to keep the problem simple, only one extra state will be added into the plant model to take into account a bias fault on the p sensor (Eq. 5.5); thus, only

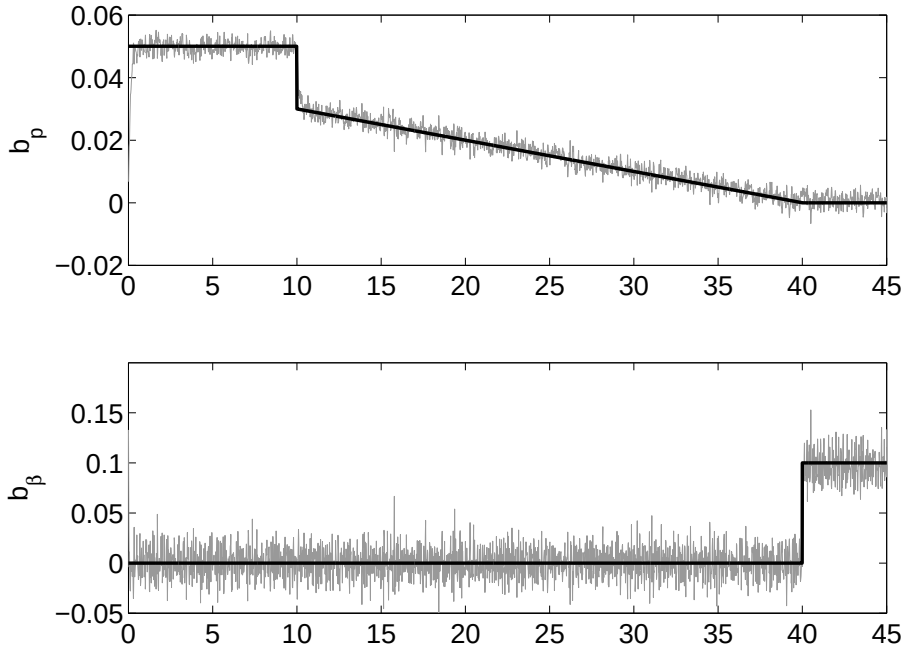

Figure 5.18 - Estimation of the bias b_p and misalignment b_β.
Noise added to both plant outputs. Black lines: real values, gray lines: estimated ones.

the full order controller case could be considered ($n_K = n$).

$$\left[\begin{array}{c} \dot{\mathbf{x}}_L \\ \dot{b}_p \\ \hline p \\ \phi \end{array}\right] = \left[\begin{array}{cc|c} \mathbf{A}_L & \mathbf{0} & \mathbf{B}_L \\ \mathbf{0} & \lambda_p & 0 \\ \hline \mathbf{C}_L & \begin{bmatrix} 1 \\ 0 \end{bmatrix} & \mathbf{D}_L \end{array}\right] \left[\begin{array}{c} \mathbf{x}_L \\ b_p \\ \hline u \end{array}\right] \tag{5.5}$$

However, the balancing of the controller (suggested in the Chapter 3) includes the removal of eigenvalues faster than the sampling frequency used for sensor data acquisition, which could result in $n_K < n$ (although $n_K > n - n_m$); thus, $n + n_K$ may vary. Therefore, as the closed-loop eigenvalues and the estimation vectors $\{\mathbf{H_1},\ \mathbf{H_2}\}$ are intended to be smoothed during the gain-scheduling process, one has to define the smoothing procedure of the CSDA-H_∞ mechanism carefully.

NOTE: as the number of closed-loop eigenvalues is small (so the number of poles), one will not employ computational intelligence for roll plane combinatoric search but, instead, select and test those combinations where all or most of the fastest poles are assigned to the estimation dynamics, according to the recommendations

of the chapter 3.

5.3.3 GA characterization

Some of the main characteristics of the GA employed in the CI-based design mechanism (Fig. 2.6) are :

- Each gene is a binary number (2^n combinations, n bits), which is explored with a crescent "deepness", that is, in the beginning of the simulation, only the most significant bit (b_n) is explored; if the elite rating is stationary, the deepness is increased by including the next significant bit in the search, and so on, finally covering all bits of the gene; if there is enough elite rating increase, the deepness is zeroed. Such strategy is aimed to implement a variant grid size in order to achieve some degree of uniform exploration in the beginning of the evolutionary process.

- Each weight $k_{\bullet\bullet}$ used in the H_∞ standard problem depicted in the Fig. A.2 is represented by two genes in the form g_1/g_2 producing a numeric interval from $1/(2^n - 1)$ up to $(2^n - 1)/1$. An entire set of weightings is called an individual, which in this case is composed of 14 genes, resulting in a huge search space order of 10^{33} for $n = 8$ bits.

- The roulette wheel is used for the selection of the individuals.

- Each run is finished by a stop criterion (standard deviation of recent best ratings).

- A record of every individual is kept in order to avoid wasted time in repeated evaluations.

- The fitness function is a fuzzy system.

- In order to save time, simulation for OBR estimation quality evaluation is only performed when the current individual presents an optimistic global rating higher than the elite's one, that is, presuming that the current individual achieves the maximum rating for estimation quality, and then computing the global rating (which includes the remaining specifications).

5.3.4 FS characterization

Regarding the scoring element, there was an improvement regarding the CSDA-LQ design, where the index-to-cost mapping was substituted by two FSs, yielding an intuitive and very simple interface for the designer to translate the specifications as fuzzy rules. Before presenting the FSs, one defines the indexes used.

Indexes. Six indexes were chosen to evaluate each individual generated by the CSDA-H_∞ mechanism: $\{t_s, M_p, u_{max}, m_g, m_p, p_{cl}\}$ (settling time, overshoot, control effort, gain and phase margins, and closed-loop poles dynamics). One may note that the rising time index is not taken into account this time because t_r seems to be a redundant specification when observing the results produced by the evolutionary process. The control effort index u_{max} is computed with the Eq. 5.6, based on the discrete output of the actuator $\beta(k)$.

$$u_{max} = \max_k \left[\beta(k)\right] \sum_k \beta(k) \tag{5.6}$$

The index p_{cl} refers to the smoothing and OBR estimation quality. Each vector of the set $\mathcal{S} = \{\mathbf{x_1}, \mathbf{x_2}\}$ to be smoothed (where $\mathbf{x_i}$ are the two designs to be compared) is composed of *(i)* closed-loop eigenvalues and *(ii)* OBR vectors $\{\mathbf{H_1},\ \mathbf{H_2}\}$ (see Chapter 3) used to produce the estimations. One devised to smooth the OBR vectors based on a supposition that this characteristic (OBR vectors smoothness) could affect the estimation produced by interpolated non-linear digital simulations.

The length of the set $\mathcal{S}$ may vary due to the controller balancing, as said before, impacting on the OBR vectors as well. Resuming: one faces here a problem to compare structures of different sizes. The chosen solution is to assign zero rating for sets with different sizes and also with different numbers of real and complex-conjugated eigenvalues. Otherwise, the p_{cl} index is computed as $p_{cl} = Q_{ne}\ (1 - Q_s)$, where Q_{ne} comes from a FS which evaluates noise and error qualities ($Q_n,\ Q_e$) of each OBR solution, and Q_s is the smoothness index.

The noise index is the maximum value in the frequency range $[f_{min}, f_{samp}/2]$ of the FFT response of the estimated variables. The error index is computed as $Q_e = \sqrt{\sum_k \left(y(k) - \hat{y}(k)\right)^2}$. The smoothness index Q_s is obtained by *(i)* arranging real and complex closed-loop eigenvalues supplied by the two vectors being compared in pairs with the smallest deviation, and then computing $s_{p1} = e^{-\log_{10}(1+10\bar{\Delta})}$, where

$\bar{\Delta}_i = |x_{i1} - x_{i2}| \,/\, \max(\{|x_{i1}|, |x_{i2}|\})$; *(ii)* repeating for the OBR vectors without re-arranging them, thus producing s_{p2}; *(iii)* finally computing $Q_s = \bar{s}_p + s_{p1}s_{p2}(1 - \bar{s}_p)$, where $\bar{s}_p = (s_{p1} + s_{p2})/2$.

NOTE: at first, the smoothing will be applied only to closed-loop eigenvalues, and later expanded to OBR vectors.

Presentation of the FSs.[1] The FS no. 1 is Sugeno-type, where the linguistic input variables are the cost function indexes $\{t_s, M_p, u_{max}, m_g, m_p, p_{cl}\}$ and the linguistic output variable is *Rating*. The linguistic values are expressed as: (i) a generalized bell-shaped function f_B, given by the triple $\langle a, b, c\rangle$ according to the Eq. 5.7a, or (ii) a Gaussian function f_G, given by the pair $\langle \sigma, c\rangle$ according to the Eq. 5.7b, or (iii) a triangular-shaped function f_T, given by the triple $\langle a, b, c\rangle$ according to the Eq. 5.7c.

$$f_B(x; a, b, c) = \left(1 + \left|\frac{x - c}{a}\right|^{2b}\right)^{-1} \tag{5.7a}$$

$$f_G(x; \sigma, c) = e^{\left[\frac{-(x-c)^2}{2\ \sigma^2}\right]} \tag{5.7b}$$

$$f_T(x; a, b, c) = max\left(min\left(\frac{x - a}{b - a}, \frac{c - x}{c - b}\right), 0\right) \tag{5.7c}$$

The FS no. 1's premises (Fig. 5.19) and universes of discourse are defined as follows:

- The linguistic variable t_s is associated with the settling time of the control system step response, where its universe of discourse is [0, 30] [s]. The linguistic value $\{large\}$ is defined as $f_B(x; 12, 3, 30)$.

- The linguistic variable M_p is associated with the overshoot size of the control system step response, where its universe of discourse is [0, 100] [%]. The linguistic value $\{satisfactory\}$ is defined as $f_G(x; 30, 0)$.

- The linguistic variable u_{max} is associated with the maximum actuation effort of the control system step response, where its universe of discourse is [0, 10] $[rad^2]$. The linguistic value $\{satisfactory\}$ is defined as $f_B(x; 0.2, 0.6, 0)$.

[1] For a better comprehension, please consult the MATLAB's FS edition GUI which can be called with the command `fuzzy`.

- The linguistic variable m_g is associated with the control system gain margin, where its universe of discourse is [0, 20] [dB]. The linguistic value $\{unsatisfactory\}$ is defined as $f_B(x; 0.5, 0.5, 0)$.

- The linguistic variable m_p is associated with the control system phase margin, where its universe of discourse is [0, 90] [^{o}]. The linguistic value $\{unsatisfactory\}$ is defined as $f_G(x; 12, 0)$.

- The linguistic variable p_{cl} is associated with the smoothness of the closed-loop eigenvalues and the OBR estimation quality, where its universe of discourse is [0, 1]. The linguistic values $\{good, bad\}$ are defined respectively as $f_G(x; 0.3, 0)$ and $f_T(x; 0.9, 1, 1.5)$.

- The linguistic variable *Rating* is associated with the total score. The linguistic values $\{good, bad\}$ are defined as the constants 1 and 0 respectively.

The FS no. 1 rules are given by the Eq. 5.8.

$$
\begin{aligned}
&R_1\text{: IF } (t_s \text{ IS } large) \text{ OR } (u_{max} \text{ IS NOT } satisfactory) \text{ OR } (m_g \text{ IS } unsatisfactory) \\
&\quad \text{OR } (m_p \text{ IS } unsatisfactory) \text{ OR } (p_{cl} \text{ IS } bad) \text{ THEN } (Rating \text{ IS } bad) \\
&R_2\text{: IF } (t_s \text{ IS NOT } large) \text{ AND } (u_{max} \text{ IS } satisfactory) \text{ AND } (m_g \text{ IS NOT } unsatisfactory) \\
&\quad \text{AND } (m_p \text{ IS NOT } unsatisfactory) \text{ AND } (p_{cl} \text{ IS } good) \text{ THEN } (Rating \text{ IS } good) \\
&R_3\text{: IF } (t_s \text{ IS NOT } large) \text{ AND } (u_{max} \text{ IS } satisfactory) \text{ AND } (m_g \text{ IS NOT } unsatisfactory) \\
&\quad \text{AND } (m_p \text{ IS NOT } unsatisfactory) \text{ AND } (p_{cl} \text{ IS NOT } bad) \text{ AND } (M_p \text{ IS } satisfactory) \\
&\quad \text{THEN } (Rating \text{ IS } good)
\end{aligned}
\tag{5.8}
$$

The FS no. 2 is Sugeno-type, where the linguistic input variables are the cost function indexes $[Q_n, Q_e]$ and the linguistic output variable is *Rating* $(= Q_{ne})$. The premises and universes of discourse are defined as follows:

- The linguistic variable Q_n is associated with the OBR estimation noise, where its universe of discourse is [0, 0.1]. The linguistic value $\{satisfactory\}$ is defined as $f_B(x; 0.0005, 0.5, 0)$.

- The linguistic variable Q_e is associated with the OBR estimation error, where its universe of discourse is [0, 1]. The linguistic value $\{satisfactory\}$ is defined as $f_B(x; 0.1, 0.5, 0)$.

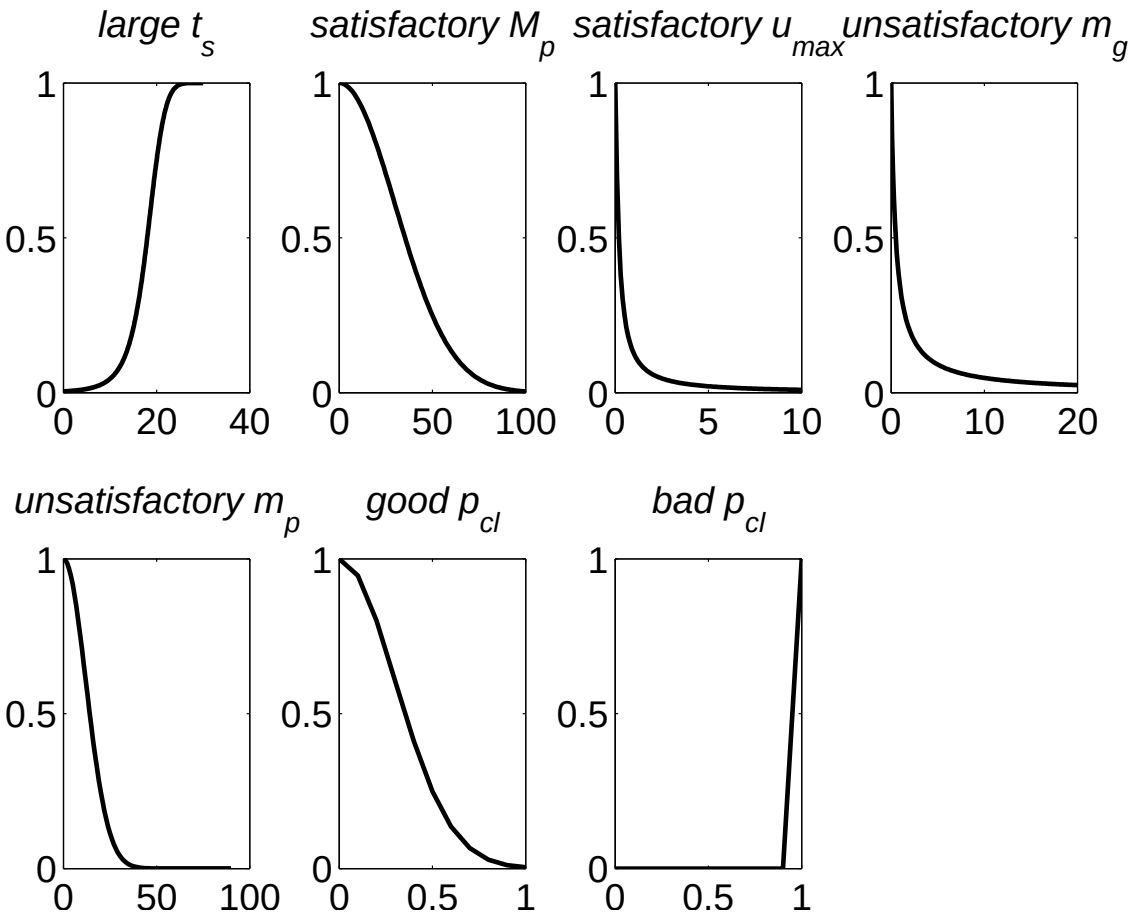

Figure 5.19 - Premises of the FS no. 1.

- The linguistic variable *Rating* is associated with the total score. The linguistic values {*good,bad*} are defined as the constants 1 and 0 respectively.

The FS no. 2 rules are given by the Eq. 5.9.

$$\begin{aligned} &R_1\text{: IF } (Q_n \text{ IS NOT } \textit{satisfactory}) \text{ OR } (Q_e \text{ IS NOT } \textit{satisfactory}) \text{ THEN } (\textit{Rating} \text{ IS } \textit{bad}) \\ &R_2\text{: IF } (Q_n \text{ IS } \textit{satisfactory}) \text{ AND } (Q_e \text{ IS } \textit{satisfactory}) \text{ THEN } (\textit{Rating} \text{ IS } \textit{good}) \end{aligned} \tag{5.9}$$

5.3.5 Results: smoothing closed-loop eigenvalues only

System specifications. After performing the CSDA simulation, one obtained the results shown in the Fig. 5.20 according to the stability, performance, smoothness and OBR indexes based on the original specifications stored in the fuzzy systems.

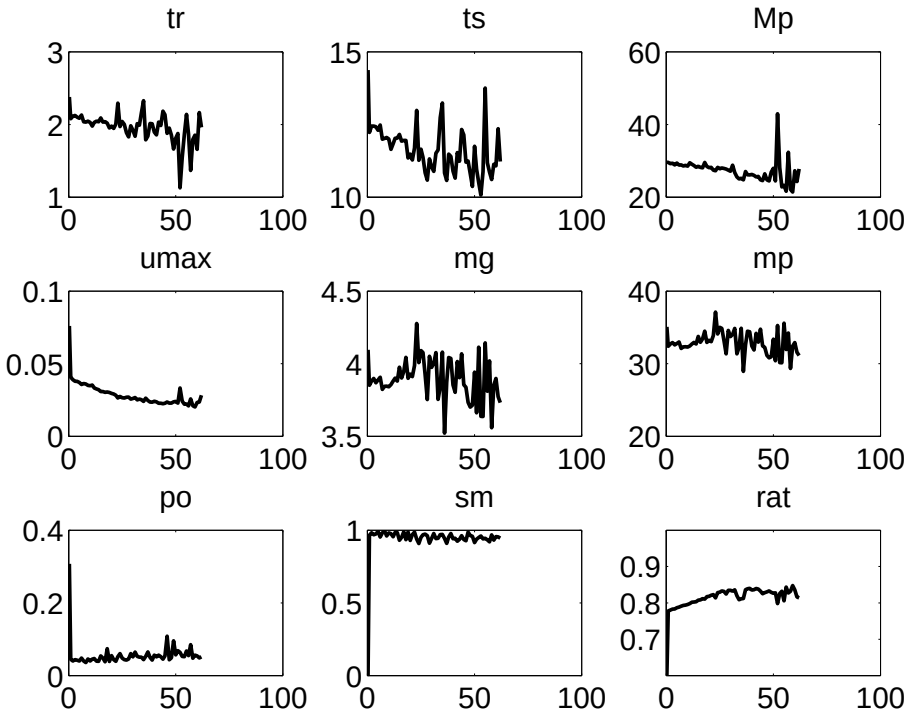

Figure 5.20 - Indexes obtained with the CSDA-H_∞ mechanism.

One can see that the rise time has an acceptable profile - not too fast in order to avoid the excitation of the bending modes - although it was not included as an specification during the CSDA procedure. The other indexes have acceptable profiles as well: multi-variable gain and phase margins values are above 3.5dB and 30^o, overshoot is around 30% (maximum of 45% in a very short period), settling time below 15s and actuation effort inferior to $0.05\,rad^2$. The smoothness index and closed-loop poles dynamics index are near to 0 and 1 respectively, which are the best values for each one. The smoothed closed-loop eigenvalues (2 complex-conjugated pairs and 3 real ones) are shown in the Fig. 5.21, and the non-smoothed OBR vectors in the Fig. 5.22.

Regarding the robustness associated with the new metric, one identified two elements (Fig 5.23) of the closed-loop state-space representation with a slow-increase behaviour on which the new metric was applied. In both cases, the system was considered stable to the modelled uncertainty (bound = 2) with a large tolerance:

Uncertain System is robustly stable to modelled uncertainty. It can tolerate up to 1.2e+003% of the modeled uncertainty. A destabilizing combination of 1.2e+003%

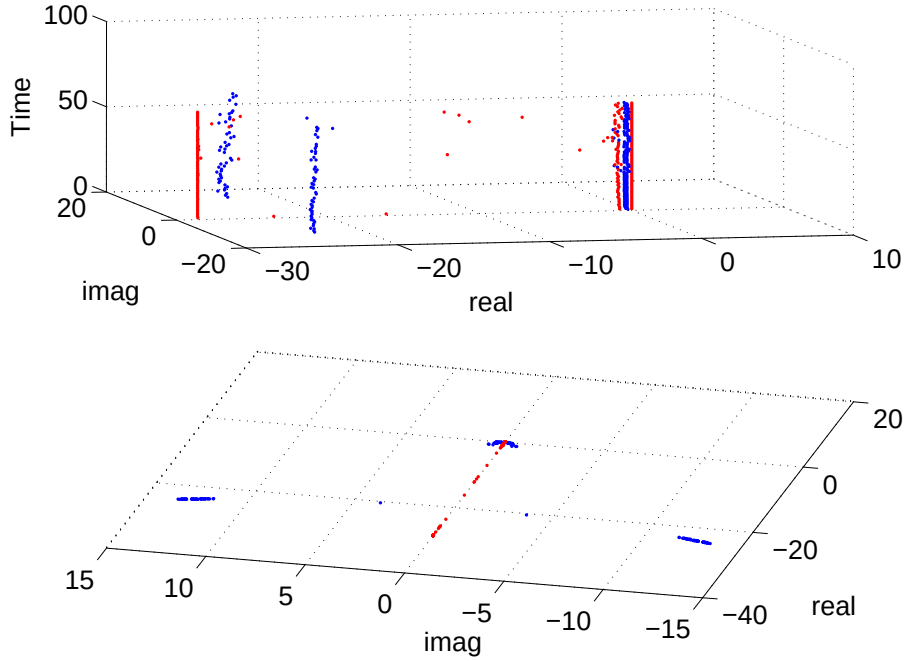

Figure 5.21 - Smoothness of the closed-loop eigenvalues.

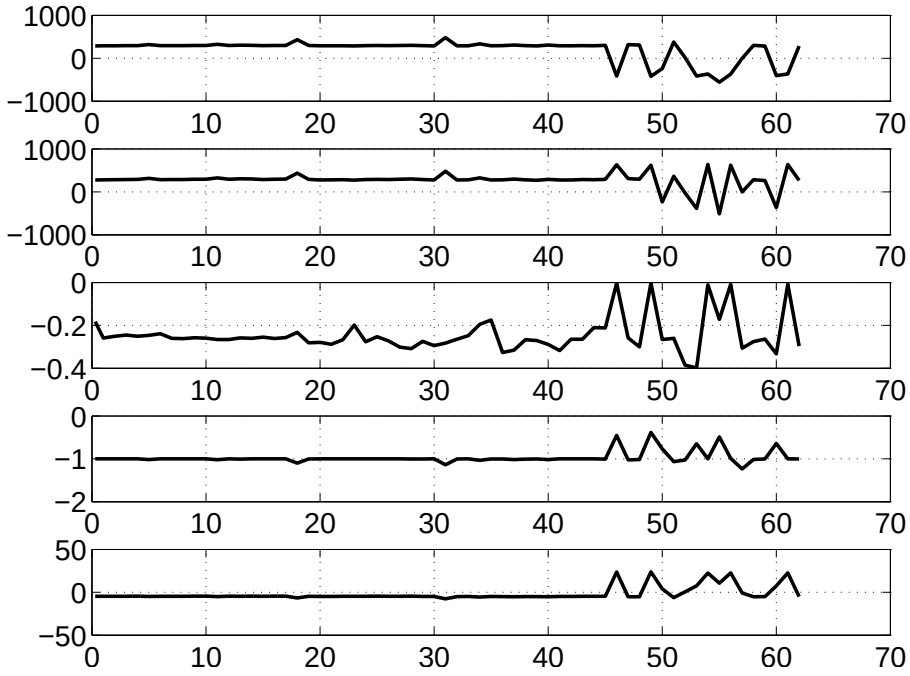

Figure 5.22 - Non-smoothed OBR vectors.
From top to bottom: H1_a1(1:3) and H2_a1(1:2) (see the Fig. 5.15).

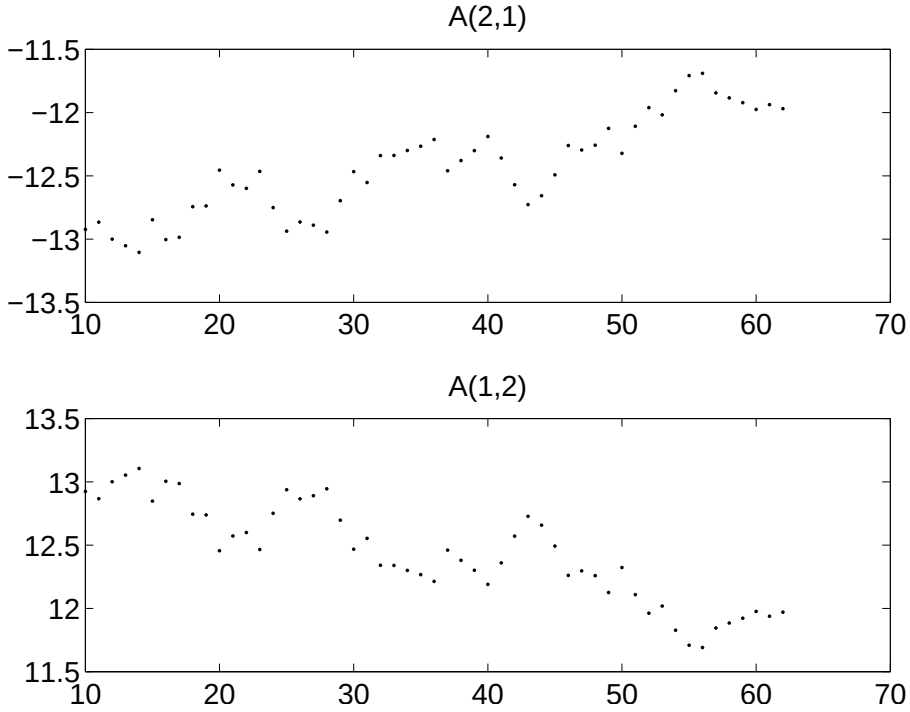

Figure 5.23 - Time variation of two elements of the closed-loop state-space matrix A_{CL}.

of the modeled uncertainty exists, causing an instability at 6.21e-010 rad/s.

Again, one emphasizes that this finding is preliminary and must be posteriorly subject to a more profound analysis.

OBR estimations from non-linear digital simulations. The Fig. 5.24 presents the results obtained from a non-linear digital simulation. One must admit that, not considering the abrupt changes occurring on the estimate $\hat{b}_p$ (to be discussed soon), the fault bias on the p sensor output has a shape which matches the real bias, and the compensated sensor output followed visibly the real variable.

5.3.6 Remarks on the non-linear digital simulation results

One supposed, at first, that OBR vectors smoothness could affect the estimation produced by interpolated non-linear digital simulations, but comparing figures 5.24 and 5.22 such assumption is hard to confirm: the abrupt changes found around 20, 25 and 40 seconds in the first figure appear to have not a clear counterpart in any of the graphs of the second one; besides, the OBR vector is notably non-smooth from 40 seconds on, while the estimate $\hat{b}_p$ is well-behaved in the same time range.

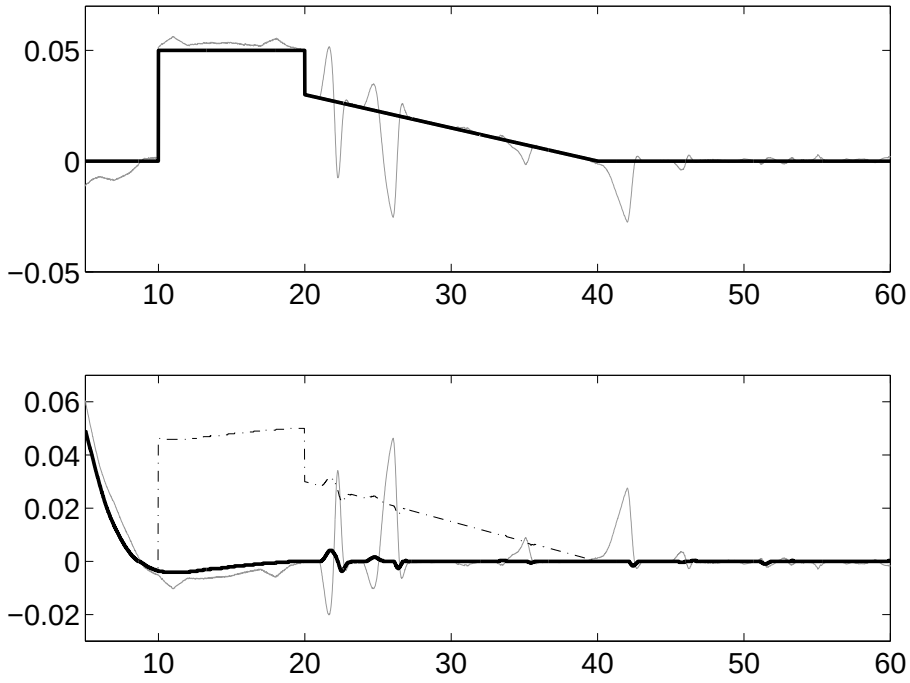

Figure 5.24 - Estimate $\hat{b}_p$ produced by non-linear digital simulation.
Top: real (black line) and estimated (grey line) biases. Bottom: real (black line), measured (dash-dotted line) and compensated (grey line) signals.

Examining other sources such as attitude references $\{\theta_{ref}, \psi_{ref}, \phi_{ref}\}$, external disturbances (Fig. 3.4), the individual elements of the state-space closed-loop matrices, one again does not find a cause for the estimation disturbances. However, those disturbances appear to be reflected in the real variable p (compare the black and grey lines in the Fig. 5.24), or they originate in the later and are amplified in the former, or are both caused by a (still unknown) common factor. Finally, one inspected the individual elements of the state-space matrices of the discrete H_∞ controller (Fig. 5.25): it was possible to identify several elements with peaks occurring at the same instant than those of the estimate $\hat{b}_p$; thus, a possible suspect (the H_∞ controller) was revealed. Unfortunately, the assumption on the OBR vectors smoothness had to be abandoned, and further investigation must be conducted in order to confirm the origin of the disturbances and devise a suitable strategy which can produce acceptable estimations. Although interesting, this investigation could not be performed due to time restrictions, but it is proposed for future research.

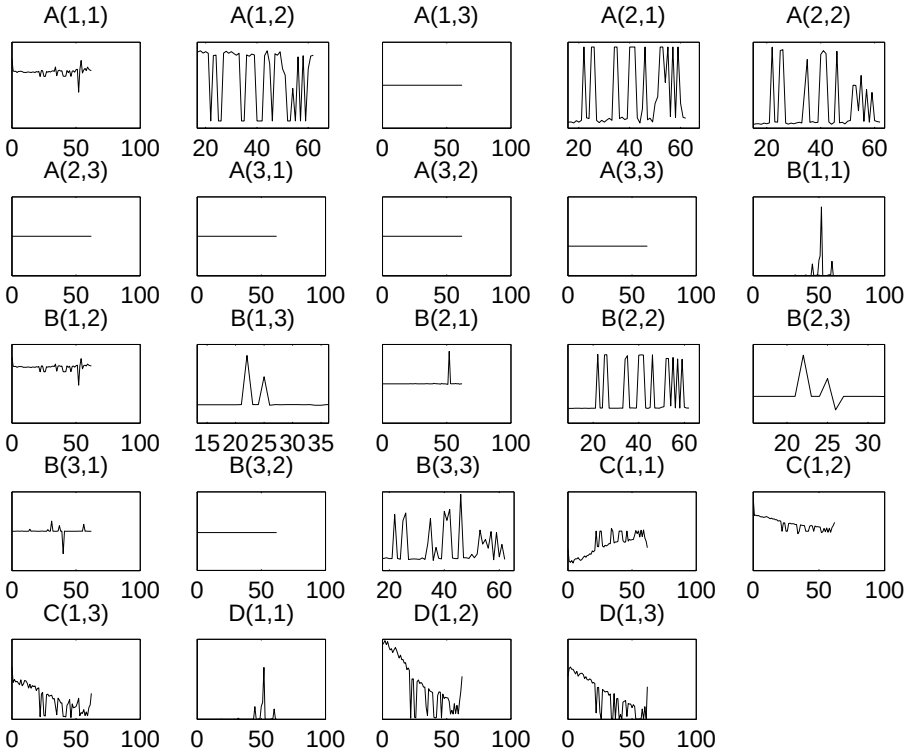

Figure 5.25 - Elements of the state-space matrices of the discrete H_∞ controller.

5.4 Conclusion

In this work, CSDA was proposed as a complement for complex CSDs, specially for the aerospace area: gain-scheduled design with controller interpolation. The first of the two case studies dealt with linear-quadratic optimization extended to the full launch vehicle trajectory. The second one replaced the original 3-gain controller by an H_∞ one, of higher order, allowing the application of the OBR technique and thus the estimation of a bias fault on the roll angular-velocity sensor; such estimation was confirmed with non-linear digital simulations, although with some imperfections, probably due to the non-smooth profile of the controller coefficients. Anyway, the investigation of the real nature of those imperfections is left for future research, together with other important tasks that could not be achieved due to time restrictions, such as the hardware-in-the-loop simulation of the CSDA implementation for the three planes of manoeuvring of the VLS launch vehicle.

6 Conclusions

6.1 Main facts

The main purpose of this work is to demonstrate the synergy between control engineering techniques and computationally-intelligent mechanisms. In this sense, one presents in the next lines few key points regarding the CSDA potential.

CSDA is not "object-oriented". *CSDA can be implemented independently of the chosen control system, controller structure, design technique, and specifications.* In this work, one combined computational intelligence with various design techniques such as linear-quadratic, H_2, H_∞, and even simple transfer functions. The invariable task is always to identify the chromosomes and genes linked to the object to be evolved (a controller or set of controllers, generally) and to translate the specifications as mathematical functions or fuzzy systems in order to allow the evaluation of generations of these objects. Finally, linear or non-linear models aimed for design and/or analysis can be freely added to the automated process. These models must be connected to the CSDA mechanism, but it is possible to develop a friendly plug-and-play environment in order to reduce code generation or adaptation, perhaps with a library of general models (simple LTI controller-actuator-plant ones) and specifications (stability and performance mainly). Such environment is didactically appealing at least, but it may offer some beneficial side effects to the most experienced users, such as to provide specifications even when they still do not exist.

CSDA provides a unified and standard framework. *Design and analysis tasks are necessarily embodied in a sequential and ordered fashion.* CSDA takes methodologies and procedures as inputs and then translate them into design, assuring repeatability during the entire process. Furthermore, posterior modifications are easily accommodated inside the whole procedure. By the other side, automated intelligence-based processes may produce non-identical solutions from different runs, in the same way that two engineers (or even a single one assuming a given span) would produce non-identical solutions when presented with the same problem. One must face that perhaps there is no such "golden solution" in everyday control engineering, but rather solutions that comply with specifications.

CSDA boosts CSD. *CSDA is aimed to accelerate the design process and explore deeply the available space of possibilities*, thus yielding better accomplishment with

the specifications; an example is provided by chapter 5 where, according to hardware-in-the-loop simulations, linear-quadratic optimization was fully achieved for the entire launch vehicle trajectory. Furthermore, mechanic and tiring tasks are not best suited for human designers but for the machine instead. However, the former ones are not expelled from the design process, neither their authority is reduced, on the contrary: there is a viewpoint change which allows the human designer to matter with more relevant questions while the machine is assigned the less interesting ones. By the other side, computational intelligence is frequently associated with computational burden; indeed, some effort is put on procedure optimization, that is, to choose the right models and evolution strategies in order to find short cuts in the design process. At the same time, computer hardware is continuously developing in size and speed, so even burden for very complex problems tends to decrease with time - thus, CSDA progress is assured.

CSDA eases the way to innovations. *CSDA allows the exploration of new forms of solutions*, and in different phases of the design process; system specifications can be extracted or tuned based on the indexes produced by preliminary set-ups. In the chapter 2, one observed that would be hypothetically possible to have on-board real-time CSDA for a satellite application; in the chapter 5, it was devised that OBR combinatoric search (a mechanic, tedious and most possibly arduous task) can be performed by means of computational intelligence; a new specification named "smoothness" was coined in order to better comply the stability issue with time-varying systems. All these ideas certainly arise in the designer's mind when their hands are free of non-creative demands; that is the baseline for CSDA, which in a extreme form will inexorably produce the very innovations.

6.2 Summary of contributions

Regarding the CI area, the main contributions are:

- Conception and implementation of new forms for interpolation of controllers, closed-loop eigenvalues and OBR vectors by adding a smoothing function in the system specifications of the CSDA mechanism.
- Conception and implementation of FSs as storing elements of the system specifications during the CSDA process.
- Proposal of the CSDA process for OBR combinatoric search, besides the

gain-scheduled controller design.

Regarding the control engineering area, the main contributions are:

- Conception of a new robustness metric associated with exponentially-varying elements of the system model.
- Considerations about the combinatoric selection for OBR computation, where *(i)* the fastest poles are not necessarily the best choice for the estimation dynamics, and *(ii)* each combinatoric (which produces the best combination of noise and error indexes) assigned to each estimate is not necessarily the same for all estimates.
- Evaluation of the interpolation action on the OBR estimations obtained from non-linear digital simulations.

6.3 Future research

Due to the time restrictions, the following questions remain for further exploration:

- Compute the GS H_∞ CSDA for the other two manoeuvring planes of the launch vehicle and execute HWIL simulations.
- Replace the weighting scalars $k_{\bullet\bullet}$ with appropriate transfer functions.
- Investigate the disturbances found in the estimate $\hat{b}_p$ (case study n. 2).
- Implement real-time satellite CSDA in the laboratory.
- Define a universal CSDA environment where models, techniques and specifications can be attached easily.
- Verify if the excitation is persistent enough for the case study considering the controller OBR.

REFERENCES

ALAZARD, D.; APKARIAN, P. Exact observer-based structures for arbitrary compensators. **International Journal of Robust and Non-linear control**, v. 9, n. 2, p. 101–118, Feb. 1999. 24

ALAZARD, D.; CUMER, C.; APKARIAN, P.; GAUVRIT, M.; FERRERES, G. **Robustesse et comande optimale**. Toulouse: Cépaduès-Éditions, 1999. 24, 25

BALAS, G.; PACKARD, A.; SAFONOV, M.; CHIANG, R. Next generation of tools for robust control. In: AMERICAN CONTROL CONFERENCE. **Proceedings...** Boston, 2004. v. 6, p. 5612–5615. 45

BALAS, G. J.; CHIANG, R. Y.; PACKARD, A. K.; SAFONOV, M. G. **Robust Control Toolbox 3 user's guide**. Natick: MathWorks, 2007. Available from: <http://www.mathworks.com>. 56, 66

BRITO, A. G.; LEITE FILHO, W. C.; RAMOS, F. O. Approach comparison for controller design of a launcher. In: 6^{th} INTERNATIONAL ESA CONFERENCE ON GUIDANCE, NAVIGATION AND CONTROL SYSTEMS. **Proceedings...** Loutraki, 2006. p. 20.1–20.6. 2, 4

CLÉMENT, G. D. B.; MAUFFREY, S. Aerospace launch vehicle control: a gain scheduling approach. **Control Engineering Practice**, v. 13, n. 3, p. 333–347, March 2005. 44, 57

COELLO, G. B. L. C. A. C.; VELDHUIZEN, D. A. van. **Evolutionary algorithms for solving multi-objective problems**. 2. ed. New York: Springer Science+Business Media, LLC, 2007. (Genetic and evolutionary computation). 3, 5

CRAENEN, B. C.; EIBEN, A. E. **Computational intelligence**. 2002. Available from: <http://www.eolss.net/>. 6

DORATO, P. A historical review of robust control. **IEEE Control Systems Magazine**, v. 7, n. 2, p. 44–47, April 1987. 42

FLEMING, P. J.; PURSHOUSE, R. C. Evolutionary algorithms in control systems engineering: a survey. **Control Engineering Practice**, v. 10, n. 11, p. 1223–1241, Nov. 2002. 1, 8

FOGEL, D. B.; ANDERSON, R. W. Revisiting bremermann's genetic algorithm. i. simultaneous mutation of all parameters. In: IEEE CONGRESS ON EVOLUTIONARY COMPUTATION. **Proceedings...** San Diego, 2000. p. 1204–1209. 8

FONSECA, C. M. M. da. **Multiobjective genetic algorithms with application to control engineering problems**. PhD Thesis (PhD) — The University of Sheffield, Sheffield, 1995. 8

FRANKLIN, G. F.; POWELL, J. D.; EMAMI-NAEINI, A. **Feedback control of dynamic systems**. 3. ed. Boston: Addison-Wesley Publishing Company, 1994. 41

GALICHET, S.; BOUKEZZOULA, R.; FOULLOY, L. Words or numbers, mamdani or sugeno fuzzy systems: a comparative study. In: BOUCHON-MEUNIER, B.; MARSALA, C.; RIFQI, M.; YAGER, R. R. (Ed.). **Uncertainty and intelligent information systems**. Singapore: World Scientific Publishing Co. Pte. Ltd., 2008. p. 291–305. 11

KIENITZ, K. H.; MOREIRA, F. J. O. **Anteprojeto de algoritmos de controle do VLS com atuadores do tipo tubeira móvel**. Brazil, April 1993. Doc. n. CTA/IAE n. 590-000000/B3033. 93, 96, 102

KONAR, A. **Computational Intelligence: principles, techniques and applications**. New York: Springer, 2005. 6, 7

LARSON, W. J.; WERTZ, J. R. **Space mission analysis and design**. 2. ed. Boston: Microcosm Inc. & Kluwer Academic Publishers, 1992. (Space Technology Series). 19

LEITE FILHO, W. C.; CARRIJO, D. S. Hardware-in-loop simulation of Brazilian launcher VLS. In: 3^{rd} ESA INTERNATIONAL CONFERENCE ON SPACECRAFT GUIDANCE, NAVIGATION AND CONTROL SYSTEMS. **Proceedings...** Noordwijk, 1997. p. 355–358. 55, 63

_____. Control system of Brazilian launcher. In: 4^{th} ESA INTERNATIONAL CONFERENCE ON SPACECRAFT GUIDANCE, NAVIGATION AND CONTROL SYSTEMS. **Proceedings...** Noordwijk, 1999. p. 401–405. 53

LEITH, D. J.; LEITHEAD, W. E. Survey of gain-scheduling analysis & design. **International Journal of Control**, v. 73, n. 11, p. 1001–1025, July 2000. 44

LI, Y.; ANG, K. H.; CHONG, G. C.; FENG, W.; TAN, K. C. CAutoCSD - evolutionary search and optimization enabled computer automated control system design. **International Journal of Automation and Computing**, 2004. 3, 5

LUENBERGER, D. G. An introduction to observers. **IEEE Transactions on Automatic Control**, AC-16, n. 6, p. 596–602, Dec. 1971. 23, 24

MAEKAWA, K.; PANG, G. K. H. Control system design automation for mechanical systems. **Journal of Intelligent & Robotic Systems**, Springer Netherlands, v. 21, p. 239–256, 1998. 3, 5

MATHWORKS. **Fuzzy Logic Toolbox 2 user's guide**. Natick: MathWorks, 2010. Available from: <http://www.mathworks.com>. 10

MEDEIROS, F. E. L.; PELLANDA, P. C.; LEITE FILHO, W. C. H_∞ analysis and synthesis by genetic algorithms of the attitude control system of the brazilian satellite launcher. In: 6^{th} INTERNATIONAL ESA CONFERENCE ON GUIDANCE, NAVIGATION AND CONTROL SYSTEMS. **Proceedings...** Loutraki, 2005. p. 21.1–21.6. 3

MENDEL, J. Fuzzy logic systems for engineering: a tutorial. **Proceedings of the IEEE**, v. 83, n. 3, p. 345 –377, March 1995. 10

MOREIRA, F. J. O.; CARRIJO, D. S. **Modelamento matemático usado no projeto do sistema de controle do VLS**. Brazil, May 1995. Doc. n. CTA/IAE n. 590-000000/B3043. 93, 96

MULLHAUPT, P.; BUCCIERI, D.; BONVIN, D. A numerical sufficiency test for the asymptotic stability of linear time-varying systems. **Automatica**, v. 43, n. 4, p. 631–638, April 2007. 44

OGATA, K. **Engenharia de controle moderno**. Rio de Janeiro: Ed. Prentice Hall do Brasil, 1985. 112

OLIVA, P.; LEITE FILHO, W. C. Rocket tracking and decoupling eigenstructure control law. **Journal of the Brazilian Society of Mechanical Sciences**, 2000. 93, 96, 101

PELLANDA, P. C.; APKARIAN, P. Une méthode d'interpolation de structures estimation/commande pour des compensateurs H_∞ et μ. In: PUBLICATIONS, H.

science (Ed.). **Conception de commandes robustes**. Paris: J. Bernussou, and A. Oustaloup, 2002. chapter 8, p. 141–187. 44

RAMOS, F. O. Combining observer-based form with computational intelligence for H_∞ controller design and interpolation. In: $10^{ÈME}$ CONGRÈS DES DOCTORANTS EDSYS (ÉCOLE DOCTORALE SYSTÈMES). **Proceedings...** Toulouse, 2009. Available from: <http://spiderman-2.laas.fr/EDSYS/>. 4

RAMOS, F. O.; ALAZARD, D. Embedding FDI in launcher attitude controllers. In: 4^{th} INTERNATIONAL CONFERENCE ON RECENT ADVANCES IN SPACE TECHNOLOGIES. **Proceedings...** Istanbul, 2009. 4, 68

_____. Observer-based realization of a computational-intelligence designed launcher attitude controller. In: AIAA GUIDANCE, NAVIGATION, AND CONTROL CONFERENCE. **Proceedings...** Chicago, 2009. 3, 4, 29

_____. Semi-automated observer-based controller design. In: 11^{th} PAN-AMERICAN CONGRESS OF APPLIED MECHANICS. **Proceedings...** Foz do Iguaçu, 2010. 4

RAMOS, F. O.; ARAUJO, E. Fuzzy-scored genetically designed controller for the VLS-1 launcher. In: IEEE WORLD CONGRESS ON COMPUTATIONAL INTELLIGENCE. **Proceedings...** Hong Kong, 2008. p. 1018–1023. 4, 8

RAMOS, F. O.; BRITO, A. G.; LEITE FILHO, W. C. PACA - a tool for design and analysis of control system. In: 6^{th} INTERNATIONAL SYMPOSIUM ON LAUNCHER TECHNOLOGY. **Proceedings...** Munich, 2005. 54

RAMOS, F. O.; LEITE FILHO, W. C. Transient effects related to a reconfigurable control design (satellite launcher). In: 15^{th} IFAC SYMPOSIUM ON AUTOMATIC CONTROL IN AEROSPACE. **Proceedings...** Bologna, 2001. 60

_____. Design upgrade and validation of a launcher vehicle attitude controller combining genetic and linear quadratic optimization. In: 19^{th} INTERNATIONAL CONGRESS OF MECHANICAL ENGINEERING. **Proceedings...** Brasilia, 2007. 3, 4, 56

_____. Extended linear quadratic design of an attitude controller through genetic optimization with variable bending rejection. In: 2^{nd} EUROPEAN CONFERENCE FOR AEROSPACE SCIENCES. **Proceedings...** Brussels, 2007. 4

_____. Extending the linear quadratic design of a launch vehicle attitude controller through genetic optimization. In: 17^{th} IFAC SYMPOSIUM ON AUTOMATIC CONTROL IN AEROSPACE. **Proceedings...** Toulouse, 2007. 2, 4, 8, 60

RAMOS, F. O.; LEITE FILHO, W. C.; MOREIRA, F. J. O. Gain computation strategy for an attitude control system. In: 17^{th} INTERNATIONAL CONGRESS OF MECHANICAL ENGINEERING. **Abstracts...** São Paulo, 2003. p. 46. 54

RAMOS, F. O.; SOUZA, L. C. G. AI-based design of a satellite attitude controller. In: 9^{th} INTERNATIONAL CONFERENCE ON MOTION AND VIBRATION CONTROL. **Proceedings...** Munich, 2008. 4, 13

_____. CI-based design of a satellite attitude controller. **Journal of Aerospace Engineering, Sciences and Applications**, II, n. 1, p. 47–52, Jan. 2011. Available from: <http://www.aeroespacial.org.br/jaesa/>. 4

RAMOS, F. O.; SOUZA, L. C. G.; ARAUJO, E. Computational intelligent satellite attitude control design. In: 59^{th} INTERNATIONAL ASTRONAUTICAL CONGRESS. **Proceedings...** Glasgow, 2008. 4

ROSENBROCK, H. H. The stability of linear time-dependent control systems. **International Journal of Electronic Control**, v. 15, n. 1, p. 73–80, July 1963. 44

RUDAS, I. J.; FODOR, J. Intelligent systems. **International Journal of Computers, Communications & Control**, III, n. S., p. 132–138, May 2008. 6

SCHUMACHER, J. Compensator synthesis using (c,a,b)-pairs. **IEEE Transactions on Automatic Control**, v. 25, n. 6, p. 1133–1138, Dec. 1980. 23

SEIBERT, G. **The history of sounding rockets and their contribution to European space research**. Noordwijk, Nov. 2006. Available from: <http://www.esa.int/esapub/hsr/HSR_38.pdf>. 51

SKOGESTAD, S.; POSTLETHWAITE, I. **Multivariable feedback control - analysis and design**. 2. ed. Chichester: John Wiley & Sons, Ltd, 2005. 41, 43, 112

SOUZA, L. C. G. Satellite attitude control system parameters optimization. In: III EUROPEAN CONFERENCE ON COMPUTATIONAL MECHANICS. **Proceedings...** Lisbon, 2006. p. 719–719. 13, 14, 21

SPECTOR, L. **Automatic quantum computer programming**. New York: Springer, 2004. 8

TAN, K. C.; LI, Y. Performance-based control system design automation via evolutionary computing. **Engineering Applications of Artificial Intelligence**, v. 14, n. 4, p. 473–486, Aug. 2001. 8

TAO, G. **Adaptive control design and analysis**. Hoboken: John Wiley & Sons, 2003. (Adaptive and learning systems for signal processing, communications and control). 29

WANG, Q.; SPRONCK, P.; TRACHT, R. An overview of genetic algorithms applied to control engineering problems. In: 2^{nd} INTERNATIONAL CONFERENCE ON MACHINE LEARNING AND AUTOMATION. **Proceedings...** Xi'an, 2003. p. 1651–1656. 8

ZADEH, L. A. Fuzzy sets. **Information and Control**, 1965. 10

APPENDIX - REVISION OF THE VLS MODELS

A.1 Objective.

This work reviews the VLS launch vehicle models presented by two principal sources ((KIENITZ; MOREIRA, 1993) and (OLIVA; LEITE FILHO, 2000)):

- The rigid body non-linear model.
- The rigid body linear coupled model.
- The rigid body linear decoupled models.
- The full linear coupled model.
- The full linear decoupled models.
- The general standard model (GSM).

A MATLAB®script was written in order to produce all the models named above (but the non-linear one) from two input files used in the design procedure at CTA/IAE (Brazilian laboratories where the VLS launch vehicle is developed).

A.2 Rigid body non-linear model of the VLS launch vehicle.

The VLS rigid body non-linear model is presented by two principal sources: CTA/IAE (KIENITZ; MOREIRA, 1993) and Oliva and Leite Filho (OLIVA; LEITE FILHO, 2000) (both based on the full mathematical description of the VLS developed in (MOREIRA; CARRIJO, 1995)). Here, one intends to produce a more detailed version and comment on some dissimilarities between both works. The Eq. A.1 represents (without time dependencies) the non-linear model ((OLIVA; LEITE FILHO, 2000), Eqs. (1)-(8)). The rotation from the coordinate axes systems $\{X,\ Y,\ Z\}$ (inertial frame) to $\{X_b,\ Y_b,\ Z_b\}$ (body frame) is shown in the Fig. A.1, along with the correspondent angles, angular velocities and linear velocities.

$$\dot{v} = -\frac{C_{n\alpha}\ P_d\ S_{ref}}{m\ U_0}\ v - g\sin(\theta)\sin(\phi) + g\cos(\theta)\sin(\psi)\cos(\phi) - U_0\ r + p\ w + \frac{F_{coy}}{m}\ r - \frac{2F_E}{m}\ \beta_y \tag{A.1a}$$

$$\dot{w} = -\frac{C_{n\alpha}\ P_d\ S_{ref}}{m\ U_0}\ w - g\sin(\theta)\cos(\phi) - g\cos(\theta)\sin(\psi)\sin(\phi) + U_0\ q - p\ v + \frac{F_{coz}}{m}\ q + \frac{2F_E}{m}\ \beta_z \tag{A.1b}$$

$$\dot{p} = -\left(\frac{C_{lp}\ P_d\ S_{ref}\ D_{ref}^2}{2\ U_0\ I_{xx}} + \frac{\dot{I}_{xx}}{I_{xx}}\right) p - \frac{(I_{zz} - I_{yy})}{I_{xx}}\ q\ r + \frac{4\ d_l\ F_E}{I_{xx}}\ \beta_r \tag{A.1c}$$

$$\dot{q} = \frac{l_{ax}\ C_{n\alpha}\ P_d\ S_{ref}}{I_{yy}\ U_0}\ w + \left(\frac{M_{coy}}{I_{yy}} - \frac{C_{mq}\ P_d\ S_{ref}\ D_{ref}^2}{2\ U_0\ I_{yy}} - \frac{\dot{I}_{yy}}{I_{yy}}\right) q - \frac{(I_{xx} - I_{zz})}{I_{yy}} p\ r - \frac{2\ l_{cx}\ F_E}{I_{yy}}\ \beta_z \tag{A.1d}$$

$$\dot{r} = -\frac{l_{ax}\ C_{n\alpha}\ P_d\ S_{ref}}{I_{zz}\ U_0}\ v + \left(\frac{M_{coz}}{I_{zz}} - \frac{C_{mq}\ P_d\ S_{ref}\ D_{ref}^2}{2\ U_0\ I_{zz}} - \frac{\dot{I}_{zz}}{I_{zz}}\right) r - \frac{(I_{yy} - I_{xx})}{I_{zz}}\ p\ q - \frac{2\ l_{cx}\ F_E}{I_{zz}}\ \beta_y \tag{A.1e}$$

$$\dot{\theta} = \frac{\cos(\phi)}{\cos(\psi)}\ q - \frac{\sin(\phi)}{\cos(\psi)}\ r \tag{A.1f}$$

$$\dot{\psi} = \sin(\phi)\ q + \cos(\phi)\ r \tag{A.1g}$$

$$\dot{\phi} = p - \tan(\psi)\cos(\phi)\ q + \tan(\psi)\sin(\phi)\ r \tag{A.1h}$$

where:

U_0 is the velocity of the vehicle relative to the axis X_b.

$C_{n\alpha}$ is the derivative of the aerodynamic normal force relative to the attack angle (α).

C_{lp} is the derivative of the roll damping moment relative to the rolling rate (p).

C_{mq} is the derivative of the pitch (yaw) moment relative to the pitch (yaw) rate.

P_d is the dynamic pressure.

S_{ref} is the reference area of the vehicle.

D_{ref} is the reference diameter of the vehicle.

m is the mass of the vehicle.

I_{xx}, I_{yy}, I_{zz} are the inertia moments relative to the axes X_b, Y_b and Z_b.

d_l is the control moment of the rolling arm.

l_{ax} is the length of the aerodynamic moment arm.

l_{cx} is the length of the pitch and yaw control arms.

F_E is the thrust force.

F_{coy}, F_{coz} are the Coriolis force components relative to the axes Y_b and Z_b.

M_{coy}, M_{coz} are the Coriolis moment components relative to the axes Y_b and Z_b.

v, w are the linear velocity components relative to the axes Y_b and Z_b.

p, q, r are the angular velocities relative to the axes $X_b,\ Y_b, Z_b$.

$\beta_y,\ \beta_z,\ \beta_r$ are nozzle deflections applied on pitch, yaw and roll planes respectively.

$\theta,\ \psi,\ \phi$ are the angular deflections required to align $Y,\ Z$ and X and Y_b, Z_b and X_b axes.

$\dot{\theta},\ \dot{\psi},\ \dot{\phi}$ are the angular velocities associated with $\theta,\ \psi$, and ϕ angles.

NOTE: pitch, yaw and roll planes are produced by the rotation of the $Y_b,\ Z_b$ and X_b axes respectively.

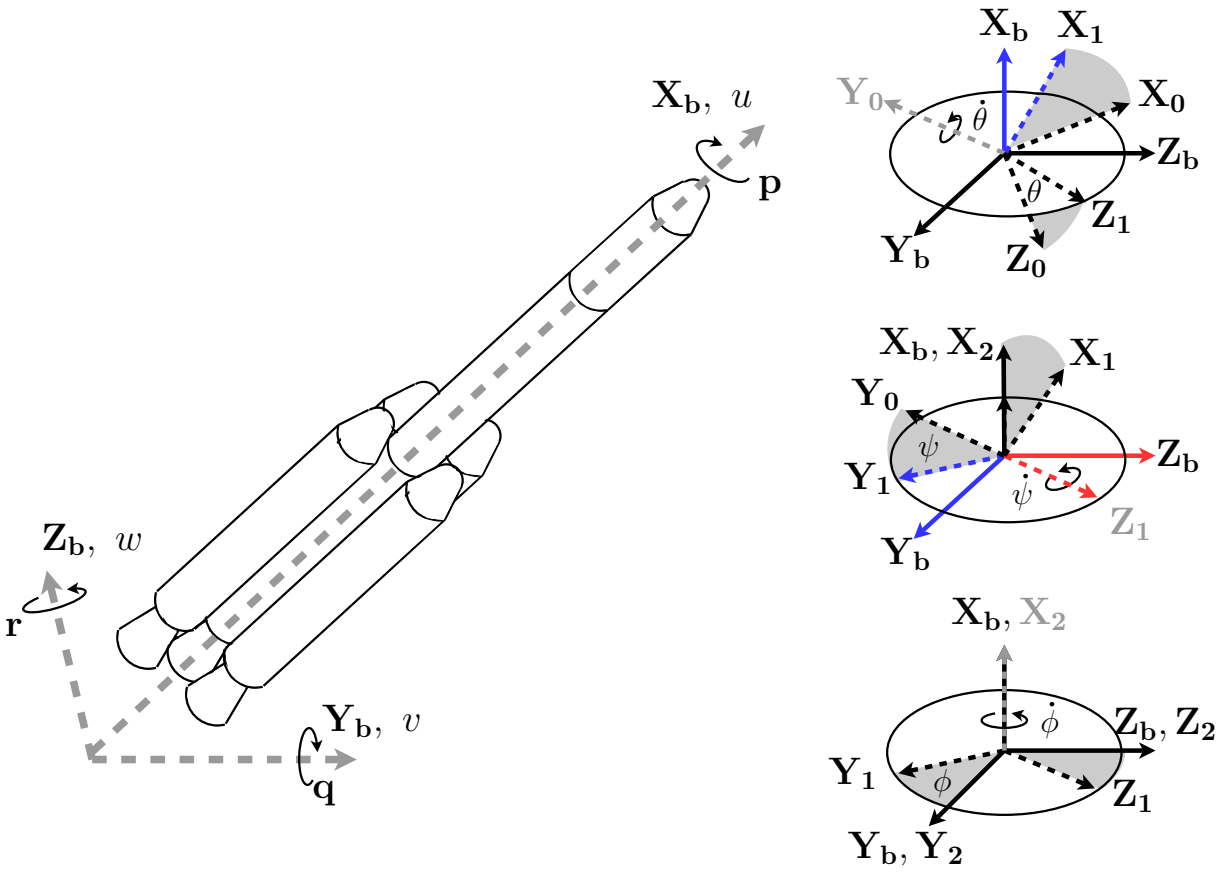

The set of axes $\{X_0, Y_0, Z_0\}$ represents the inertial system and $\{X_b, Y_b, Z_b\}$ the body system. The planes formed by the coloured pairs of axes are perpendicular to the axis of the next frame rotation.

Figure A.1 - Transformation between systems of coordinate axes of the VLS vehicle.

Remarks:

- The equation for $\dot{u}$ is given in the reference (KIENITZ; MOREIRA, 1993) but not in (OLIVA; LEITE FILHO, 2000)) where, according to the authors, "*it is not necessary because there is no thrust control*".

- In the reference (OLIVA; LEITE FILHO, 2000), some coefficients are repeated (*e.g.,* $C_{n\alpha}$ in the $\dot{v}$ equation should be $C_{n\beta}$, as shown in (KIENITZ; MOREIRA, 1993)), probably due to a presumed equivalence between the pitch and yaw planes of manoeuvring.

- The Coriolis forces do not appear in the reference (KIENITZ; MOREIRA, 1993) (but they are shown in (OLIVA; LEITE FILHO, 2000), although as an approximation compared with the mathematical model (MOREIRA; CARRIJO, 1995)). The Coriolis moments appear in both references, as approximations compared with (MOREIRA; CARRIJO, 1995). For both force and moments, the reference (OLIVA; LEITE FILHO, 2000) has a little disagreement with (MOREIRA; CARRIJO, 1995), because the latter includes the angular velocities into the Coriolis terms.

- The reference (KIENITZ; MOREIRA, 1993) takes into account the disturbance input (wind components in Y_b and Z_b axes), but (OLIVA; LEITE FILHO, 2000) does not.

Here, for the sake of completeness, one will firstly adopt the full set of equations ($\dot{u}$ included) and add the Coriolis terms and the disturbance inputs, substituting some expressions by coefficients (as named by (KIENITZ; MOREIRA, 1993)) and rearranging. Also, the occurrences of the single variable F_E in (OLIVA; LEITE FILHO, 2000) will be replaced by the individual components F_{Ex}, F_{Ey} and F_{Ez}. The nomenclature of the variables was mostly kept. Finally, one arrives at the definitive set of the VLS non-linear equations, as seen in the Eq. A.2.

$$\dot{u} = -\frac{C_{x0}\ P_d\ S_{ref}}{m} + \frac{F_{Ex}}{m} + v\ r - w\ q - g\cos(\theta)\cos(\psi) \tag{A.2a}$$

$$\dot{v} = -Y_\beta\ \beta + Y_{\beta y}\ \beta_y - \left(\frac{2\ \dot{m}\ x_e}{m} + u\right) r + w\ p - g\sin(\theta)\sin(\phi) + g\cos(\theta)\sin(\psi)\cos(\phi) \tag{A.2b}$$

$$\dot{w} = -Z_\alpha\ \alpha + Z_{\beta z}\ \beta_z + \left(\frac{2\ \dot{m}\ x_e}{m} + u\right) q - v\ p - g\sin(\theta)\cos(\phi) - g\cos(\theta)\sin(\psi)\sin(\phi) \tag{A.2c}$$

$$\dot{p} = -L_p\ p + \frac{(I_{yy} - I_{zz})}{I_{xx}}\ q\ r + L_{\beta x}\ \beta_r \tag{A.2d}$$

$$\dot{q} = M_\alpha\ \alpha - M_{\beta z}\ \beta_z - M_q\ q - \frac{(I_{xx} - I_{zz})}{I_{yy}}\ p\ r \tag{A.2e}$$

$$\dot{r} = -N_\beta\ \beta + N_{\beta y}\ \beta_y - N_r\ r + \frac{(I_{xx} - I_{yy})}{I_{zz}}\ p\ q \tag{A.2f}$$

$$\dot{\theta} = \frac{\cos(\phi)}{\cos(\psi)}\ q - \frac{\sin(\phi)}{\cos(\psi)}\ r \tag{A.2g}$$

$$\dot{\psi} = \sin(\phi)\ q + \cos(\phi)\ r \tag{A.2h}$$

$$\dot{\phi} = p - \tan(\psi)\cos(\phi)\ q + \tan(\psi)\sin(\phi)\ r \tag{A.2i}$$

with:

$Y_\beta = \dfrac{C_{n\beta}\ P_d\ S_{ref}}{m}$, $Y_{\beta y} = \dfrac{F_{Ey}}{m}$, $Z_\alpha = \dfrac{C_{n\alpha}\ P_d\ S_{ref}}{m}$, $Z_{\beta z} = \dfrac{F_{Ez}}{m}$, $L_{\beta x} = \dfrac{l_{cx}\ F_{Ex}}{I_{xx}}$,

$L_p = \left(\dfrac{C_{lp}\ P_d\ S_{ref}\ D_{ref}^2}{2\ u\ I_{xx}} + \dfrac{\dot{I}_{xx}}{I_{xx}}\right)$, $M_\alpha = \dfrac{l_{ax}\ C_{n\alpha}\ P_d\ S_{ref}}{I_{yy}}$, $M_{\beta z} = \dfrac{l_{cx}\ F_{Ez}}{I_{yy}}$,

$M_q = \left(\dfrac{C_{mq}\ P_d\ S_{ref}\ D_{ref}^2}{2\ u\ I_{yy}} + \dfrac{\dot{I}_{yy}}{I_{yy}} - \dfrac{\dot{m}\ x_e^2}{I_{yy}}\right)$, $N_\beta = \dfrac{l_{ax}\ C_{n\beta}\ P_d\ S_{ref}}{I_{zz}}$, $N_{\beta y} = \dfrac{l_{cx}\ F_{Ey}}{I_{zz}}$,

$N_r = \left(\dfrac{C_{nr}\ P_d\ S_{ref}\ D_{ref}^2}{2\ u\ I_{zz}} + \dfrac{\dot{I}_{zz}}{I_{zz}} - \dfrac{\dot{m}\ x_e^2}{I_{zz}}\right)$, $\beta = \tan^{-1}\left(\dfrac{v - v_v}{u}\right)$, $\alpha = \tan^{-1}\left(\dfrac{w - w_v}{u}\right)$

where:

u is the velocity component in the axis X_b.

x_e is the length of the gases exhaustion arm ($\approx l_{cx}$).

F_{Ex}, F_{Ey}, F_{Ez} are the thrust force components in the axes X_b, Y_b, Z_b.

C_{x0} is the coefficient of aerodynamic drag.

$C_{n\beta}$ is the derivative of the aerodynamic normal force relative to the slipping lateral angle.

β, α are the slipping lateral angle and the attack angle.
v_v, w_v are the wind components in the axes Y_b, Z_b.

A.3 Rigid body linear models of the VLS launch vehicle.

In this section, the VLS linear coupled model and the decoupled ones (for each manoeuvring plane) will be presented and inspected.

A.3.1 Numerical data.

The numerical data used in this work are shown in the Table A.1, associated with the flight time interval $t_{max} \pm 1[s]$, where t_{max} is the instant of time when the aerodynamic pressure P_d is maximal.

A.3.2 Rigid body linear coupled model.

Regarding the full set of non-linear equations of the VLS launch vehicle (Eq. A.2):

- The longitudinal velocity u can be viewed as a known time-varying parameter U, because the thrust force is function of the engines energy profiles, which are known. Therefore, Eq. A.2a is discarded, and the variable u is substituted by the parameter U in the remaining equations.

- Due to the large value of U, the small angle approximation is suitable[1] to the angles β and α.

Now, one rewrites the full set of the rigid body non-linear equations, resulting in the Eq. A.3:

[1]Small angle approximation: $tan(x) \approx x$ and $tan^{-1}(x) \approx x$.

Table A.1 - Parameters of the VLS model around $t_{max} \pm 1[s]$. Units in MKS, angles in radians.

Parameter	Value @			Δ[%]	
	$t_{max} - 1$[s]	$t_{max}[s]$	$t_{max} + 1$[s]	$t_{max} - 1$[s]	$t_{max} + 1$[s]
$\bar{Y}_\beta$	48.9809	48.8415	48.4431	0.29	-0.82
$\bar{Y}_{\beta y}$	20.7997	21.0547	21.4026	-1.2	1.7
$\bar{Z}_\alpha$	48.9809	48.8415	48.4431	0.29	-0.82
$\bar{Z}_{\beta z}$	20.1978	20.5001	20.8069	-1.5	1.5
$\bar{L}_p$	0.10602	0.098859	0.091059	7.2	-7.9
$\bar{L}_{\beta x}$	59.4865	61.0492	62.8248	-2.6	2.9
$\bar{M}_\alpha$	4.1586	4.077	3.9895	2	-2.1
$\bar{M}_{\beta z}$	-7.3075	-7.3734	-7.4377	-0.89	0.87
$\bar{M}_q$	0.012673	0.013955	0.01539	-9.2	10
$\bar{N}_\beta$	4.1543	4.0726	3.9852	2	-2.1
$\bar{N}_\beta y$	-7.5174	-7.5648	-7.6423	-0.63	1
$\bar{N}_r$	0.0073421	0.0087795	0.01038	-16	18
$\bar{u} = \bar{U}$	621.3418	645.5643	670.4573	-3.8	3.9
$\bar{v}$	-0.0017395	-0.0016109	-0.0014967	8	-7.1
$\bar{w}$	1.8281	1.9034	1.9867	-4	4.4
$\bar{p}$	0	0	0	0	0
$\bar{q}$	-0.0047798	-0.0046546	-0.0045338	2.7	-2.6
$\bar{r}$	0	0	0	0	0
$\bar{\theta}$	-0.33573	-0.3405	-0.34514	-1.4	1.4
$\bar{\psi}$	0	0	0	0	0
$\bar{\phi}$	0	0	0	0	0
$\dot{\bar{\theta}}$	-0.0047798	-0.0046546	-0.0045338	2.7	-2.6
$\dot{\bar{\psi}}$	0	0	0	0	0
$\dot{\bar{\phi}}$	0	0	0	0	0
$\bar{g}$	9.7765	9.7747	9.7728	0.019	-0.019
$\bar{m}$	31212.378	30713.478	30216.475	1.6	-1.6
$\dot{\bar{m}}$	-500.0652	-497.7389	-496.2699	0.47	-0.3
$\bar{x}_e$	-5.0416	-5.0641	-5.0867	-0.44	0.45
$\bar{I}_{xx}$	24458.292	23770.038	23082.511	2.9	-2.9
$\bar{I}_{yy}$	434937.31	432429.63	429980.65	0.58	-0.57
$\bar{I}_{zz}$	435391.3	432893.18	430453.18	0.58	-0.56
$\bar{K}_{B,1}$	-16.2279	-16.3397	-16.5089	-0.68	1
$\bar{K}_{B,2}$	12.694	12.7706	12.8922	-0.6	0.95
$\bar{\omega}_{B,1}$	29.4187	29.5478	29.6768	-0.44	0.44
$\bar{\omega}_{B,2}$	80.2636	80.4232	80.5829	-0.2	0.2
ζ_M	0.002	0.002	0.002	-	-

$$\dot{v} = -\frac{Y_\beta}{U}\ v + \frac{Y_\beta}{U}\ v_v + Y_{\beta y}\ \beta_y - \left(\frac{2\ \dot{m}\ x_e}{m} + U\right) r + w\ p - g\sin(\theta)\sin(\phi) + g\cos(\theta)\sin(\psi)\cos(\phi) \tag{A.3a}$$

$$\dot{w} = -\frac{Z_\alpha}{U}\ w + \frac{Z_\alpha}{U}\ w_v + Z_{\beta z}\ \beta_z + \left(\frac{2\ \dot{m}\ x_e}{m} + U\right) q - v\ p - g\sin(\theta)\cos(\phi) - g\cos(\theta)\sin(\psi)\sin(\phi) \tag{A.3b}$$

$$\dot{p} = -L_p\ p + \frac{(I_{yy} - I_{zz})}{I_{xx}}\ q\ r + L_{\beta x}\ \beta_r \tag{A.3c}$$

$$\dot{q} = \frac{M_\alpha}{U}\ w - \frac{M_\alpha}{U}\ w_v - M_{\beta z}\ \beta_z - M_q\ q - \frac{(I_{xx} - I_{zz})}{I_{yy}}\ p\ r \tag{A.3d}$$

$$\dot{r} = -\frac{N_\beta}{U}\ v + \frac{N_\beta}{U}\ v_v + N_{\beta y}\ \beta_y - N_r\ r + \frac{(I_{xx} - I_{yy})}{I_{zz}}\ p\ q \tag{A.3e}$$

$$\dot{\theta} = \frac{\cos(\phi)}{\cos(\psi)}\ q - \frac{\sin(\phi)}{\cos(\psi)}\ r \tag{A.3f}$$

$$\dot{\psi} = \sin(\phi)\ q + \cos(\phi)\ r \tag{A.3g}$$

$$\dot{\phi} = p - \tan(\psi)\cos(\phi)\ q + \tan(\psi)\sin(\phi)\ r \tag{A.3h}$$

with:
$Y_\beta = \dfrac{C_{n\beta}\ P_d\ S_{ref}}{m},\ Y_{\beta y} = \dfrac{F_{Ey}}{m},\ Z_\alpha = \dfrac{C_{n\alpha}\ P_d\ S_{ref}}{m},\ Z_{\beta z} = \dfrac{F_{Ez}}{m},\ L_{\beta x} = \dfrac{l_{cx}\ F_{Ex}}{I_{xx}},$
$L_p = \left(\dfrac{C_{lp}\ P_d\ S_{ref}\ D_{ref}^2}{2\ U\ I_{xx}} + \dfrac{\dot{I}_{xx}}{I_{xx}}\right),\ M_\alpha = \dfrac{l_{ax}\ C_{n\alpha}\ P_d\ S_{ref}}{I_{yy}},\ M_{\beta z} = \dfrac{l_{cx}\ F_{Ez}}{I_{yy}},$
$M_q = \left(\dfrac{C_{mq}\ P_d\ S_{ref}\ D_{ref}^2}{2\ U\ I_{yy}} + \dfrac{\dot{I}_{yy}}{I_{yy}} - \dfrac{\dot{m}\ x_e^2}{I_{yy}}\right),\ N_\beta = \dfrac{l_{ax}\ C_{n\beta}\ P_d\ S_{ref}}{I_{zz}},\ N_{\beta y} = \dfrac{l_{cx}\ F_{Ey}}{I_{zz}},$
$N_r = \left(\dfrac{C_{nr}\ P_d\ S_{ref}\ D_{ref}^2}{2\ U\ I_{zz}} + \dfrac{\dot{I}_{zz}}{I_{zz}} - \dfrac{\dot{m}\ x_e^2}{I_{zz}}\right)$

The linearisation process is found in the section A.6, producing the Eq. A.4:

$$\dot{\mathbf{x}} = \mathbf{A}\ \mathbf{x} + \mathbf{B_u}\ \mathbf{u} + \mathbf{B_d}\ \mathbf{d},\ \mathbf{x} = [w\ q\ \theta\ v\ r\ \psi\ p\ \phi\ ]^T,\ \mathbf{u} = [\beta_z\ \beta_y\ \beta_r]^T \text{ and } \mathbf{d} = [v_v\ w_v]^T \tag{A.4}$$

with:

$$\mathbf{A} = \begin{bmatrix} -\frac{\bar{Z}_\alpha}{\bar{U}} & \frac{2\ \dot{\bar{m}}\ \bar{x}_e}{\bar{m}} + \bar{U} & A_{13} & -\bar{p} & 0 & A_{16} & -\bar{v} & A_{18} \\ \frac{\bar{M}_\alpha}{\bar{U}} & -\bar{M}_q & 0 & 0 & -\frac{(\bar{I}_{xx} - \bar{I}_{zz})}{\bar{I}_{yy}}\ \bar{p} & 0 & -\frac{(\bar{I}_{xx} - \bar{I}_{zz})}{\bar{I}_{yy}}\ \bar{r} & 0 \\ 0 & \frac{\cos(\bar{\phi})}{\cos(\bar{\psi})} & 0 & 0 & -\frac{\sin(\bar{\phi})}{\cos(\bar{\psi})} & A_{36} & 0 & A_{38} \\ \bar{p} & 0 & A_{43} & -\frac{\bar{Y}_\beta}{\bar{U}} & -\left(\frac{2\ \dot{\bar{m}}\ \bar{x}_e}{\bar{m}} + \bar{U}\right) & A_{46} & \bar{w} & A_{48} \\ 0 & \frac{(\bar{I}_{xx} - \bar{I}_{yy})}{\bar{I}_{zz}}\ \bar{p} & 0 & -\frac{\bar{N}_\beta}{\bar{U}} & -\bar{N}_r & 0 & \frac{(\bar{I}_{xx} - \bar{I}_{yy})}{\bar{I}_{zz}}\ \bar{q} & 0 \\ 0 & \sin(\bar{\phi}) & 0 & 0 & \cos(\bar{\phi}) & 0 & 0 & A_{68} \\ 0 & \frac{(\bar{I}_{yy} - \bar{I}_{zz})}{\bar{I}_{xx}}\bar{r} & 0 & 0 & \frac{(\bar{I}_{yy} - \bar{I}_{zz})}{\bar{I}_{xx}}\ \bar{q} & 0 & -\bar{L}_p & 0 \\ 0 & -\tan(\bar{\psi})\cos(\bar{\phi}) & 0 & 0 & \tan(\bar{\psi})\sin(\bar{\phi}) & A_{86} & 1 & A_{88} \end{bmatrix},$$

$$\mathbf{B}_u = \begin{bmatrix} \bar{Z}_{\beta z} & 0 & 0 \\ -\bar{M}_{\beta z} & 0 & 0 \\ 0 & 0 & 0 \\ 0 & \bar{Y}_{\beta y} & 0 \\ 0 & \bar{N}_{\beta y} & 0 \\ 0 & 0 & 0 \\ 0 & 0 & \bar{L}_{\beta x} \\ 0 & 0 & 0 \end{bmatrix}, \quad \mathbf{B}_d = \begin{bmatrix} 0 & \frac{\bar{Z}_\alpha}{\bar{U}} \\ 0 & -\frac{\bar{M}_\alpha}{\bar{U}} \\ 0 & 0 \\ \frac{\bar{Y}_\beta}{\bar{U}} & 0 \\ \frac{\bar{N}_\beta}{\bar{U}} & 0 \\ 0 & 0 \\ 0 & 0 \\ 0 & 0 \end{bmatrix}$$

where:

$$A_{13} = -\bar{g}\ \cos(\bar{\theta})\ \cos(\bar{\phi}) + \bar{g}\sin(\bar{\theta})\sin(\bar{\psi})\sin(\bar{\phi}),\ A_{16} = -\bar{g}\cos(\bar{\theta})\cos(\bar{\psi})\sin(\bar{\phi}),$$
$$A_{18} = \bar{g}\ \sin(\bar{\theta})\ \sin(\bar{\phi}) - \bar{g}\cos(\bar{\theta})\sin(\bar{\psi})\cos(\bar{\phi}),\ A_{36} = \frac{\cos(\bar{\phi})\ \bar{q} - \sin(\bar{\phi})\ \bar{r}}{\sqrt{1-\bar{\psi}^2}},$$
$$A_{38} = \frac{-\sin(\bar{\phi})\ \bar{q} - \cos(\bar{\phi})\ \bar{r}}{\cos(\bar{\psi})},\ A_{43} = -\bar{g}\ \cos(\bar{\theta})\ \sin(\bar{\phi}) - \bar{g}\sin(\bar{\theta})\sin(\bar{\psi})\cos(\bar{\phi}),$$
$$A_{46} = \bar{g}\cos(\bar{\theta})\cos(\bar{\psi})\cos(\bar{\phi}),\ A_{48} = -\bar{g}\ \sin(\bar{\theta})\ \cos(\bar{\phi}) - \bar{g}\cos(\bar{\theta})\sin(\bar{\psi})\sin(\bar{\phi}),$$
$$A_{68} = \cos(\bar{\phi})\ \bar{q} - \sin(\bar{\phi})\ \bar{r},\ A_{86} = \frac{-\cos(\bar{\phi})\ \bar{q} + \sin(\bar{\phi})\ \bar{r}}{\cos^2(\bar{\psi})},$$
$$A_{88} = \tan(\bar{\psi})\left[\sin(\bar{\phi})\ \bar{q} + \cos(\bar{\phi})\ \bar{r}\right]$$

Remarks:

- The reference (OLIVA; LEITE FILHO, 2000) does not include the terms

A_{36}, A_{38}, A_{68}, A_{86}, and A_{88} in the state space description of the linear coupled model of the VLS launch vehicle.

- The reference (KIENITZ; MOREIRA, 1993) considers only decoupled models for all manoeuvring planes in the design stage. The linear coupled model is not presented. The non-linear model is employed in more realistic simulations during the final analysis phases.

The matrices $\mathbf{A}$, $\mathbf{B}_u$ and $\mathbf{B}_d$ in the Eq. A.4 assume the following values at t_{max}:

$$\mathbf{A} = \begin{bmatrix} -0.0757 & 645.7285 & -9.2135 & 0 & 0 & 0 & 0.0016 & 0 \\ 0.0063 & -0.0140 & 0 & 0 & 0 & 0 & 0 & 0 \\ 0 & 1.0000 & 0 & 0 & 0 & -0.0047 & 0 & 0 \\ 0 & 0 & 0 & -0.0757 & -645.7285 & 9.2135 & 1.9034 & 3.2643 \\ 0 & 0 & 0 & -0.0063 & -0.0088 & 0 & 0.0044 & 0 \\ 0 & 0 & 0 & 0 & 1.0000 & 0 & 0 & -0.0047 \\ 0 & 0 & 0 & 0 & 0.0001 & 0 & -0.0989 & 0 \\ 0 & 0 & 0 & 0 & 0 & 0.0047 & 1.0000 & 0 \end{bmatrix},$$

$$\mathbf{B}_u = \begin{bmatrix} 20.5001 & 0 & 0 \\ 7.3734 & 0 & 0 \\ 0 & 0 & 0 \\ 0 & 21.0547 & 0 \\ 0 & -7.5648 & 0 \\ 0 & 0 & 0 \\ 0 & 0 & 61.0492 \\ 0 & 0 & 0 \end{bmatrix}, \quad \mathbf{B}_d = \begin{bmatrix} 0 & 0.0757 \\ 0 & -0.0063 \\ 0 & 0 \\ 0.0757 & 0 \\ 0.0063 & 0 \\ 0 & 0 \\ 0 & 0 \\ 0 & 0 \end{bmatrix}$$

A.3.3 Rigid body linear decoupled models.

It is easier to design the control system if the three planes of manoeuvring are decoupled, which is accomplished when the angle ϕ and the angular velocity p are small enough[2] (KIENITZ; MOREIRA, 1993). In such case, the Eq. A.5 holds:

[2]Verify the elements outside the blocks $A_{1-3,1-3}$, $A_{4-6,4-6}$ and $A_{7-8,7-8}$ of the matrix $\mathbf{A}$ (Eq. A.4) and the product $\mathbf{Ax}$.

$$\begin{bmatrix} \dot{w} \\ \dot{q} \\ \dot{\theta} \end{bmatrix} \approx \begin{bmatrix} -\frac{\bar{Z}_\alpha}{\bar{U}} & \frac{2\ \bar{\dot{m}}\ \bar{x}_e}{\bar{m}} + \bar{U} & -\bar{g}\cos(\bar{\theta}) \\ \frac{\bar{M}_\alpha}{\bar{U}} & -\bar{M}_q & 0 \\ 0 & 1 & 0 \end{bmatrix} \begin{bmatrix} w \\ q \\ \theta \end{bmatrix} + \begin{bmatrix} \bar{Z}_{\beta z} \\ -\bar{M}_{\beta z} \\ 0 \end{bmatrix} \beta_z + \begin{bmatrix} \frac{\bar{Z}_\alpha}{\bar{U}} \\ -\frac{\bar{M}_\alpha}{\bar{U}} \\ 0 \end{bmatrix} w_v \tag{A.5a}$$

$$\begin{bmatrix} \dot{v} \\ \dot{r} \\ \dot{\psi} \end{bmatrix} \approx \begin{bmatrix} -\frac{\bar{Y}_\beta}{\bar{U}} & -\left(\frac{2\ \bar{\dot{m}}\ \bar{x}_e}{\bar{m}} + \bar{U}\right) & \bar{g}\cos(\bar{\theta}) \\ -\frac{\bar{N}_\beta}{\bar{U}} & -N_r & 0 \\ 0 & 1 & 0 \end{bmatrix} \begin{bmatrix} v \\ r \\ \psi \end{bmatrix} + \begin{bmatrix} \bar{Y}_{\beta y} \\ \bar{N}_{\beta y} \\ 0 \end{bmatrix} \beta_y + \begin{bmatrix} \frac{\bar{Y}_\beta}{\bar{U}} \\ \frac{\bar{N}_\beta}{\bar{U}} \\ 0 \end{bmatrix} v_v \tag{A.5b}$$

$$\begin{bmatrix} \dot{p} \\ \dot{\phi} \end{bmatrix} \approx \begin{bmatrix} -\bar{L}_p & 0 \\ 1 & 0 \end{bmatrix} \begin{bmatrix} p \\ \phi \end{bmatrix} + \begin{bmatrix} \bar{L}_{\beta x} \\ 0 \end{bmatrix} \beta_r \tag{A.5c}$$

A.3.4 Transfer functions of the rigid body decoupled dynamics.

The transfer functions associated to the state-space descriptions of the Eq. A.5 are shown in the Eq. A.6.

$$G_{w\beta}(s) = \frac{w(s)}{\beta_z(s)} = \frac{\bar{Z}_{\beta z}s^2 + \left[\bar{Z}_{\beta z}\bar{M}_q - \bar{M}_{\beta z}\left(\bar{U} + \frac{2\bar{m}\bar{x}_e}{\bar{m}}\right)\right]s + \bar{M}_{\beta z}\ \bar{g}\ \cos(\bar{\theta})}{s^3 + (\bar{M}_q + \frac{\bar{Z}_\alpha}{\bar{U}})\ s^2 + \left[\frac{1}{\bar{U}}\left(\bar{Z}_\alpha\bar{M}_q - \frac{2\bar{M}_\alpha\bar{m}\bar{x}_e}{\bar{m}}\right) - \bar{M}_\alpha\right]s + \frac{\bar{M}_\alpha\bar{g}}{\bar{U}}\cos(\bar{\theta})} \tag{A.6a}$$

$$G_{wd}(s) = \frac{w(s)}{w_v(s)} = \frac{\frac{\bar{M}_\alpha}{\bar{U}}s^2 - \left[\frac{1}{\bar{U}}\left(\bar{Z}_\alpha\bar{M}_q + \frac{2\bar{M}_\alpha\bar{m}\bar{x}_e}{\bar{m}}\right) + \bar{M}_\alpha\right]s + \bar{M}_{\beta z}\ \bar{g}\ \cos(\bar{\theta})}{s^3 + (\bar{M}_q + \frac{\bar{Z}_\alpha}{\bar{U}})\ s^2 + \left[\frac{1}{\bar{U}}\left(\bar{Z}_\alpha\bar{M}_q - \frac{2\bar{M}_\alpha\bar{m}\bar{x}_e}{\bar{m}}\right) - \bar{M}_\alpha\right]s + \frac{\bar{M}_\alpha\bar{g}}{\bar{U}}\cos(\bar{\theta})} \tag{A.6b}$$

$$G_{q\beta}(s) = \frac{q(s)}{\beta_z(s)} = \frac{\left[-\bar{M}_{\beta z}s + \frac{1}{\bar{U}}\left(\bar{M}_\alpha\bar{Z}_{\beta z} - \bar{Z}_\alpha\bar{M}_{\beta z}\right)\right]s}{s^3 + (\bar{M}_q + \frac{\bar{Z}_\alpha}{\bar{U}})\ s^2 + \left[\frac{1}{\bar{U}}\left(\bar{Z}_\alpha\bar{M}_q - \frac{2\bar{M}_\alpha\bar{m}\bar{x}_e}{\bar{m}}\right) - \bar{M}_\alpha\right]s + \frac{\bar{M}_\alpha\bar{g}}{\bar{U}}\cos(\bar{\theta})} \tag{A.6c}$$

$$G_{qd}(s) = \frac{q(s)}{w_v(s)} = \frac{-\frac{\bar{M}_\alpha}{\bar{U}}s^2}{s^3 + (\bar{M}_q + \frac{\bar{Z}_\alpha}{\bar{U}})\ s^2 + \left[\frac{1}{\bar{U}}\left(\bar{Z}_\alpha\bar{M}_q - \frac{2\bar{M}_\alpha\bar{m}\bar{x}_e}{\bar{m}}\right) - \bar{M}_\alpha\right]s + \frac{\bar{M}_\alpha\bar{g}}{\bar{U}}\cos(\bar{\theta})} \tag{A.6d}$$

$$G_{\theta\beta}(s) = \frac{\theta(s)}{\beta_z(s)} = \frac{-\bar{M}_{\beta z}s + \frac{1}{\bar{U}}\left(\bar{M}_\alpha\bar{Z}_{\beta z} - \bar{Z}_\alpha\bar{M}_{\beta z}\right)}{s^3 + (\bar{M}_q + \frac{\bar{Z}_\alpha}{\bar{U}})\ s^2 + \left[\frac{1}{\bar{U}}\left(\bar{Z}_\alpha\bar{M}_q - \frac{2\bar{M}_\alpha\bar{m}\bar{x}_e}{\bar{m}}\right) - \bar{M}_\alpha\right]s + \frac{\bar{M}_\alpha\bar{g}}{\bar{U}}\cos(\bar{\theta})} \tag{A.6e}$$

$$G_{\theta d}(s) = \frac{\theta(s)}{w_v(s)} = \frac{-\frac{\bar{M}_\alpha}{\bar{U}}s}{s^3 + (\bar{M}_q + \frac{\bar{Z}_\alpha}{\bar{U}})\ s^2 + \left[\frac{1}{\bar{U}}\left(\bar{Z}_\alpha\bar{M}_q - \frac{2\bar{M}_\alpha\bar{m}\bar{x}_e}{\bar{m}}\right) - \bar{M}_\alpha\right]s + \frac{\bar{M}_\alpha\bar{g}}{\bar{U}}\cos(\bar{\theta})} \tag{A.6f}$$

$$G_{v\beta}(s) = \frac{v(s)}{\beta_y(s)} = \frac{\bar{Y}_{\beta y}s^2 + \left[\bar{Y}_{\beta y}\bar{N}_r - \bar{N}_{\beta y}\left(\bar{U} + \frac{2\bar{m}\bar{x}_e}{\bar{m}}\right)\right]s + \bar{N}_{\beta y}\ \bar{g}\ \cos(\bar{\theta})}{s^3 + (\bar{N}_r + \frac{\bar{Y}_\beta}{\bar{U}})\ s^2 + \left[\frac{1}{\bar{U}}\left(\bar{Y}_\beta\bar{N}_r - \frac{2\bar{N}_\beta\bar{m}\bar{x}_e}{\bar{m}}\right) - \bar{N}_\beta\right]s + \frac{\bar{N}_\beta\bar{g}}{\bar{U}}\cos(\bar{\theta})} \tag{A.6g}$$

$$G_{vd}(s) = \frac{v(s)}{v_v(s)} = \frac{\frac{\bar{Y}_\beta}{\bar{U}}s^2 + \left[\frac{1}{\bar{U}}\left(\bar{Y}_\beta\bar{N}_r - \frac{2\bar{N}_\beta\bar{m}\bar{x}_e}{\bar{m}}\right) - \bar{N}_\beta\right]s + \bar{N}_{\beta y}\ \bar{g}\ \cos(\bar{\theta})}{s^3 + (\bar{N}_r + \frac{\bar{Y}_\beta}{\bar{U}})\ s^2 + \left[\frac{1}{\bar{U}}\left(\bar{Y}_\beta\bar{N}_r - \frac{2\bar{N}_\beta\bar{m}\bar{x}_e}{\bar{m}}\right) - \bar{N}_\beta\right]s + \frac{\bar{N}_\beta\bar{g}}{\bar{U}}\cos(\bar{\theta})} \tag{A.6h}$$

$$G_{r\beta}(s) = \frac{r(s)}{\beta_y(s)} = \frac{\left[\bar{N}_{\beta y}s + \frac{1}{\bar{U}}\left(\bar{Y}_\beta\bar{N}_{\beta y} - \bar{N}_\beta\bar{Y}_{\beta y}\right)\right]s}{s^3 + (\bar{N}_r + \frac{\bar{Y}_\beta}{\bar{U}})\ s^2 + \left[\frac{1}{\bar{U}}\left(\bar{Y}_\beta\bar{N}_r - \frac{2\bar{N}_\beta\bar{m}\bar{x}_e}{\bar{m}}\right) - \bar{N}_\beta\right]s + \frac{\bar{N}_\beta\bar{g}}{\bar{U}}\cos(\bar{\theta})} \tag{A.6i}$$

$$G_{rd}(s) = \frac{r(s)}{v_v(s)} = \frac{-\frac{\bar{N}_\beta}{\bar{U}}s^2}{s^3 + (\bar{N}_r + \frac{\bar{Y}_\beta}{\bar{U}})\ s^2 + \left[\frac{1}{\bar{U}}\left(\bar{Y}_\beta\bar{N}_r - \frac{2\bar{N}_\beta\bar{m}\bar{x}_e}{\bar{m}}\right) - \bar{N}_\beta\right]s + \frac{\bar{N}_\beta\bar{g}}{\bar{U}}\cos(\bar{\theta})} \tag{A.6j}$$

$$G_{\psi\beta}(s) = \frac{\psi(s)}{\beta_y(s)} = \frac{\bar{N}_{\beta y}s + \frac{1}{\bar{U}}\left(\bar{Y}_\beta\bar{N}_{\beta y} - \bar{N}_\beta\bar{Y}_{\beta y}\right)}{s^3 + (\bar{N}_r + \frac{\bar{Y}_\beta}{\bar{U}})\ s^2 + \left[\frac{1}{\bar{U}}\left(\bar{Y}_\beta\bar{N}_r - \frac{2\bar{N}_\beta\bar{m}\bar{x}_e}{\bar{m}}\right) - \bar{N}_\beta\right]s + \frac{\bar{N}_\beta\bar{g}}{\bar{U}}\cos(\bar{\theta})} \tag{A.6k}$$

$$G_{\psi d}(s) = \frac{\psi(s)}{v_v(s)} = \frac{-\frac{\bar{N}_\beta}{\bar{U}}s}{s^3 + (\bar{N}_r + \frac{\bar{Y}_\beta}{\bar{U}})\ s^2 + \left[\frac{1}{\bar{U}}\left(\bar{Y}_\beta\bar{N}_r - \frac{2\bar{N}_\beta\bar{m}\bar{x}_e}{\bar{m}}\right) - \bar{N}_\beta\right]s + \frac{\bar{N}_\beta\bar{g}}{\bar{U}}\cos(\bar{\theta})} \tag{A.6l}$$

$$G_{p\beta}(s) = \frac{p(s)}{\beta_r(s)} = \frac{\bar{L}_{\beta x}}{s + \bar{L}_p} \tag{A.6m}$$

$$G_{\phi\beta}(s) = \frac{\phi(s)}{\beta_r(s)} = \frac{\bar{L}_{\beta x}}{\left(s + \bar{L}_p\right)s} \tag{A.6n}$$

A.4 Full linear models.

This section presents the rigid body models of the launch vehicle added to the bending and torsional modes.

A.4.1 Bending and torsional modes.

These modes are described by the following differential equations for pitch (bending), yaw (bending) and roll (torsional) planes:

$$\ddot{\theta}_{B,i}(t) = K_{\theta,i}\ \beta_z(t) - 2\zeta_{\theta,i}\ \omega_{\theta,i}\ \dot{\theta}(t) - \omega^2_{\theta,i}\ \theta(t) \tag{A.7a}$$

$$\ddot{\psi}_{B,i}(t) = K_{\psi,i}\ \beta_y(t) - 2\zeta_{\psi,i}\ \omega_{\psi,i}\ \dot{\psi}(t) - \omega^2_{\psi,i}\ \psi(t) \tag{A.7b}$$

$$\ddot{\phi}_{T,i}(t) = K_{\phi,i}\ \beta_r(t) - 2\zeta_{\phi,i}\ \omega_{\phi,i}\ \dot{\phi}(t) - \omega^2_{\phi,i}\ \phi(t) \tag{A.7c}$$

where i is the number of the mode; for the VLS launch vehicle, torsional modes and all bending modes but the 1^{st} and the 2^{nd} are neglected due to their high normal frequency ($\omega_{\theta,i},\ \omega_{\psi,i},\ \omega_{\phi,i}$), very above the control cut-off frequency. Furthermore, due to the symmetry of the launch vehicle, $K_{\theta,i} = K_{\psi,i} \triangleq K_{B,i}$ and $\omega_{\theta,i} = \omega_{\psi,i} \triangleq \omega_{B,i}$. Finally, $\zeta_{\theta,i} = \zeta_{\psi,i} = \zeta_{\phi,i} \triangleq \zeta_M = 0.002\ \forall\ i$.

The generic transfer function of the last set of equations is:

$$G_{Bi}(s) = \frac{\bar{K}_{Fi}}{s^2 + 2\ \zeta_M\ \bar{\omega}_{B,i}\ s + \bar{\omega}^2_{B,i}},\ i = 1, 2 \tag{A.8}$$

A.4.2 Full linear coupled model.

Including the two first bending modes for each one of the pitch and yaw planes of manoeuvring (states $\theta_{Bi1},\ \theta_{Bi2},\ \psi_{Bi1}$ and ψ_{Bi2}) in the rigid body linear coupled model (Eq. A.4), one arrives at the Eq. A.9.

$$\dot{\mathbf{x}} = \mathbf{A}\ \mathbf{x} + \mathbf{B_u}\ \mathbf{u} + \mathbf{B_d}\ \mathbf{d}, \tag{A.9}$$

$$\mathbf{x} = [w\ q\ \theta\ \theta_{B11}\ \theta_{B12}\ \theta_{B21}\ \theta_{B22}\ v\ r\ \psi\ \psi_{B11}\ \psi_{B12}\ \psi_{B21}\ \psi_{B22}\ p\ \phi\ ]^T,$$

$$\mathbf{u} = [\beta_z\ \beta_y\ \beta_r]^T \text{ and } \mathbf{d} = [v_v\ w_v]^T$$

with:

$$\mathbf{B}_u = \begin{bmatrix} \bar{Z}_{\beta z} & 0 & 0 \\ -\bar{M}_{\beta z} & 0 & 0 \\ 0 & 0 & 0 \\ 0 & 0 & 0 \\ K_{B,1} & 0 & 0 \\ 0 & 0 & 0 \\ K_{B,2} & 0 & 0 \\ 0 & \bar{Y}_{\beta y} & 0 \\ 0 & \bar{N}_{\beta y} & 0 \\ 0 & 0 & 0 \\ 0 & 0 & 0 \\ 0 & K_{B,1} & 0 \\ 0 & 0 & 0 \\ 0 & K_{B,2} & 0 \\ 0 & 0 & \bar{L}_{\beta x} \\ 0 & 0 & 0 \end{bmatrix}, \quad \mathbf{B}_d = \begin{bmatrix} 0 & \frac{\bar{Z}_\alpha}{\bar{U}} \\ 0 & -\frac{\bar{M}_\alpha}{\bar{U}} \\ 0 & 0 \\ 0 & 0 \\ 0 & 0 \\ 0 & 0 \\ 0 & 0 \\ \frac{\bar{Y}_\beta}{\bar{U}} & 0 \\ \frac{\bar{N}_\beta}{\bar{U}} & 0 \\ 0 & 0 \\ 0 & 0 \\ 0 & 0 \\ 0 & 0 \\ 0 & 0 \\ 0 & 0 \\ 0 & 0 \end{bmatrix}, \text{ and (see next page),}$$

$$
\mathbf{A} = \begin{bmatrix}
-\frac{\bar{Z}_\alpha}{\bar{U}} & \frac{2\ \dot{\bar{m}}\ \bar{x}_e}{\bar{m}} + \bar{U} & * & 0 & 0 & 0 & 0 & -\bar{p} & 0 & * & 0 & 0 & 0 & 0 & -\bar{v} & * \\
\frac{\bar{M}_\alpha}{\bar{U}} & -\bar{M}_q & 0 & 0 & 0 & 0 & 0 & 0 & -\frac{\left(\bar{I}_{xx} - \bar{I}_{zz}\right)}{\bar{I}_{yy}}\ \bar{p} & 0 & 0 & 0 & 0 & 0 & -\frac{\left(\bar{I}_{xx} - \bar{I}_{zz}\right)}{\bar{I}_{yy}}\ \bar{r} & 0 \\
0 & \frac{\cos(\bar{\phi})}{\cos(\bar{\psi})} & 0 & 0 & 0 & 0 & 0 & 0 & -\frac{\sin(\bar{\phi})}{\cos(\bar{\psi})} & * & 0 & 0 & 0 & 0 & 0 & * \\
0 & 0 & 0 & 0 & 1 & 0 & 0 & 0 & 0 & 0 & 0 & 0 & 0 & 0 & 0 & 0 \\
0 & 0 & 0 & * & * & 0 & 0 & 0 & 0 & 0 & 0 & 0 & 0 & 0 & 0 & 0 \\
0 & 0 & 0 & 0 & 0 & 0 & 1 & 0 & 0 & 0 & 0 & 0 & 0 & 0 & 0 & 0 \\
0 & 0 & 0 & 0 & 0 & * & * & 0 & 0 & 0 & 0 & 0 & 0 & 0 & 0 & 0 \\
\bar{p} & 0 & * & 0 & 0 & 0 & 0 & -\frac{\bar{Y}_\beta}{\bar{U}} & -\left(\frac{2\ \dot{\bar{m}}\ \bar{x}_e}{\bar{m}} + \bar{U}\right) & * & 0 & 0 & 0 & 0 & \bar{w} & * \\
0 & \frac{\left(\bar{I}_{xx} - \bar{I}_{yy}\right)}{\bar{I}_{zz}}\ \bar{p} & 0 & 0 & 0 & 0 & 0 & -\frac{\bar{N}_\beta}{\bar{U}} & -\bar{N}_r & 0 & 0 & 0 & 0 & 0 & \frac{\left(\bar{I}_{xx} - \bar{I}_{yy}\right)}{\bar{I}_{zz}}\ \bar{q} & 0 \\
0 & \sin(\bar{\phi}) & 0 & 0 & 0 & 0 & 0 & 0 & \cos(\bar{\phi}) & 0 & 0 & 0 & 0 & 0 & 0 & * \\
0 & 0 & 0 & 0 & 0 & 0 & 0 & 0 & 0 & 0 & 0 & 1 & 0 & 0 & 0 & 0 \\
0 & 0 & 0 & 0 & 0 & 0 & 0 & 0 & 0 & 0 & * & * & 0 & 0 & 0 & 0 \\
0 & 0 & 0 & 0 & 0 & 0 & 0 & 0 & 0 & 0 & 0 & 0 & 1 & 0 & 0 & 0 \\
0 & 0 & 0 & 0 & 0 & 0 & 0 & 0 & 0 & 0 & 0 & 0 & 0 & * & * & 0 \\
0 & \frac{\left(\bar{I}_{yy} - \bar{I}_{zz}\right)}{\bar{I}_{xx}}\bar{r} & 0 & 0 & 0 & 0 & 0 & 0 & \frac{\left(\bar{I}_{yy} - \bar{I}_{zz}\right)}{\bar{I}_{xx}}\ \bar{q} & 0 & 0 & 0 & 0 & 0 & -\bar{L}_p & 0 \\
0 & -\tan(\bar{\psi})\cos(\bar{\phi}) & 0 & 0 & 0 & 0 & 0 & 0 & \tan(\bar{\psi})\sin(\bar{\phi}) & * & 0 & 0 & 0 & 0 & 1 & * \\
\end{bmatrix}, \text{ where:}
$$

$A_{1,3} = -\bar{g}\ \cos(\bar{\theta})\ \cos(\bar{\phi}) + \bar{g}\sin(\bar{\theta})\sin(\bar{\psi})\sin(\bar{\phi}),\ A_{1,10} = -\bar{g}\cos(\bar{\theta})\cos(\bar{\psi})\sin(\bar{\phi}),\ A_{1,16} = \bar{g}\ \sin(\bar{\theta})\ \sin(\bar{\phi}) - \bar{g}\cos(\bar{\theta})\sin(\bar{\psi})\cos(\bar{\phi}),$
$A_{3,10} = \frac{\cos(\bar{\phi})\ \bar{q} - \sin(\bar{\phi})\ \bar{r}}{\sqrt{1-\bar{\psi}^2}},\ A_{3,16} = \frac{-\sin(\bar{\phi})\ \bar{q} - \cos(\bar{\phi})\ \bar{r}}{\cos(\bar{\psi})},\ A_{5,4} = -\omega_{B,1}^2,\ A_{5,5} = -2\ \zeta_{B,1}\ \omega_{B,1},\ A_{7,6} = -\omega_{B,2}^2,\ A_{7,7} = -2\zeta_{B,2}\ \omega_{B,2},$
$A_{8,3} = -\bar{g}\ \cos(\bar{\theta})\ \sin(\bar{\phi}) - \bar{g}\sin(\bar{\theta})\sin(\bar{\psi})\cos(\bar{\phi}),\ A_{8,10} = \bar{g}\cos(\bar{\theta})\cos(\bar{\psi})\cos(\bar{\phi}),\ A_{8,16} = -\bar{g}\ \sin(\bar{\theta})\ \cos(\bar{\phi}) - \bar{g}\cos(\bar{\theta})\sin(\bar{\psi})\sin(\bar{\phi}),$
$A_{10,16} = \cos(\bar{\phi})\ \bar{q} - \sin(\bar{\phi})\ \bar{r},\ A_{12,11} = -\omega_{B,1}^2,\ A_{12,12} = -2\zeta_{B,1}\ \omega_{B,1},\ A_{14,13} = -\omega_{B,2}^2,\ A_{14,14} = -2\zeta_{B,2}\ \omega_{B,2},\ A_{16,10} = \frac{-\cos(\bar{\phi})\ \bar{q} + \sin(\bar{\phi})\ \bar{r}}{\cos^2(\bar{\psi})},$
$A_{16,16} = \tan(\bar{\psi})\left[\sin(\bar{\phi})\ \bar{q} + \cos(\bar{\phi})\ \bar{r}\right]$

A.4.3 Full linear decoupled models.

The same assumptions made in the section A.3.3 are adopted here for the full linear model, resulting in the set of equations A.10. Furthermore, the full linear decoupled model for the roll plane is the same given earlier for the rigid body (Eq. A.5c, where the output equation is $[p\ \phi]^T = \mathbf{I}\ [p\ \phi]^T + [0\ 0]^T\ \beta_r$), since the torsional modes were neglected.

$$\begin{bmatrix} \dot{w} \\ \dot{q} \\ \dot{\theta} \\ \dot{\theta}_{B11} \\ \dot{\theta}_{B12} \\ \dot{\theta}_{B21} \\ \dot{\theta}_{B22} \end{bmatrix} \approx \begin{bmatrix} -\bar{Z}_\alpha/\bar{U} & (2\ \bar{\dot{m}}\ \bar{x}_e)/\bar{m} + \bar{U} & -\bar{g}\cos(\bar{\theta}) & 0 & 0 & 0 & 0 \\ \bar{M}_\alpha/\bar{U} & -\bar{M}_q & 0 & 0 & 0 & 0 & 0 \\ 0 & 1 & 0 & 0 & 0 & 0 & 0 \\ 0 & 0 & 0 & 0 & 1 & 0 & 0 \\ 0 & 0 & 0 & -\bar{\omega}_{B,1}^2 & -2\zeta_{B,1}\ \bar{\omega}_{B,1} & 0 & 0 \\ 0 & 0 & 0 & 0 & 0 & 0 & 1 \\ 0 & 0 & 0 & 0 & 0 & -\bar{\omega}_{B,2}^2 & -2\zeta_{B,2}\ \bar{\omega}_{B,2} \end{bmatrix} \begin{bmatrix} w \\ q \\ \theta \\ \theta_{B11} \\ \theta_{B12} \\ \theta_{B21} \\ \theta_{B22} \end{bmatrix} + \begin{bmatrix} \bar{Z}_{\beta z} \\ -\bar{M}_{\beta z} \\ 0 \\ 0 \\ K_{B,1} \\ 0 \\ K_{B,2} \end{bmatrix} \beta_z + \begin{bmatrix} \bar{Z}_\alpha/\bar{U} \\ -\bar{M}_\alpha/\bar{U} \\ 0 \\ 0 \\ 0 \\ 0 \\ 0 \end{bmatrix} w_v \tag{A.10a}$$

$$\begin{bmatrix} q_F \\ \theta_F \end{bmatrix} = \begin{bmatrix} 0 & 1 & 0 & 0 & 1 & 0 & 1 \\ 0 & 0 & 1 & 1 & 0 & 1 & 0 \end{bmatrix} \begin{bmatrix} w \\ q \\ \theta \\ \theta_{B11} \\ \theta_{B12} \\ \theta_{B21} \\ \theta_{B22} \end{bmatrix} + \begin{bmatrix} 0 \\ 0 \end{bmatrix} \beta_z + \begin{bmatrix} 0 \\ 0 \end{bmatrix} w_v$$

$$\begin{bmatrix} \dot{v} \\ \dot{r} \\ \dot{\psi} \\ \dot{\psi}_{B11} \\ \dot{\psi}_{B12} \\ \dot{\psi}_{B21} \\ \dot{\psi}_{B22} \end{bmatrix} \approx \begin{bmatrix} -\bar{Y}_\beta/\bar{U} & -\left(2\ \bar{\dot{m}}\ \bar{x}_e/\bar{m} + \bar{U}\right) & \bar{g}\cos(\bar{\theta}) & 0 & 0 & 0 & 0 \\ -\bar{N}_\beta/\bar{U} & -N_r & 0 & 0 & 0 & 0 & 0 \\ 0 & 1 & 0 & 0 & 0 & 0 & 0 \\ 0 & 0 & 0 & 0 & 1 & 0 & 0 \\ 0 & 0 & 0 & -\bar{\omega}_{B,1}^2 & -2\zeta_{B,1}\ \bar{\omega}_{B,1} & 0 & 0 \\ 0 & 0 & 0 & 0 & 0 & 0 & 1 \\ 0 & 0 & 0 & 0 & 0 & -\bar{\omega}_{B,2}^2 & -2\zeta_{B,2}\ \bar{\omega}_{B,2} \end{bmatrix} \begin{bmatrix} v \\ r \\ \psi \\ \psi_{B11} \\ \psi_{B12} \\ \psi_{B21} \\ \psi_{B22} \end{bmatrix} + \begin{bmatrix} \bar{Y}_{\beta y} \\ \bar{N}_{\beta y} \\ 0 \\ 0 \\ K_{B,1} \\ 0 \\ K_{B,2} \end{bmatrix} \beta_y + \begin{bmatrix} \bar{Y}_\beta/\bar{U} \\ \bar{N}_\beta/\bar{U} \\ 0 \\ 0 \\ 0 \\ 0 \\ 0 \end{bmatrix} v_v \tag{A.10b}$$

$$\begin{bmatrix} r_F \\ \psi_F \end{bmatrix} = \begin{bmatrix} 0 & 1 & 0 & 0 & 1 & 0 & 1 \\ 0 & 0 & 1 & 1 & 0 & 1 & 0 \end{bmatrix} \begin{bmatrix} v \\ r \\ \psi \\ \psi_{B11} \\ \psi_{B12} \\ \psi_{B21} \\ \psi_{B22} \end{bmatrix} + \begin{bmatrix} 0 \\ 0 \end{bmatrix} \beta_y + \begin{bmatrix} 0 \\ 0 \end{bmatrix} v_v$$

A.5 VLS launch vehicle general standard model.

The general standard models (GSMs) of each manoeuvring plane of the launch vehicle are developed, with which a robust controller can be designed. In this work, in order to reduce the complexity of the design, the GSMs of the pitch and yaw planes are assumed equal, supposing vehicle symmetry.

A.5.1 Structure of the GSM.

The pitch plane will be chosen to illustrate detailedly the building method of the GSM, which can be applied to the other two manoeuvring planes. The mathematical description of the GSM is given by the Eq. A.11 ($G_L(s) = G_{\theta\beta}(s) + \sum G_{Bi}(s)$, $k_{\bullet\bullet}$ are scalars), associated with the Fig. A.2.

$$\begin{bmatrix} z_u \\ z_q \\ z_\theta \\ z_{e\theta} \\ \tilde{q} \\ \tilde{\theta} \end{bmatrix} = \begin{bmatrix} 0 & 0 & 0 & 0 & k_{zu} \\ 0 & 0 & k_{zq}\,k_{wd}\,G_{\theta d}s & k_{zq}\,k_{wu}\,G_L G_A s & k_{zq}\,G_L G_A\,s \\ 0 & 0 & k_{z\theta}\,k_{wd}\,G_{\theta d} & k_{z\theta}\,k_{wu}\,G_L G_A & k_{z\theta}\,G_L G_A \\ 0 & G_{e\theta}\,k_{w\theta} & -k_{wd}\,G_{e\theta}\,G_{\theta d} & -k_{wu}\,G_{e\theta}\,G_L G_A & -G_{e\theta}\,G_L G_A \\ k_{wq} & 0 & -k_{wd}\,G_{\theta d}\,s & -k_{wu}\,G_L G_A\,s & -G_L G_A\,s \\ 0 & k_{w\theta} & -k_{wd}\,G_{\theta d} & -k_{wu}\,G_L G_A & -G_L G_A \end{bmatrix} \begin{bmatrix} w_q \\ w_\theta \\ w_d \\ w_u \\ u \end{bmatrix} \tag{A.11}$$

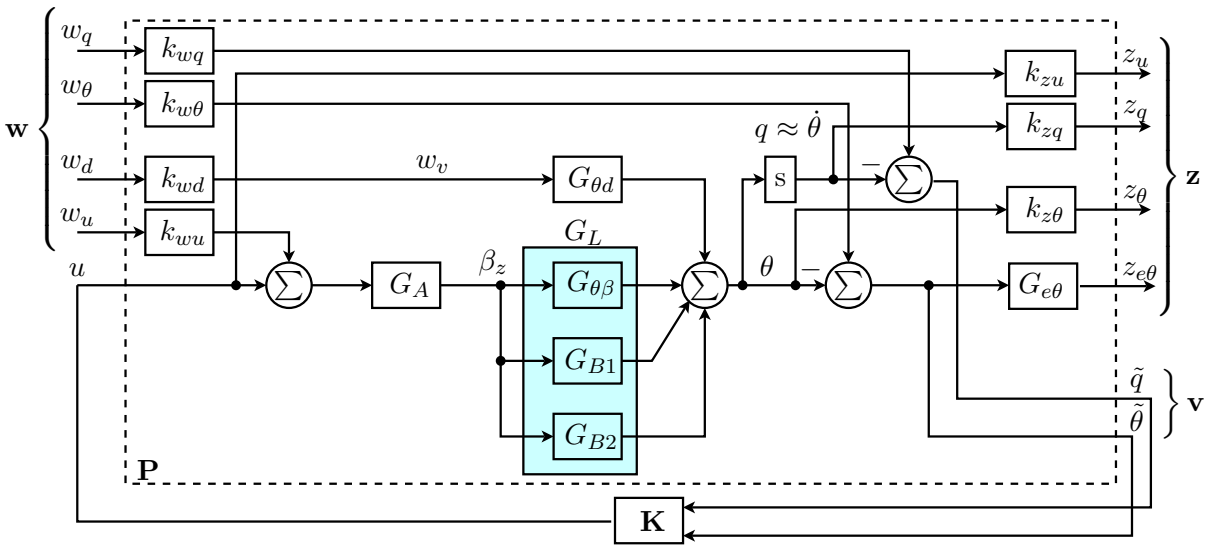

Figure A.2 - GSM of the VLS launch vehicle (pitch plane).

The following transfer functions will be considered:

a) $G_{\theta\beta}$ (Eq. A.6e) and $G_{\theta d}$ (Eq. A.6f) are the transfer functions of the linear rigid body decoupled model with respect to the control input β_z and disturbance input w_v respectively.

b) G_{B1} and G_{B2} are the transfer functions of the 1^{st} and 2^{nd} bending modes, given by the Eq. A.8.

c) G_A is the actuator transfer function, given by the Eq. A.12:

$$G_A(s) = \frac{\lambda_a}{s + \lambda_a} \tag{A.12}$$

d) $G_{e\theta}$ is the transfer function representing the (approximated) integral of the error signal $k_{w\theta}\, w_\theta - \theta$:

$$G_{e\theta}(s) = \frac{1}{s + \epsilon_{e\theta}} \tag{A.13}$$

This transfer function is required to cancel the steady-state error to a step function at input w_θ (or otherwise reference input θ_{ref}). The parameter $\epsilon_{e\theta}$ is necessary to comply with the properties required for the GSM, which will be given soon.

A.5.2 Development of the GSM state equations.

The atmospheric phase of the VLS flight trajectory is associated with a set of aerodynamic coefficients, but some of them become null when the vehicle is outside the atmosphere. Due to this aspect, the development of the GSM will be presented for these two conditions, namely: full set and reduced set.

A.5.2.1 Full set of coefficients.

In this section, the pitch plane GSM will be developed, based on the Eq. A.11. First, one observes a common term given by:

$$h(s) = k_{wd}\, G_{\theta d}(s)\, w_d(s) + G_L(s) G_A(s)\, [u(s) + k_{wu}\, w_u(s)] = k_{wd}\, G_{\theta d}(s)\, w_d(s) + G_L(s)\, \beta_z(s) \tag{A.14}$$

One may rewrite the Eq. A.14 in a fractional form:

$$h(s) = k_{wd}\,\frac{G_{\theta d,n}(s)}{G_{\theta d,d}(s)} w_d(s) + \frac{G_{L,n}(s)}{G_{L,d}(s)}\beta_z(s) \tag{A.15}$$

$$\text{where } \begin{cases} G_{L,n}(s) = G_{\theta\beta,n}(s)\,G_{B1,d}(s)\,G_{B2,d}(s) + G_{B1,n}(s)G_{\theta\beta,d}(s)\,G_{B2,d}(s) + G_{B2,n}(s)\,G_{\theta\beta,d}(s)\,G_{B1,d}(s) \\ G_{L,d}(s) = G_{\theta\beta,d}(s)\,G_{B1,d}(s)\,G_{B2,d}(s) \end{cases}$$

As $G_{\theta\beta,d}(s) = G_{\theta d,d}(s) \triangleq G_{\theta,d}(s)$, and considering the advice given by ((SKOGESTAD; POSTLETHWAITE, 2005), Chapter 4), associated with the unstable disturbance model $G_{\theta d}(s)$, in order to avoid internal pole-zero cancellations the Eq. A.15 is redefined as:

$$G_{L,d}(s)h(s) = k_{wd}\,G_{\theta d,n}(s)\,G_{B1,d}(s)\,G_{B2,d}(s)\,w_d(s) + G_{L,n}(s)\beta_z(s)$$

or, given the degree of each of the transfer functions A.6e, A.6f and A.8, then:

$$\left[s^7 + \sum_{i=0}^{6}\left(a_{1i}s^i\right)\right] h(s) = k_{wd}\sum_{i=1}^{5}\left(a_{2i}s^i\right)\,w_d(s) + \sum_{i=0}^{5}\left(a_{3i}s^i\right)\beta_z(s) \tag{A.16}$$

The inverse Laplace transform produces:

$$\begin{aligned} h^{(7)}(t) \;+\; & a_{16}\,h^{(6)}(t) + a_{15}\,h^{(5)}(t) + a_{14}\,h^{(4)}(t) + a_{13}\,h^{(3)}(t) + a_{12}\,\ddot{h}(t) + a_{11}\,\dot{h}(t) + a_{10}\,h(t) = \\ & k_{wd}\;a_{25}\,w_d^{(5)}(t) + k_{wd}\;a_{24}\,w_d^{(4)}(t) + k_{wd}\;a_{23}\,w_d^{(3)}(t) + k_{wd}\;a_{22}\,\ddot{w}_d(t) + k_{wd}\;a_{21}\,\dot{w}_d(t) + \\ & a_{35}\,\beta_z^{(5)}(t) + a_{34}\,\beta_z^{(4)}(t) + a_{33}\,\beta_z^{(3)}(t) + a_{32}\,\ddot{\beta}_z(t) + a_{31}\,\dot{\beta}_z(t) + a_{30}\,\beta_z(t) \end{aligned} \tag{A.17}$$

The Eq. A.17 contains derivatives of the inputs, thus the following realization in state space is necessary (see for example, (OGATA, 1985), pp. 763-766):

$$x_1(t) \;=\; \rho_0 h(t) + \eta_0\,w_d(t) + \mu_0\,\beta_z(t) = h(t)$$

$$\begin{aligned} x_2(t) \;&=\; \dot{x}_1(t) + \rho_1 h(t) + \eta_1\,w_d(t) + \mu_1\,\beta_z(t) \\ &= \dot{h}(t) + a_{16}\,h(t) \Rightarrow \dot{x}_1(t) = x_2(t) - a_{16}x_1(t) \end{aligned}$$

$$
\begin{aligned}
x_3(t) &= \dot{x}_2(t) + \rho_2 h(t) + \eta_2\, w_d(t) + \mu_2\, \beta_z(t) \\
&= \ddot{h}(t) + a_{16}\, \dot{h}(t) + a_{15}\, h(t) - k_{wd}\; a_{25}\, w_d(t) - a_{35}\beta_z(t) \\
&\Rightarrow \dot{x}_2(t) = x_3(t) - a_{15}x_1(t) + k_{wd}\; a_{25}\, w_d(t) + a_{35}\beta_z(t)
\end{aligned}
$$

$$
\begin{aligned}
x_4(t) &= \dot{x}_3(t) + \rho_3 h(t) + \eta_3\, w_d(t) + \mu_3\, \beta_z(t) = \\
&\quad h^{(3)}(t) + a_{16}\, \ddot{h}(t) + a_{15}\, \dot{h}(t) - k_{wd}\; a_{25}\, \dot{w}_d(t) - a_{35}\, \dot{\beta}_z(t) \\
&\quad + a_{14}\, h(t) - k_{wd}\; a_{24}\, w_d(t) - a_{34}\, \beta_z(t) \\
&\quad \Rightarrow \dot{x}_3(t) = x_4(t) - a_{14}x_1(t) + k_{wd}\; a_{24}\, w_d(t) + a_{34}\beta_z(t)
\end{aligned}
$$

$$
\begin{aligned}
x_5(t) &= \dot{x}_4(t) + \rho_4 h(t) + \eta_4\, w_d(t) + \mu_4\, \beta_z(t) = \\
&\quad h^{(4)}(t) + a_{16}\, h^{(3)}(t) + a_{15}\, \ddot{h}(t) - k_{wd}\; a_{25}\, \ddot{w}_d(t) - a_{35}\, \ddot{\beta}_z(t) \\
&\quad + a_{14}\, \dot{h}(t) - k_{wd}\; a_{24}\, \dot{w}_d(t) - a_{34}\, \dot{\beta}_z(t) + a_{13}\, h(t) - k_{wd}\; a_{23}\, w_d(t) - a_{33}\, \beta_z(t) \\
&\quad \Rightarrow \dot{x}_4(t) = x_5(t) - a_{13}x_1(t) + k_{wd}\; a_{23}\, w_d(t) + a_{33}\beta_z(t)
\end{aligned}
$$

$$
\begin{aligned}
x_6(t) &= \dot{x}_5(t) + \rho_5 h(t) + \eta_5\, w_d(t) + \mu_5\, \beta_z(t) = \\
&\quad h^{(5)}(t) + a_{16}\, h^{(4)}(t) + a_{15}\, h^{(3)}(t) - k_{wd}\; a_{25}\, w_d^{(3)}(t) - a_{35}\, \beta_z^{(3)}(t) \\
&\quad + a_{14}\, \ddot{h}(t) - k_{wd}\; a_{24}\, \ddot{w}_d(t) - a_{34}\, \ddot{\beta}_z(t) + a_{13}\, \dot{h}(t) - k_{wd}\; a_{23}\, \dot{w}_d(t) \\
&\quad - a_{33}\, \dot{\beta}_z(t) + a_{12}\, h(t) - k_{wd}\; a_{22}\, w_d(t) - a_{32}\, \beta_z(t) \\
&\quad \Rightarrow \dot{x}_5(t) = x_6(t) - a_{12}x_1(t) + k_{wd}\; a_{22}\, w_d(t) + a_{32}\beta_z(t)
\end{aligned}
$$

$$
\begin{aligned}
x_7(t) &= \dot{x}_6(t) + \rho_6 h(t) + \eta_6\, w_d(t) + \mu_6\, \beta_z(t) \\
&\quad = h^{(6)}(t) + a_{16}\, h^{(5)}(t) + a_{15}\, h^{(4)}(t) - k_{wd}\; a_{25}\, w_d^{(4)}(t) - a_{35}\, \beta_z^{(4)}(t) \\
&\quad + a_{14}\, h^{(3)}(t) - k_{wd}\; a_{24}\, w_d^{(3)}(t) - a_{34}\, \beta_z^{(3)}(t) + a_{13}\, \ddot{h}(t) - k_{wd}\; a_{23}\, \ddot{w}_d(t) \\
&\quad - a_{33}\, \ddot{\beta}_z(t) + a_{12}\, \dot{h}(t) - k_{wd}\; a_{22}\, \dot{w}_d(t) - a_{32}\, \dot{\beta}_z(t) + a_{11}\, h(t) \\
&\quad - k_{wd}\; a_{21}\, w_d(t) - a_{31}\, \beta_z(t) \\
&\quad \Rightarrow \dot{x}_6(t) = x_7(t) - a_{11}x_1(t) + k_{wd}\; a_{21}\, w_d(t) + a_{31}\beta_z(t)
\end{aligned}
$$

$$
\begin{aligned}
\dot{x}_7(t) \;=\;& h^{(7)}(t) + a_{16}\, h^{(6)}(t) + a_{15}\, h^{(5)}(t) + a_{14}\, h^{(4)}(t) + a_{13}\, h^{(3)}(t) + a_{12}\, \ddot{h}(t) + a_{11}\, \dot{h}(t) \\
& - k_{wd}\; a_{25}\, w_d^{(5)}(t) - k_{wd}\; a_{24}\, w_d^{(4)}(t) - k_{wd}\; a_{23}\, w_d^{(3)}(t) - k_{wd}\; a_{22}\, \ddot{w}_d(t) - k_{wd}\; a_{21}\, \dot{w}_d(t) \\
& - a_{35}\, \beta_z^{(5)}(t) - a_{34}\, \beta_z^{(4)}(t) - a_{33}\, \beta_z^{(3)}(t) - a_{32}\, \ddot{\beta}_z(t) - a_{31}\, \dot{\beta}_z(t) = -a_{10}\, h(t) + a_{30}\, \beta_z(t) \\
& \Rightarrow \dot{x}_7(t) = -a_{10} x_1(t) + a_{30} \beta_z(t)
\end{aligned}
$$

An additional state is required for $z_{e\theta}$:

$$
z_{e\theta}(s) = x_8(s) = G_{e\theta}(s)\, \tilde{\theta}(s) = G_{e\theta}(s)\; [k_{w\theta}\; w_\theta(s) - h(s)] = G_{e\theta}(s)\; [k_{w\theta}\; w_\theta(s) - x_1(s)]
$$

Then, substituting the Eq. A.13 and applying the inverse Laplace transform:

$$
\dot{x}_8(t) = k_{w\theta}\; w_\theta(t) - x_1(t) - \epsilon_{e\theta}\; x_8(t)
$$

Finally, one adds the actuator state: $\dot{x}_9(t) = -\lambda_a\; x_9(t) + \lambda_a\, (u(t) + k_{wu}\; w_u(t))$, where $x_9(t) = \beta_z(t)$. Returning to the Eq. A.11, one can see that[3]: $z_\theta(s) = k_{z\theta}\, h(s)$, $z_q(s) = k_{zq}\, h(s)\, s$, $\tilde{q}(s) = k_{wq}\, w_q(s) - h(s)\, s$, and $\tilde{\theta}(s) = k_{w\theta}\, w_\theta(s) - h(s)$. Therefore, the state space description of the pitch plane GSM is given by the Eqs. A.18 and A.19, where $\mathbf{x} = [x_1\; x_2\; \cdots\; x_9]^T$, $\mathbf{z} = [z_u\; z_q\; z_\theta\; z_{e\theta}]^T$, $\mathbf{v} = \left[\tilde{q}\; \tilde{\theta}\right]^T$ and $\mathbf{w} = [w_q\; w_\theta\; w_d\; w_u]^T$.

$$
\begin{bmatrix} \dot{\mathbf{x}}(t) \\ \mathbf{z}(t) \\ \mathbf{v}(t) \end{bmatrix} = \mathbf{P} \begin{bmatrix} \mathbf{x}(t) \\ \mathbf{w}(t) \\ u(t) \end{bmatrix} = \left[\begin{array}{c|c|c} \mathbf{A} & \mathbf{B}_1 & \mathbf{B}_2 \\ \hline \mathbf{C}_1 & \mathbf{D}_{11} & \mathbf{D}_{12} \\ \hline \mathbf{C}_2 & \mathbf{D}_{21} & \mathbf{D}_{22} \end{array}\right] \begin{bmatrix} \mathbf{x}(t) \\ \mathbf{w}(t) \\ u(t) \end{bmatrix} \tag{A.18}
$$

[3]Note also that $\dot{h}(t) = x_2(t) - a_{16}\, x_1(t)$.

$$\mathbf{P} = \left[\begin{array}{cccccccc|cccc|c}
-a_{16} & 1 & 0 & 0 & 0 & 0 & 0 & 0 & 0 & 0 & 0 & 0 & 0 & 0 \\
-a_{15} & 0 & 1 & 0 & 0 & 0 & 0 & 0 & a_{35} & 0 & 0 & k_{wd}\ a_{25} & 0 & 0 \\
-a_{14} & 0 & 0 & 1 & 0 & 0 & 0 & 0 & a_{34} & 0 & 0 & k_{wd}\ a_{24} & 0 & 0 \\
-a_{13} & 0 & 0 & 0 & 1 & 0 & 0 & 0 & a_{33} & 0 & 0 & k_{wd}\ a_{23} & 0 & 0 \\
-a_{12} & 0 & 0 & 0 & 0 & 1 & 0 & 0 & a_{32} & 0 & 0 & k_{wd}\ a_{22} & 0 & 0 \\
-a_{11} & 0 & 0 & 0 & 0 & 0 & 1 & 0 & a_{31} & 0 & 0 & k_{wd}\ a_{21} & 0 & 0 \\
-a_{10} & 0 & 0 & 0 & 0 & 0 & 0 & 0 & a_{30} & 0 & 0 & 0 & 0 & 0 \\
-1 & 0 & 0 & 0 & 0 & 0 & 0 & -\epsilon_{e\theta} & 0 & 0 & k_{w\theta} & 0 & 0 & 0 \\
0 & 0 & 0 & 0 & 0 & 0 & 0 & 0 & -\lambda_a & 0 & 0 & 0 & \lambda_a\ k_{wu} & \lambda_a \\
\hline
0 & 0 & 0 & 0 & 0 & 0 & 0 & 0 & 0 & 0 & 0 & 0 & 0 & k_{zu} \\
-k_{zq}\, a_{16} & k_{zq} & 0 & 0 & 0 & 0 & 0 & 0 & 0 & 0 & 0 & 0 & 0 & 0 \\
k_{z\theta} & 0 & 0 & 0 & 0 & 0 & 0 & 0 & 0 & 0 & 0 & 0 & 0 & 0 \\
0 & 0 & 0 & 0 & 0 & 0 & 0 & 1 & 0 & 0 & 0 & 0 & 0 & 0 \\
\hline
a_{16} & -1 & 0 & 0 & 0 & 0 & 0 & 0 & 0 & k_{wq} & 0 & 0 & 0 & 0 \\
-1 & 0 & 0 & 0 & 0 & 0 & 0 & 0 & 0 & 0 & k_{w\theta} & 0 & 0 & 0
\end{array}\right] \tag{A.19}$$

A.5.2.2 Reduced set of coefficients.

For the pitch plane considered here, the subsets of the coefficients $\left\{\bar{M}_\alpha, \bar{Z}_\alpha\right\}$ (set 1) and $\left\{\bar{M}_q, \bar{M}_{\beta z}, \bar{Z}_{\beta z}\right\}$ (set 2) become null after the atmospheric phase, but in different superimposed intervals (see Fig. A.3). These sets produce the following effects:

- The transfer function $G_{\theta d}$ becomes zero due to the set 1, being removed from the GSM (Fig. A.2) together with the weighting value k_{wd} and the input w_d.
- Set 1 also makes the transfer function $G_{\theta\beta}$ (Eq. A.6e) to become:

$$G_{\theta\beta}(s) = \frac{\theta(s)}{\beta_z(s)} = -\frac{\bar{M}_{\beta z}}{s^2 + \bar{M}_q\ s} \tag{A.20}$$

- The set 2 finally removes the rigid body transfer function from the GSM, which means that practically there is no control action acting on the vehicle (burn-out of the second and third stages).

Equation A.11 was rewritten as Eq. A.21 in order to reflect the described changes.

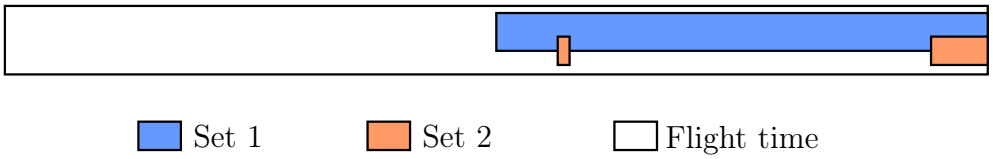

Figure A.3 - Intervals for null coefficients of the subsets 1 and 2 (illustrative view).

$$\begin{bmatrix} z_u \\ z_q \\ z_\theta \\ z_{e\theta} \\ \tilde{q} \\ \tilde{\theta} \end{bmatrix} = \begin{bmatrix} 0 & 0 & 0 & k_{zu} \\ 0 & 0 & k_{zq}\,k_{wu}\,G_L G_A s & k_{zq}\,G_L G_A s \\ 0 & 0 & k_{z\theta}\,k_{wu}\,G_L G_A & k_{z\theta}\,G_L G_A \\ 0 & G_{e\theta}\,k_{w\theta} & -k_{wu}\,G_{e\theta}\,G_L G_A & -G_{e\theta}\,G_L G_A \\ k_{wq} & 0 & -k_{wu}\,G_L G_A s & -G_L G_A s \\ 0 & k_{w\theta} & -k_{wu}\,G_L G_A & -G_L G_A \end{bmatrix} \begin{bmatrix} w_q \\ w_\theta \\ w_u \\ u \end{bmatrix} \tag{A.21}$$

The Eq. A.16 is affected by the set 1 with the coefficients $a_{10},\ a_{2i}$ and a_{30} equal to zero, which also changes the state-space realization to:

$$\dot{x}_1(t) = x_2(t) - a_{16}x_1(t)\dot{x}_2(t) = x_3(t) - a_{15}x_1(t) + a_{35}\beta_z(t)$$

$$\dot{x}_3(t) = x_4(t) - a_{14}x_1(t) + a_{34}\beta_z(t)\dot{x}_4(t) = x_5(t) - a_{13}x_1(t) + a_{33}\beta_z(t)$$

$$\dot{x}_5(t) = x_6(t) - a_{12}x_1(t) + a_{32}\beta_z(t)\dot{x}_6(t) = -a_{11}\,x_1(t) + a_{31}\beta_z(t)$$

The other two additional states for $z_{e\theta}(s)$ and the actuator are renamed as $\dot{x}_7(t)$ and $\dot{x}_8$. The final general standard equation for the reduced set of coefficients is given

by the Eq. A.22.

$$\mathbf{P} = \left[\begin{array}{cccccccc|cccc|c}
-a_{16} & 1 & 0 & 0 & 0 & 0 & 0 & 0 & 0 & 0 & 0 & 0 & 0 \\
-a_{15} & 0 & 1 & 0 & 0 & 0 & 0 & a_{35} & 0 & 0 & k_{wd}\ a_{25} & 0 & 0 \\
-a_{14} & 0 & 0 & 1 & 0 & 0 & 0 & a_{34} & 0 & 0 & k_{wd}\ a_{24} & 0 & 0 \\
-a_{13} & 0 & 0 & 0 & 1 & 0 & 0 & a_{33} & 0 & 0 & k_{wd}\ a_{23} & 0 & 0 \\
-a_{12} & 0 & 0 & 0 & 0 & 1 & 0 & a_{32} & 0 & 0 & k_{wd}\ a_{22} & 0 & 0 \\
-a_{11} & 0 & 0 & 0 & 0 & 0 & 0 & a_{31} & 0 & 0 & k_{wd}\ a_{21} & 0 & 0 \\
-1 & 0 & 0 & 0 & 0 & 0 & -\epsilon_{e\theta} & 0 & 0 & k_{w\theta} & 0 & 0 & 0 \\
0 & 0 & 0 & 0 & 0 & 0 & 0 & -\lambda_a & 0 & 0 & 0 & \lambda_a\ k_{wu} & \lambda_a \\
\hline
0 & 0 & 0 & 0 & 0 & 0 & 0 & 0 & 0 & 0 & 0 & 0 & k_{zu} \\
-k_{zq}\, a_{16} & k_{zq} & 0 & 0 & 0 & 0 & 0 & 0 & 0 & 0 & 0 & 0 & 0 \\
k_{z\theta} & 0 & 0 & 0 & 0 & 0 & 0 & 0 & 0 & 0 & 0 & 0 & 0 \\
0 & 0 & 0 & 0 & 0 & 0 & 1 & 0 & 0 & 0 & 0 & 0 & 0 \\
\hline
a_{16} & -1 & 0 & 0 & 0 & 0 & 0 & 0 & k_{wq} & 0 & 0 & 0 & 0 \\
-1 & 0 & 0 & 0 & 0 & 0 & 0 & 0 & 0 & k_{w\theta} & 0 & 0 & 0
\end{array}\right] \tag{A.22}$$

A.5.3 Properties of the GSM.

To be used in the multi-variable control design, the matrix $\mathbf{P}$ must comply with the following properties: *(i)* the pair $(\mathbf{A}, \mathbf{B}_2)$ must be stabilizable[4]; *(ii)* the pair $(\mathbf{A}, \mathbf{C}_2)$ must be detectable[5]; *(iii)* the matrices $\mathbf{D}_{12}$ and $\mathbf{D}_{21}$ must have full rank[6]; *(iv)* the matrix $[\mathbf{A} - s\mathbf{I}\ \ \mathbf{B}_2;\ \ \mathbf{C}_1\ \ \mathbf{D}_{12}]$ must have left inverse for all $s = jw, w \in \Re$; *(v)* the matrix $[\mathbf{A} - s\mathbf{I}\ \ \mathbf{B}_1;\ \ \mathbf{C}_2\ \ \mathbf{D}_{21}]$ must have right inverse for all $s = jw, w \in \Re$; *(vi)* $\mathbf{D}_{11} = \mathbf{0}, \mathbf{D}_{22} = \mathbf{0}$.

One can see that properties *(iii)* and *(vi)* are already satisfied by the model $\mathbf{P}$ (given that $k_{zu},\ k_{wq}$ and $k_{w\theta} \neq 0$), resulting from the procedure of development given earlier.

[4]A pair $\mathbf{A}, \mathbf{B}$ is stabilizable if there exists some matrix $\mathbf{F}$ such that $(\mathbf{A} + \mathbf{BF})$ is stable (the real part of each eigenvalue of $(\mathbf{A} + \mathbf{BF})$ is negative).

[5]A pair $\mathbf{A}, \mathbf{C}$ is detectable if there exists some matrix $\mathbf{L}$ such that $(\mathbf{A} + \mathbf{LC})$ is stable (the real part of each eigenvalue of $(\mathbf{A} + \mathbf{LC})$ is negative).

[6]A matrix $\mathbf{M} \in R^{m \times n}$ has full rank if $rank(\mathbf{M}) = min(m, n)$.

A.5.4 GSM of the roll plane.

The block diagram representing the roll plane GSM and its mathematical description are seen in the Fig. A.4 and the Eq. A.23 respectively.

$$\begin{bmatrix} z_u \\ z_p \\ z_\phi \\ z_{e\phi} \\ \tilde{p} \\ \tilde{\phi} \end{bmatrix} = \begin{bmatrix} 0 & 0 & 0 & k_{zu} \\ 0 & 0 & k_{zp}\, k_{wu}\, G_{\phi\beta} G_A s & k_{zp}\, G_{\phi\beta} G_A\, s \\ 0 & 0 & k_{z\phi}\, k_{wu}\, G_{\phi\beta} G_A & k_{z\phi}\, G_{\phi\beta} G_A \\ 0 & G_{e\phi}\, k_{w\phi} & -k_{wu}\, G_{e\phi}\, G_{\phi\beta} G_A & -G_{e\phi}\, G_{\phi\beta} G_A \\ k_{wp} & 0 & -k_{wu}\, G_{\phi\beta} G_A\, s & -G_{\phi\beta} G_A\, s \\ 0 & k_{w\phi} & -k_{wu}\, G_{\phi\beta} G_A & -G_{\phi\beta} G_A \end{bmatrix} \begin{bmatrix} w_p \\ w_\phi \\ w_u \\ u \end{bmatrix} \tag{A.23}$$

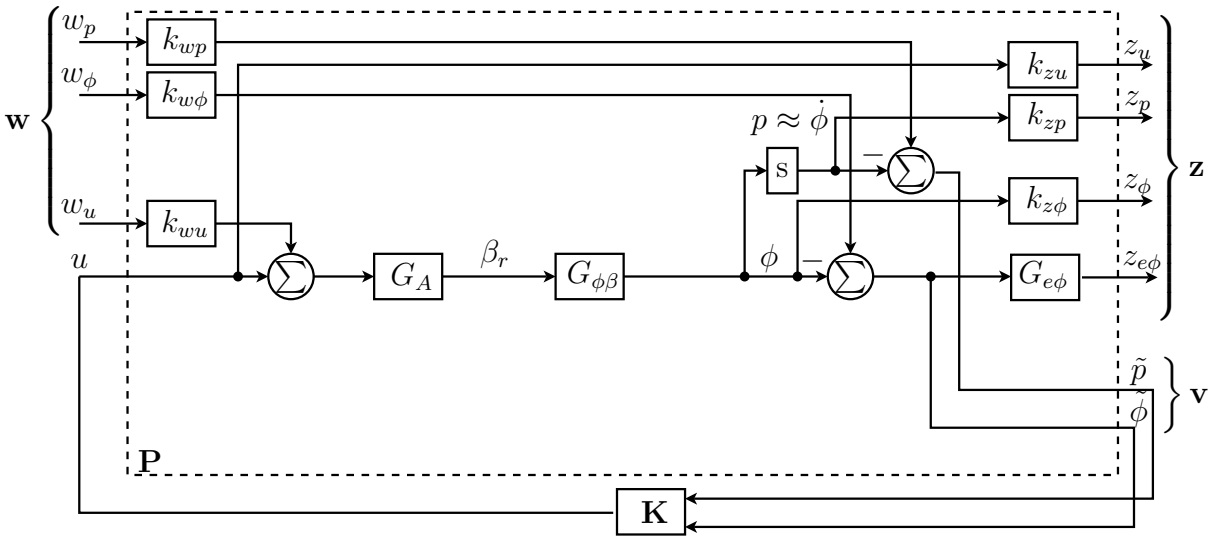

Figure A.4 - GSM of the VLS launch vehicle (roll plane).

Repeating the procedure followed in the section A.5.2.1, one starts by identifying a common term given by:

$$h(s) = G_{\phi\beta}(s) G_A(s) \left[u(s) + k_{wu}\, w_u(s)\right] = \frac{G_{\phi\beta,n}(s)}{G_{\phi\beta,d}(s)}\ \beta_r(s) \tag{A.24}$$

Recalling the Eq. A.6n, one readily defines $\dot{x}_1(t) = x_2(t) - \bar{L}_p\ x_1(t)$ and $\dot{x}_2(t) = \bar{L}_{\beta x}\ \beta_r(t)$, where $x_1(t) = h(t)$. The remaining states are: $\dot{x}_3(t) = k_{w\phi} w_\phi(t) -$

$x_1(t) - \epsilon_{e\phi} x_3(t)$ (where $x_3(t) = z_{e\phi}(t)$), and the actuator state $\dot{x}_4(t) = -\lambda_a\ x_4(t) + \lambda_a\,(u(t) + k_{wu}\ w_u(t))$, where $x_4(t) = \beta_r(t)$. Returning to the Eq. A.23, one can see that[7]: $z_\phi(s) = k_{z\phi}\,h(s)$, $z_p(s) = k_{zp}\,h(s)\,s$, $\tilde{p}(s) = k_{wp}\,w_p(s) - h(s)\,s$, and $\tilde{\phi}(s) = k_{w\phi}\,w_\phi(s) - h(s)$. Therefore, the state space description of the roll plane GSM is given by the Eqs. A.18 and A.25, where $\mathbf{x} = [x_1\ x_2\ \cdots\ x_4]^T$, $\mathbf{z} = [z_u\ z_p\ z_\phi\ z_{e\phi}]^T$, $\mathbf{v} = \left[\tilde{p}\ \tilde{\phi}\right]^T$ and $\mathbf{w} = [w_p\ w_\phi\ w_u]^T$.

$$\mathbf{P} = \left[\begin{array}{cccc|cccc} -\bar{L}_p & 1 & 0 & 0 & 0 & 0 & 0 & 0 \\ 0 & 0 & 0 & \bar{L}_{\beta x} & 0 & 0 & 0 & 0 \\ -1 & 0 & -\epsilon_{e\phi} & 0 & 0 & k_{w\phi} & 0 & 0 \\ 0 & 0 & 0 & -\lambda_a & 0 & 0 & \lambda_a\ k_{wu} & \lambda_a \\ \hline 0 & 0 & 0 & 0 & 0 & 0 & 0 & k_{zu} \\ -k_{zp}\bar{L}_p & k_{zp} & 0 & 0 & 0 & 0 & 0 & 0 \\ k_{z\phi} & 0 & 0 & 0 & 0 & 0 & 0 & 0 \\ 0 & 0 & 1 & 0 & 0 & 0 & 0 & 0 \\ \hline \bar{L}_p & -1 & 0 & 0 & k_{wp} & 0 & 0 & 0 \\ -1 & 0 & 0 & 0 & 0 & k_{w\phi} & 0 & 0 \end{array}\right] \tag{A.25}$$

It is important to observe that the parameter $\bar{L}_{\beta x}$ is zero after the burn-out of the 1^{st} stage engines, and thus the Eq. A.25 is discarded; in such condition, the roll plane control is achieved by other means (not considered in this work.)

A.6 Linearisation of the VLS rigid body non-linear model.

The method of linearisation chosen here is based on the approximation of a Taylor series of a given multi-variable function $f(\mathbf{x})$ with $\mathbf{x} = [x_1\ x_2 \cdots x_d]^T$ around a linearisation point $\bar{\mathbf{x}} = [\bar{x}_1\ \bar{x}_2 \cdots \bar{x}_d]^T$:

$$f^{\bar{\mathbf{x}}}(\mathbf{x}) = \sum_{n_1=0}^{\infty} \cdots \sum_{n_d=0}^{\infty} \frac{(x_1 - \bar{x}_1)^{n_1} \cdots (x_d - \bar{x}_d)^{n_d}}{n_1! \cdots n_d!} \left[\frac{\partial^{n_1+\cdots+n_d}}{\partial x_1^{n_1} \cdots \partial x_d^{n_d}} f(\mathbf{x})\right]_{\mathbf{x}=\bar{\mathbf{x}}}$$

and respective *Jacobians*. First, consider two scalar functions $f_i = f_i(\dot{x}_i) = \dot{x}_i$ and $g_i = g_i(\mathbf{x}, \mathbf{u})$, $\mathbf{x} \in \Re^{mx1}$ and $\mathbf{u} \in \Re^{nx1}$, so that $f_i(\dot{x}_i) = g_i(\mathbf{x}, \mathbf{u})$, and also the triple $(\bar{\dot{\mathbf{x}}}, \bar{\mathbf{x}}, \bar{\mathbf{u}})$ corresponding to the reference point of linearisation $\mathscr{P}$, $f_i\,|_{\mathscr{P}} \triangleq f_i^{\mathscr{P}} = g_i^{\mathscr{P}} \triangleq g_i\,|_{\mathscr{P}}$. The first terms of the Taylor series can be used as an approximation of

[7] Note also that $\dot{h}(t) = x_2(t) - \bar{L}_p\,x_1(t)$.

the functions considered, so that:

$$f_i^{\mathscr{P}} + \left.\frac{\partial f_i(\dot{x}_i)}{\partial \dot{x}_i}\right|_{\mathscr{P}} (\dot{x}_i - \dot{\bar{x}}_i) \approx f_i(\dot{x}_i) = g_i(\mathbf{x},\mathbf{u}) \approx g_i^{\mathscr{P}} + \left.\frac{\partial g_i(\mathbf{x},\mathbf{u})}{\partial \mathbf{x}}\right|_{\mathscr{P}} (\mathbf{x} - \bar{\mathbf{x}}) + \left.\frac{\partial g_i(\mathbf{x},\mathbf{u})}{\partial \mathbf{u}}\right|_{\mathscr{P}} (\mathbf{u} - \bar{\mathbf{u}})$$

which simplifies to:

$$\dot{x}_i - \dot{\bar{x}}_i \approx \left.\frac{\partial g_i(\mathbf{x},\mathbf{u})}{\partial \mathbf{x}}\right|_{\mathscr{P}} \mathbf{x} + \left.\frac{\partial g_i(\mathbf{x},\mathbf{u})}{\partial \mathbf{u}}\right|_{\mathscr{P}} \mathbf{u} - \left.\frac{\partial g_i(\mathbf{x},\mathbf{u})}{\partial \mathbf{x}}\right|_{\mathscr{P}} \bar{\mathbf{x}} - \left.\frac{\partial g_i(\mathbf{x},\mathbf{u})}{\partial \mathbf{u}}\right|_{\mathscr{P}} \bar{\mathbf{u}}$$

If one considers in the last equation that the second element of the left side is $f_i^{\mathscr{P}}$ and the two last ones of the right side are $-g_i^{\mathscr{P}}$, it follows that $\dot{x}_i - f_i^{\mathscr{P}} \approx g_i(\mathbf{x},\mathbf{u}) - g_i^{\mathscr{P}}$, and therefore:

$$\dot{x}_i \approx \left.\frac{\partial g_i(\mathbf{x},\mathbf{u})}{\partial \mathbf{x}}\right|_{\mathscr{P}} \mathbf{x} + \left.\frac{\partial g_i(\mathbf{x},\mathbf{u})}{\partial \mathbf{u}}\right|_{\mathscr{P}} \mathbf{u} = \mathbf{a}_i^T\ \mathbf{x} + \mathbf{b}_i^T\ \mathbf{u} \tag{A.26}$$

where $\mathbf{a}_i^T$ and $\mathbf{b}_i^T$ are row vectors of the state-space matrices $\mathbf{A}^{mxm} = [\mathbf{a}_1\ \mathbf{a}_2\ \cdots \mathbf{a}_m]^T$ and $\mathbf{B}^{mxn} = [\mathbf{b}_1\ \mathbf{b}_2\ \cdots \mathbf{b}_n]^T$ of the linear system $\mathbf{A}\ \mathbf{x} + \mathbf{B}\ \mathbf{u}$. However, considering the VLS model, in order to separate the effects of the control inputs from the disturbance inputs, two matrices $\mathbf{B}_u$ and $\mathbf{B}_d$ will be assigned respectively to each set, according to the Eq. A.27 (where $\mathbf{x} = [w\ q\ \theta\ v\ r\ \psi\ p\ \phi\ ]^T$, $\mathbf{u} = [\beta_z\ \beta_y\ \beta_r\ ]^T$ and $\mathbf{d} = [v_v\ w_v]^T$):

$$\dot{\mathbf{x}} = \mathbf{A}\ \mathbf{x} + \mathbf{B_u}\ \mathbf{u} + \mathbf{B_d}\ \mathbf{d} \tag{A.27}$$

NOTE: in the next lines, a given parameter $\bar{\gamma}$ and respective variable $\gamma(t)$ are associated as $\bar{\gamma} = \gamma(t)|_{\mathscr{P}}$.

The linearisation of the VLS non-linear model (Eq. A.3) requires the partial derivatives shown in the Eq. A.26. The state space matrices of the VLS linear model, according to the Eq. A.27, are:

$$\mathbf{A} = \begin{bmatrix} -\frac{\bar{Z}_\alpha}{\bar{U}} & \frac{2\ \bar{\dot{m}}\ \bar{x}_e}{\bar{m}} + \bar{U} & A_{13} & -\bar{p} & 0 & A_{16} & -\bar{v} & A_{18} \\ \frac{\bar{M}_\alpha}{\bar{U}} & -\bar{M}_q & 0 & 0 & -\frac{\left(\bar{I}_{xx} - \bar{I}_{zz}\right)}{\bar{I}_{yy}}\ \bar{p} & 0 & -\frac{\left(\bar{I}_{xx} - \bar{I}_{zz}\right)}{\bar{I}_{yy}}\ \bar{r} & 0 \\ 0 & \frac{\cos(\bar{\phi})}{\cos(\bar{\psi})} & 0 & 0 & -\frac{\sin(\bar{\phi})}{\cos(\bar{\psi})} & A_{36} & 0 & A_{38} \\ \bar{p} & 0 & A_{43} & -\frac{\bar{Y}_\beta}{\bar{U}} & -\left(\frac{2\ \bar{\dot{m}}\ \bar{x}_e}{\bar{m}} + \bar{U}\right) & A_{46} & \bar{w} & A_{48} \\ 0 & \frac{\left(\bar{I}_{xx} - \bar{I}_{yy}\right)}{\bar{I}_{zz}}\ \bar{p} & 0 & -\frac{\bar{N}_\beta}{\bar{U}} & -\bar{N}_r & 0 & \frac{\left(\bar{I}_{xx} - \bar{I}_{yy}\right)}{\bar{I}_{zz}}\ \bar{q} & 0 \\ 0 & \sin(\bar{\phi}) & 0 & 0 & \cos(\bar{\phi}) & 0 & 0 & A_{68} \\ 0 & \frac{\left(\bar{I}_{yy} - \bar{I}_{zz}\right)}{\bar{I}_{xx}}\bar{r} & 0 & 0 & \frac{\left(\bar{I}_{yy} - \bar{I}_{zz}\right)}{\bar{I}_{xx}}\ \bar{q} & 0 & -\bar{L}_p & 0 \\ 0 & -\tan(\bar{\psi})\cos(\bar{\phi}) & 0 & 0 & \tan(\bar{\psi})\sin(\bar{\phi}) & A_{86} & 1 & A_{88} \end{bmatrix},$$

$$\mathbf{B}_u = \begin{bmatrix} \bar{Z}_{\beta z} & 0 & 0 \\ -\bar{M}_{\beta z} & 0 & 0 \\ 0 & 0 & 0 \\ 0 & \bar{Y}_{\beta y} & 0 \\ 0 & \bar{N}_{\beta y} & 0 \\ 0 & 0 & 0 \\ 0 & 0 & \bar{L}_{\beta x} \\ 0 & 0 & 0 \end{bmatrix},\ \mathbf{B}_d = \begin{bmatrix} 0 & \frac{\bar{Z}_\alpha}{\bar{U}} \\ 0 & -\frac{\bar{M}_\alpha}{\bar{U}} \\ 0 & 0 \\ \frac{\bar{Y}_\beta}{\bar{U}} & 0 \\ \frac{\bar{N}_\beta}{\bar{U}} & 0 \\ 0 & 0 \\ 0 & 0 \\ 0 & 0 \end{bmatrix}$$

where:

$$A_{13} = -\bar{g}\ \cos(\bar{\theta})\ \cos(\bar{\phi}) + \bar{g}\sin(\bar{\theta})\sin(\bar{\psi})\sin(\bar{\phi}),\ A_{16} = -\bar{g}\cos(\bar{\theta})\cos(\bar{\psi})\sin(\bar{\phi}),$$
$$A_{18} = \bar{g}\ \sin(\bar{\theta})\ \sin(\bar{\phi}) - \bar{g}\cos(\bar{\theta})\sin(\bar{\psi})\cos(\bar{\phi}),\ A_{36} = \frac{\cos(\bar{\phi})\ \bar{q} - \sin(\bar{\phi})\ \bar{r}}{\sqrt{1-\bar{\psi}^2}},$$
$$A_{38} = \frac{-\sin(\bar{\phi})\ \bar{q} - \cos(\bar{\phi})\ \bar{r}}{\cos(\bar{\psi})},\ A_{43} = -\bar{g}\ \cos(\bar{\theta})\ \sin(\bar{\phi}) - \bar{g}\sin(\bar{\theta})\sin(\bar{\psi})\cos(\bar{\phi}),$$
$$A_{46} = \bar{g}\cos(\bar{\theta})\cos(\bar{\psi})\cos(\bar{\phi}),\ A_{48} = -\bar{g}\ \sin(\bar{\theta})\ \cos(\bar{\phi}) - \bar{g}\cos(\bar{\theta})\sin(\bar{\psi})\sin(\bar{\phi}),$$
$$A_{68} = \cos(\bar{\phi})\ \bar{q} - \sin(\bar{\phi})\ \bar{r},\ A_{86} = \frac{-\cos(\bar{\phi})\ \bar{q} + \sin(\bar{\phi})\ \bar{r}}{\cos^2(\bar{\psi})},\ A_{88} = \tan(\bar{\psi})\left[\sin(\bar{\phi})\ \bar{q} + \cos(\bar{\phi})\ \bar{r}\right]$$

AUTOMATISATION DE LA SYNTHÈSE H-INFINIE DE COMPENSATEURS ET DE LEURS RÉALISATIONS SOUS FORME ESTIMATION-COMMANDE

Fausto DE OLIVEIRA RAMOS

Ce mémoire présente les avantages de combiner des techniques établies dans le domaine de l'ingénierie de contrôle avec des éléments de l'intelligence calculatoire, en fournissant un certain niveau d'automatisation et la possibilité d'explorer des propositions innovantes pour une meilleure conformité avec les spécifications. L'adoption de cette philosophie est justifiée par la complexité de certains systèmes, où des multiples exigences contradictoires doivent être remplies à chaque point de fonctionnement. Il est évident que le problème initial doit être adapté, soit par des simplifications ou des linéarisations. L'automaticien doit définir et proposer des structures et des techniques liées à la résolution du problème. Il se rendra compte parfois que certains choix doivent être faits au détriment d'autres solutions qui pourraient également être explorées. Dans ce contexte, un mécanisme basé sur l'intelligence calculatoire peut accélérer le développement du projet et élargir les horizons de la recherche révélant de nouvelles possibilités. L'apport de ce mécanisme est évalué sur deux études de cas, toutes deux basées sur un modèle variant dans le temps d'un véhicule de lancement, où le séquencement de gain est appliqué aux techniques quadratique linéaire et H-infini. L'interpolation étant un facteur important pour la stabilité en raison des paramètres variables du modèle, on comprend le lissage de certains éléments du système de contrôle dans les spécifications de conception telles que la stabilité, la performance et la robustesse. De ces deux scénarios, un mécanisme basé sur l'intelligence, qui se compose d'un algorithme génétique (responsable d'un processus évolutif en miroir de la sélection darwinienne naturelle) et les systèmes flous (qui comprend les spécifications de conception) est responsable de la recherche et de la sélection des contrôleurs plus conformes aux critères. Dans le cas linéaire quadratique, à part le lissage des gains du régulateur, on obtient l'optimisation du système de contrôle pour toute la trajectoire du véhicule, un fait qui est évalué et aussi validé par des simulations *hardware-in-the-loop*. Dans le cas H-infini, le pro-

blème est plus complexe : d'une part, en tenant compte spécifiquement de l'aspect robuste et d'autre part pour les systèmes variants dans le temps, il est proposé dans ce mémoire une métrique pour évaluer l'impact des variations exponentielles dans le modèle du système concernant la stabilité robuste du système contrôlé, ce qui est particulièrement utile pour un évènement réel qui se produit pendant le vol du véhicule de lancement utilisé dans les études des cas analysés. La mesure est simple et basée sur les fonctions existantes au sein du logiciel MATLAB. De plus, on ajoute aux objectifs précités la duplication des fonctions du compensateur, permettant de l'utiliser également en tant qu'observateur, à l'utilité évidente pour détecter et isoler les défauts. Comme l'objectif concerne la qualité des estimés fournis par les contrôleurs interpolés sous la forme estimation-commande lors de simulations non linéaires, le lissage est appliqué aux gains utilisés pour obtenir ces estimations à partir du vecteur d'état du contrôleur, et aux valeurs des pôles en boucle fermée pour assurer la stabilité du système à chaque point de fonctionnement. Enfin, l'une des tâches requises par cette technique est le choix de la dynamique d'estimation (parmi l'ensemble des pôles en boucle fermée), afin de fournir les meilleures estimés en présence de bruits de mesures et de divers défauts à détecter et à isoler; l'intelligence calculatoire peut être encore utilisée pour definir cette dynamique dans des situations où le nombre de pôles, et donc des combinaisons est très élevé. En conséquence, l'objectif principal de ce travaille est de permettre l'étude des possibilités découlant de la synergie entre l'intelligence calculatoire et l'ingénierie de contrôle, pour que ces professionnels considèrent ces outils modernes comme un moyen d'obtenir de meilleurs résultats tenant en compte les spécifications.

Mots clés: contrôle, synthèse, automatisation, forme estimation-commande, intelligence calculatoire, robustesse.

AUTOMATION OF H-INFINITY CONTROLLER DESIGN AND ITS OBSERVER-BASED REALIZATION

Fausto DE OLIVEIRA RAMOS

This work discusses the advantages of combining established techniques in the field of control engineering with elements of artificial intelligence, providing a certain level of automation and the ability to explore innovative proposals for better compliance with design specifications. The rationale for adopting this philosophy is justified by the complexity of certain systems, where multiple conflicting requirements must be met for each operating point. It is almost inevitable that the original problem must be adapted (either through simplifications or linearizations) in order to become feasible. If on one hand the designer must define and propose structures and techniques related to solving the problem, sometimes he will realize that certain choices should be made at the expense of other alternatives that could also be explored. In this context, a mechanism based on computational intelligence can accelerate the development of the project and expand the horizons of research revealing new possibilities, which is shown here in two case studies, both based on a time-variant model of a launch vehicle, where gain-scheduling is applied with the linear quadratic and H-infinity techniques. Since interpolation is an important factor for stability because of the varying parameters of the model, one includes the smoothing of certain elements of the control system into the design specifications such as stability, performance and robustness. From these two scenarios a mechanism based on intelligence, which consists of a genetic algorithm (responsible for an evolutionary process mirrored from the Darwinian natural selection) and fuzzy systems (which comprises the design specifications) searches for controllers and selects those ones that best comply with the specifications. In the linear-quadratic case, besides the smoothing of the controller gains, one obtains the optimization of the control system for the entire vehicle trajectory, a fact which is not only demonstrated but also validated through hardware- in-the-loop simulations. In the H-infinity case, the focus is more complex: firstly, taking into account the robust aspect specifically for time-varying systems, it is proposed in this paper a metric for assessing the impact of exponential variations

in the plant model regarding the robust stability of the control system. The metric is simple and based on existing functions within MATLAB®. Moreover, one adds to the aforementioned objectives the functional duplication of the controller, allowing to use it also as an observer, with obvious utility for detecting and isolating faults; as the greatest interest lies in the quality of the estimation of the interpolated controllers in observer form during non-linear digital simulations, the smoothing is applied to the gains used to obtain these estimates from the state vector controller, and to the values of the closed-loop eigenvalues as well to ensure system stability at each operating point. Finally, one of the tasks required by this technique is the choice of the closed-loop combinatoric in order to provide the best characteristics in relation to noise and signal error for each estimate: again the computational intelligence can be used to select these combinations in situations where the number of poles and thus combinations is considerably high. Therefore, the main objective of this work is to allow the contemplation of the possibilities arising from the synergy between computational intelligence and control engineering, motivating these professionals to experiment modern tools as a way to obtain better results in meeting the design specifications.

Keywords: control, design, automation, observer-based realization, computational intelligence, robustness.

Automatisation de la synthèse *H*∞ de compensateurs et de leurs réalisations sous forme estimation-commande

Ce mémoire présente les avantages de combiner des techniques établies dans le domaine de l'ingénierie de contrôle avec des éléments de l'intelligence calculatoire, en fournissant un certain niveau d'automatisation et la possibilité d'explorer des propositions innovantes pour une meilleure conformité avec les spécifications. L'adoption de cette philosophie est justifiée par la complexité de certains systèmes, où des multiples exigences contradictoires doivent être remplies à chaque point de fonctionnement. L'automaticien se rendra compte parfois que certains choix doivent être faits au détriment d'autres solutions qui pourraient également être explorées. Dans ce contexte, un mécanisme basé sur l'intelligence calculatoire peut accélérer le développement du projet et révéler de nouvelles possibilités. L'apport de ce mécanisme est évalué sur deux études de cas, toutes deux basées sur un modèle variant dans le temps d'un véhicule de lancement, où le séquencement de gain est appliqué aux techniques quadratique linéaire et H-infinie. Dans le cas linéaire quadratique, à part le lissage des gains du régulateur, on obtient l'optimisation du système de contrôle pour toute la trajectoire du véhicule, un fait qui est validé par des simulations hardware-in-the-loop. Dans le cas H-infini, on ajoute la duplication fonctionnelle du compensateur, permettant de l'utiliser également en tant qu'observateur; l'intelligence calculatoire peut être utilisée pour définir la choix de la dynamique d'estimation dans des situations où le nombre des combinaisons (pôles en boucle fermée) est très élevé, afin de fournir les meilleures estimés.

Mots clés : contrôle, synthèse, automatisation, forme estimation-commande, intelligence calculatoire, robustesse.

Automation of *H*∞ controller design and its observer-based realization

This thesis presents the advantages of combining established techniques in the field of control engineering with elements of computational intelligence, providing some level of automation and the ability to explore innovative proposals to improve compliance with specifications. The adoption of this
philosophy is justified by the complexity of some systems, where multiple conflicting requirements must be met at each operating point. The control engineer will realize that some choices must be made at the expense of other solutions that could also be explored. In this context, a mechanism based on computational intelligence can accelerate the development of the project and reveal new possibilities. The contribution of this mechanism is evaluated in two case studies, both based on a time-varying model of a launch vehicle, where gain scheduling is combined with linear quadratic techniques and H-infinity. For the linear quadratic case, besides the smoothing of the controller gains, we obtain the optimization of the control system for the entire flight path of the vehicle, a fact that is validated by hardware-in-the-loop simulations. For the H-infinity case, we add the functional duplication of the compensator, allowing its use also as an observer; computational intelligence can be used to define the choice of the dynamic estimation in situations where the number of combinations (closed-loop poles) is very high, in order to provide the best estimates.

Keywords: control, design, automation, observer-based realization, computational intelligence, robustness.